



HAL
open science

Production of γ -valerolactone, a green platform molecule

Jose Delgado Liriano

► **To cite this version:**

Jose Delgado Liriano. Production of γ -valerolactone, a green platform molecule. Chemical and Process Engineering. Normandie Université; Åbo akademi, 2023. English. NNT: 2023NORMIR13. tel-04299852

HAL Id: tel-04299852

<https://theses.hal.science/tel-04299852v1>

Submitted on 22 Nov 2023

HAL is a multi-disciplinary open access archive for the deposit and dissemination of scientific research documents, whether they are published or not. The documents may come from teaching and research institutions in France or abroad, or from public or private research centers.

L'archive ouverte pluridisciplinaire **HAL**, est destinée au dépôt et à la diffusion de documents scientifiques de niveau recherche, publiés ou non, émanant des établissements d'enseignement et de recherche français ou étrangers, des laboratoires publics ou privés.



Normandie Université

INSA | INSTITUT NATIONAL
DES SCIENCES
APPLIQUÉES
ROUEN NORMANDIE

THÈSE

Pour obtenir le diplôme de doctorat

Spécialité GENIE DES PROCÉDES

Préparée au sein de l'INSA Rouen Normandie

**En cotutelle internationale avec Åbo Akademi University - Turku, Finlande ,
FINLANDE**

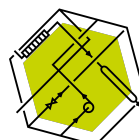
Production of γ -valerolactone, a green platform molecule

**Présentée et soutenue par
JOSE DELGADO LIRIANO**

**Thèse soutenue le 28/06/2023
devant le jury composé de**

M. LAURENT FALK	DIRECTEUR DE RECHERCHE, Université de Lorraine	Rapporteur
M. PASCAL FONGARLAND	PROFESSEUR DES UNIVERSITÉS, Université Claude Bernard Lyon 1	Rapporteur
MME PIA DAMLIN	ASSOCIATE PROFESSOR, University of Turku, Finlande	Membre
M. OSKAR KARLSTROM	ASSOCIATE PROFESSOR, University of Turku, Finlande	Membre
M. TAPIO SALMI	PROFESSEUR, Abo Akademi, Finlande	Président du jury
M. HENRIK GRENMAN	PROFESSEUR, ABO AKADEMI UNIVERSITY - TURKU, FINLANDE	Directeur de thèse
M. SEBASTIEN LEVENEUR	MAITRE DE CONFERENCES DES UNIVERSITES HDR, Institut national des sciences appliquées de Rouen	Directeur de thèse

Thèse dirigée par SEBASTIEN LEVENEUR (LABORATOIRE DE SECURITE DES PROCÉDES CHIMIQUES) et HENRIK GRENMAN (LABORATOIRE DE SECURITE DES PROCÉDES CHIMIQUES)



LSPC
Laboratoire
de sécurité
des procédés
chimiques

Production of gamma valerolactone, a green platform molecule

Jose Emilio Delgado Liriano



LSPC
Laboratoire
de sécurité
des procédés
chimiques



Institut National des Sciences Appliquées de Rouen and Åbo Akademi University
2023

INSA | INSTITUT NATIONAL
DES SCIENCES
APPLIQUÉES
ROUEN NORMANDIE



THESE

Pour obtenir le diplôme de doctorat

Spécialité Génie des Procédés

**Préparée au sein de « l'Institut National des Sciences Appliquées de Rouen Normandie » et
« Åbo Akademi University »**

Production of γ valerolactone, a green platform molecule

Présentée et soutenue par

Jose Emilio DELGADO LIRIANO

**Thèse soutenue publiquement le 28 juin 2023 à Turku, Finlande
devant le jury composé de**

Pascal FONGARLAND	Professeur , Université de Lyon, Lyon, France	Rapporteur
Laurent FALK	Directeur de recherche, Université de Lorraine, Nancy, France	Rapporteur
Pia DAMLIN	Adjunt Professor, University of Turku, Turku, Finlande	Examinatrice
Oskar KARLSTRÖM	Associate Professor, University of Turku, Turku, Finlande	Examineur
Tapio SALMI	Professeur Academique, Åbo Akademi University, Turku, Finlande	Président
Henrik GRÉNMAN	Professeur, Åbo Akademi University, Turku, Finlande	Directeur de thèse
Sébastien LEVENEUR	MCF-HDR, LSPC, INSA Rouen, Rouen, France	Directeur de thèse

Thèse dirigée par Sébastien LEVENEUR (INSA Rouen Normandie) et Henrik GRÉNMAN (Åbo Akademi University)

Curriculum Vitae



Jose Emilio Delgado Liriano

Born in 1989, Santo Domingo, Dominican Republic

Education

Oct 2019 – Mar 2023

PhD candidate in chemical engineering (double degree)
LSPC, INSA Rouen Normandy & Laboratory of industrial
chemistry and reaction engineering, Åbo Akademi University

Sept 2017 – Sept 2019

Master's in science and Technology, Process Engineering
INSA Rouen Normandy

Aug 2007 – Apr 2015

Bachelor's in chemical engineering
Department of Chemical Engineering, Universidad Autonoma
de Santo Domingo, UASD

Acknowledgments

This work was conducted as a double degree project (cotutelle) between the Laboratoire de Sécurité des Procédés Chimiques (LSPC) at Institut National des Sciences Appliquées (INSA) de Rouen Normandie (France) and the Laboratory of Industrial Chemistry and Reaction Engineering (TKR) at Åbo Akademi University (Finland). The Ministry of High Education, Science and Technology of the Dominican Republic (MESCYT) has gratefully acknowledged financial support.

Thanks to the members of the jury for accepting in reviewing this work. Research director, Pascal Fongarland, Research Professor Laurent Falk, Adjoint Professor Pia Damlin, Associate Professor Oskar Karlström, and Academic Professor, Tapio Salmi. I would thank my supervisors, Professor Sebastien Leveneur and Professor Henrik Grénman, which have greatly helped and assisted me during the development of this work. Without them, I would not have been able to get to this point; I admire your professionalism and knowledge. I want to thank Professor Sebastien Leveneur for his incredible dedication and devotion to work and his humanistic approach to treating everyone. I am incredibly thankful for his openness and availability whenever I have questions. He has always been there for any difficulties I may have had during all these years. I would also like to thank Professor Henrik Grénman for his involvement in this thesis, his scientific input, suggestions, and guidance. I admire his out-of-the-box thinking, which gave great perspectives in solving challenging problems. To you both, thank you. Thanks to my CSI members, Françoise Maugé, Dominique Seguin, and Pasi Tolvanen for their support and guidance during the development of the Thesis.

When I first arrived in Finland, I felt very welcomed by all the people of the industrial chemistry and reaction engineering laboratory in Abo Akademi. To Academy Professor Tapio Salmi and Professor Dmitry Murzin, thank you for your teachings; I admire your in-depth knowledge. I also want to thank Kari Eränen, Atte Aho, Narendra Kumar, Pasi Tolvanen, and Päivi Mäki-Arvela for your laboratory analysis and experiments assistance. I would also like to thank my friends and colleagues in Finland: Adriana, Moldir, Umara, Soudabeh, Matias, Lu, Ole, Christoph, Ananias, Wander, Mouad, Maria, Mark, Jay-pee, Zuzana, Ekaterina, Nemanja and

Jogi. You made me feel welcomed in a great environment, and your friendship and companionship are something that I keep dearly.

I would also like to thank the people in LSPC at INSA for all their support. I want to thank Bruno Daronat, Raphael Delamare, and Jean-Pierre Hebert for all the assistance in the realization of experiments, Sylvie Poubelle, and Maria Pereira for their help in commandes and being dear friends. I am also thankful to Christine Devouge-Boyer and Mélanie Mignot for their assistance in the analytical methods and analysis from COBRA. I want to thank Isabelle Polaert, Alain Ledoux and Corine Lacour for their support. To my colleagues and friends from LSPC, you made me feel at home; thanks to Mickael, Chetna, Yanjun, Sarah, Jie, Daniele, Sindi, Giulia, Youssef, Flora, Yudong. Monica, and Aurelia. I am grateful to you all.

To my family from CALIOPE, I want to thank Elizabeth, Lilivet, Balkydia, Katia, Rosy, Clara, Sarita, Yessica, Pahola, Leandro, Oscar, Juan Ernesto, Angel, César, Veronica, Rafael, Michael, Jennifer, Wenel, Erny, Luis B., Guillermina, Sharon, Gabriel, and Otoniel. I cannot express my gratitude to you for being part of my life here in France.

To my friends in the Dominican Republic, I would like to thank Lusmerlin, Joan, Miguel, Ivan, Chanel, Nelson, Marvin, and Leandro. I would also like to thank my family; your support and guidance has helped me through everything: Thanks to my parents, Orietta and Jose Luis, for always supporting and guiding me. To my late aunt Maricarmen, te amo y espero que descanses en paz Jose Manuel and Laura, thanks for all the encouragement. Especially to my aunt Angela (chachi); thank you for the unconditional love, to my grandmother Elsa, my aunts and uncles, Maria Elvira, Margot, Millo, Luis, Anita, and Aramis. My cousins, Lucia, Alicia, Noelia, Miguel, Camila, Pablito, y Desi, Thank you for everything.

Thank you all for all your support and guidance.

Publications and oral communications

Publications

- I. S. Capecci, Y. Wang, **J. Delgado**, V. Casson Moreno, M. Mignot, H. Grenman, D. Yu. Murzin, S. Leveneur, Bayesian statistics to elucidate the kinetics of γ -valerolactone from n-butyl levulinate hydrogenation over Ru/C, *Industrial & Engineering Chemistry Research*, 2021, 60, 31, 11725–11736. <https://doi.org/10.1021/acs.iecr.1c02107>.
- II. **Jose Delgado**, Wenel Naudy Vasquez Salcedo, Giulia Bronzetti, Valeria Casson Moreno, Mélanie Mignot, Julien Legros, Christoph Held, Henrik Grénman, Sébastien Leveneur, Kinetic model assessment for the synthesis of γ -valerolactone from n-butyl levulinate and levulinic acid hydrogenation over the synergy effect of dual catalysts Ru/C and Amberlite IR-120, *Chemical Engineering Journal*, Volume 430, Part 3, 15 February 2022, 133053, <https://doi.org/10.1016/j.cej.2021.133053>.
- III. **Jose Delgado**, Wenel Naudy Vasquez Salcedo, Christine Devouge-Boyer, Jean-Pierre Hebert, Julien Legros, Bruno Renou, Christoph Held, Henrik Grénman, Sébastien Leveneur, Reaction enthalpies for the hydrogenation of alkyl levulinates and levulinic acid on Ru/C– influence of experimental conditions and alkyl chain length, *Process Safety and Environmental Protection*, 171, March 2023, Pages 289-298, <https://doi.org/10.1016/j.psep.2023.01.025>

Oral Communications:

- I. **Jose Emilio DELGADO LIRIANO**, Wenel Naudy VASQUEZ SALCEDO, Jean-Pierre HEBERT, Christoph HELD, Henrik GRÉNMAN, Sébastien LEVENEUR; “Adiabatic Hydrogenation of Alkyl Levulinates” International Symposium on Green Chemistry (ISGC) 2022, La Rochelle, France.

II. **Jose Emilio DELGADO LIRIANO**, Wenel Naudy VASQUEZ SALCEDO, Sebastien LEVENEUR; “Production of γ -Valerolactone: Reaction Enthalpies & Kinetic study”. Faculty of Engineering Scientific Conference 2021, Veszprém, Hungary.

Author contributions:

- I. **J. Delgado** assisted in performing the analysis and writing the manuscript.
- II. **J. Delgado** performed the experiments, participated in model assessment, and wrote the manuscript.
- III. **J. Delgado** performed the experiments, model assessment, and wrote the manuscript.

Abstract

Non-renewable feedstock should be replaced with renewable resources in the production of energy, chemical commodities, and materials to increase sustainability. Biomass, especially 2nd generation biomass sources such as forest residues and agricultural waste are good renewable candidates for the production of biofuels, materials, and chemicals.

Different compounds can be obtained from biomass, among which, some have been classified as platform molecules due to the versatile possibilities in their further transformation to value added products. Among these platform molecules, γ -valerolactone (GVL) is a valuable molecule that may be used as a precursor for high-value materials, as a combustible additive, and as a non-toxic non-polar solvent with good physical and chemical properties. This thesis is focused on studying the production of γ -valerolactone from alkyl levulinates from a kinetic and thermodynamic perspective.

The production proceeds via a two-step reaction pathway, which comprises catalytic hydrogenation of alkyl levulinates followed by an internal cyclization to form GVL. A Ru/C solid catalyst was used to enhance the hydrogenation of levulinates with molecular hydrogen.

In the first part of the work, the influence of experimental parameters such as hydrogen pressure, temperature, and initial reactant concentration on the reaction rates and selectivity were investigated using butyl levulinate as a reference reactant. A mathematical model was proposed for the reaction kinetics using Bayesian inference. An autoclave was used to investigate experimentally the reaction kinetics in isothermal and isobaric conditions. The reactant and product concentrations were analyzed by GC-FID. It was observed that the cyclization was the rate limiting step in the GVL production.

In the second part, the hydrogenation of levulinic acid (LA) and butyl levulinate to GVL was investigated. The motivation comes from the fact that the solvolysis of glucose or fructose to butyl levulinate also leads to the production of LA as a side product. A sulfonic resin, Amberlite IR120, was used to accelerate the internal cyclization reaction. A kinetic model considering the dual catalyst system, Ru/C and Amberlite IR120, was obtained via Bayesian inference. A cross-validation method, K-fold method, was used to evaluate the predictive ability of the models.

Risks related to the production of GVL can be understood and evaluated with the help of thermodynamics. Reaction enthalpy is a key thermodynamic factor in thermal risk assessment, as it contributes to the severity of risks involved. The values of the reaction enthalpies for both reaction steps considering five *n*-alkyl levulinates (from methyl to pentyl levulinates) were determined. Batch calorimeters operated under isothermal and isobaric conditions were utilized in the experiments. A Mettler Toledo RC1mx calorimeter was used for the hydrogenation reaction, while a Tian Calvet C80 microcalorimeter was used for the cyclization reaction. The influence of parameters such as temperature, alkyl substituent, solvent effect, and initial concentration on the reaction rates and selectivity was studied for the hydrogenation reaction.

The current work contributes to the production of biomass derived γ -valerolactone, a green platform molecule.

Résumé

L'utilisation de ressources non renouvelables devraient être remplacées par de ressources renouvelables pour la production d'énergie et de matériaux, afin d'assurer un approvisionnement plus stable et plus respectueux de l'environnement. La biomasse, en particulier les sources de biomasse de deuxième génération, notamment les cultures forestières, les résidus forestiers et les déchets agricoles, sont de bons candidats renouvelables pour la production de biocarburants, de matériaux ou de produits chimiques.

Différents composés peuvent être obtenus à partir de la biomasse, parmi lesquels certains ont été considérés comme des molécules plateformes, aptes à obtenir plusieurs matériaux à haute valeur ajoutée. Parmi ces molécules plateformes, la γ -valérolactone (GVL) est une molécule polyvalente qui peut être utilisée comme précurseur de matériaux à plus grande valeur ajoutée, comme additif combustible et, ce qui est plus important, comme solvant apolaire non toxique en raison de ses propriétés physiques et chimiques. Cette thèse se centre sur l'étude des méthodes d'obtention de la γ -valérolactone à partir de lévulinate d'alkyle dans un point de vue cinétique et thermodynamique.

La voie réactionnelle est composée par deux réactions subséquentes, une réaction d'hydrogénation catalytique des lévulinate d'alkyle suivie d'une cyclisation interne pour former la GVL. Un catalyseur solide Ru/C et de l'hydrogène moléculaire ont été utilisés pour effectuer la réaction d'hydrogénation.

Dans la première partie, l'influence de différents paramètres expérimentaux, tels que la pression d'hydrogène, la température et les concentrations initiales sur les vitesses de réaction et la sélectivité ont été étudiées en utilisant le lévulinate du butyle comme réactif de référence. Un modèle cinétique a été proposé en utilisant l'inférence bayésienne. Un autoclave a été utilisé pour les expériences cinétiques dans des conditions isothermes et isobares et les concentrations étaient mesurées par GC-FID. Les concentrations ont été utilisées comme observables. Il a été observé que l'étape de cyclisation était plus lente, ce qui limitait le rendement en GVL.

Dans la deuxième partie, l'hydrogénation de l'acide lévulinique (LA) et du lévulinate du butyle pour la production de GVL a été étudiée. Cette étude est motivée par le fait que la solvolysse du glucose ou du fructose en BL conduit également à la production d'acide lévulinique. Une résine sulfonique, l'Amberlite IR120, a été utilisée pour accélérer la réaction de cyclisation interne. Un modèle cinétique prenant en compte ce double système catalytique, Ru/C et Amberlite IR120, a été obtenu par inférence bayésienne. Une méthode de validation croisée, la méthode K-fold, a été utilisée pour évaluer la prévisibilité des modèles.

Les risques liés à la production de GVL peuvent être compris et évalués grâce à la thermodynamique. L'enthalpie de réaction est une constante thermodynamique clé dans l'évaluation des risques thermiques, car elle contribue à la gravité d'un tel risque. Les valeurs des enthalpies de réaction pour les deux réactions concernant les cinq premiers levulinales de n-alkyle (de méthyle aux lévulinales de pentyle) ont été estimées. Des calorimètres discontinues dans des conditions isothermes et isobariques ont été utilisés. Un calorimètre Mettler Toledo RC1mx a été utilisé pour la réaction d'hydrogénation, tandis qu'un microcalorimètre Tian Calvet C80 a été utilisé pour la réaction de cyclisation. L'influence de paramètres tels que la température, le substituant alkyle, l'effet du solvant et la concentration initiale a été étudiée pour la réaction d'hydrogénation.

Ce travail contribue à la valorisation de la biomasse comme alternative aux sources non renouvelables dans la production de γ -valérolactone, une molécule plate-forme verte.

Referat

Industriella omställningen från användning av fossila råvaror till att producera energi och material från förnybara resurser är nödvändig. Biomassa, särskilt andra generationens biomassakällor som till exempel skogsbruksrester och jordbruksavfall är goda förnybara alternativ för produktion av biobränslen, material och kemikalier.

Biomassa är en källa för mångsidiga kemiska föreningar, varav en del betraktas som plattformsmolekyler som är speciellt lämpliga för vidareförädling till produkter med högt mervärde. Bland dessa plattformsmolekyler är γ -valerolakton (GVL), som kan användas för att producera material med högt värde, som en bränsletillsats och som ett icke-toxiskt opolärt lösningsmedel med goda fysikaliska och kemiska egenskaper. Denna avhandling fokuserar på att studera metoder för framställning av γ -valerolakton från alkyllevulinater ur ett kinetiskt och termodynamiskt perspektiv.

Reaktionen sker i två steg genom katalytisk hydrogenering av alkyllevulinater och en intramolekylär cyklisering för att bilda GVL. En fast Ru/C-katalysator användes för att genomföra hydreringsreaktionen med molekylärt väte.

I den första delen av avhandlingen undersöktes inverkan av olika parametrar som till exempel vätetryck, temperatur och initial reaktantkoncentration på reaktionshastigheten med butyllevulinat som referensreagens. En matematisk modell föreslogs för reaktionskinetiken med hjälp av Bayesiansk inferens. En autoklav användes för att utföra de kinetiska experimenten vid isotermiska och isobariska förhållanden. Reaktant- och produktkoncentrationerna analyserades med GC-FID. Det observerades att cykliseringssteget var långsammare jämfört med hydrogeneringen, vilket begränsade GVL utbytet.

I den andra delen undersöktes hydrering av levulinsyra (LA) och butyllevulinat för produktion av GVL. Motiveringen för denna undersökning härstammar från det faktum att solvolys av glukos eller fruktos leder till produktion av både butyllevulinat och LA. En sulfonharts-katalysator, Amberlite IR120, användes för att påskynda den interna cykliseringsreaktionen. En matematisk modell för reaktionskinetiken, som beaktar båda reaktionsstegen med katalysatorerna Ru/C och Amberlite IR120, erhöles genom Bayesisk

inferens. En korsvalideringsmetod, K-fold-metoden, användes för att utvärdera modellernas extrapoleringsförmåga.

Termodynamik kan utnyttjas för att estimeras och förstå risker relaterade till produktion av GVL. Reaktionsentalpin är en viktig termodynamisk konstant i termisk riskbedömning eftersom den är väsentlig för att bedöma hur kosekvenserna av en olycka. Reaktionsentalpin bestämdes för båda reaktionsstegen för fem n-alkyllevuliner (från metyl- till pentyllevulinat). Satsvis fungerande kalorimetrar användes under isotermiska och isobariska förhållanden. En Mettler Toledo RC1mx-kalorimeter användes för att undersöka hydreringsreaktionen och en Tian Calvet C80-mikrokalorimeter användes för cykliseringsreaktionen. Inverkan av parametrar som temperatur, alkylsubstituent, lösningsmedelseffekt och initialkoncentrationer på reaktionsentalpin undersöktes för hydreringsreaktionen.

Avhandlingen bidrar till ökad förståelse i effektivare produktion av γ -valerolakton, en grön plattformmolekyl.

Table of Contents

Chapter 1 - Context of the study	17
1.1. Introduction	17
1.2. Platform molecules.....	18
1.3. Lignocellulosic biomass	18
1.3.1. Composition of lignocellulosic biomass	18
1.3.2. Cellulose.....	19
1.3.3. Hemicellulose.....	20
1.3.4. Lignin	20
1.3.5. Extraction of LCB compounds.....	20
1.4. Sugars and bio-sourced platform molecules.....	21
1.5. Levulinic Acid.....	23
1.6. Alkyl levulinates.....	24
1.7. Gamma-valerolactone: a green platform molecule	28
1.8. GVL applications	29
1.8.1. Solvent.....	29
1.8.2. Synthesis of chemical compounds.....	30
1.8.3. Fuel additive	32
1.9. Production methods.....	32
1.10. Reaction pathways.....	34
1.10.1. Hydrogenation	34
1.10.2. Cyclization / Lactonization.....	38
1.11. Catalysis	39
1.11.1. Noble metals.....	40
1.11.2. Non-noble metals	42
1.12. Mathematical modeling	42
1.12.1. Bayesian inference	43
1.13. Objectives.....	43
Chapter 2 - Materials and Equipments	45
2.1. Materials.....	45
2.2. Equipment	46
2.2.1. Kinetic experiments.....	46

2.2.2. Calorimetry.....	47
2.2.3. Transesterification	48
2.2.4. Analytical equipment	50
2.2.5. Catalyst characterization	51
2.3. Reaction pathway	54
Chapter 3 - Bayesian statistic evaluation for kinetic models on butyl levulinate hydrogenation to γ -valerolactone	56
3.1. Introduction	56
3.2. Experimental procedure	57
3.3. Experimental results	57
3.3.1. Effect of temperature.....	58
3.3.2. Effect of pressure.....	59
3.3.3. Catalyst loading.....	61
3.4. Kinetic models.....	62
3.5. Material balances.....	67
3.6. Bayesian statistical method	68
3.7. Modeling results.....	70
3.7.1. Model 4 – LH2 with catalyzed cyclization step	71
3.7.2. Model 2 – LH1 with catalyzed cyclization step	73
3.7.3. Model 8 – NCLH1 with catalyzed cyclization step.....	74
3.8. Conclusions	77
Chapter 4 - Kinetic model assessment for butyl levulinate and levulinic acid hydrogenation over dual catalysts	78
4.1. Introduction	78
4.2. Experimental procedure	79
4.3. Experimental results	81
4.3.1. Effect of temperature.....	81
4.3.2. Effect of hydrogen hydrostatic pressure.....	82
4.3.3. Effect of ruthenium catalyst loading	83
4.3.4. Effect of Amberlite IR120 loading.....	84
4.3.5. Effect of levulinic acid (LA) concentration.....	85
4.4. Kinetic modeling	86
4.4.1. Rate expressions for the hydrogenation step	87
4.4.2. Rate expressions for the cyclization step.....	91
4.5. Material balances.....	92
4.6. Modeling	94

4.6.1. Modeling results: Non-competitive Langmuir Hinshelwood 1.2	97
4.6.2. Modeling results: Non-competitive Langmuir Hinshelwood 2.2	103
4.7. Cross-validation: K-fold method	110
4.8. Conclusions and perspectives	112
Chapter 5 - Substituent effect on Reaction Enthalpies for the hydrogenation of alkyl levulinates into γ -valerolactone	114
5.1. Introduction	114
5.2. Calorimetry	116
5.2.1. Calorimetry measurements	116
5.2.2. Synthesis of n-propyl levulinate and n-pentyl levulinate by transesterification:	119
5.3. Experimental results	120
5.3.1. Cyclization reactions	121
5.3.2. Hydrogenation reactions	123
5.3.3. Hydrogenation and cyclization of propyl and pentyl levulinate	132
5.4. Conclusions	135
General conclusions and perspectives	137
Notations	140
References	144
Annexes	163
List of figures	163
List of Tables	168
Publications	Erreur ! Signet non défini.

Chapter 1 - Context of the study

1.1. Introduction

The demand for energy and materials has been steadily growing over the last century. This increase is related to the growing global population and the development of industries, such as the agrochemical and plastics sectors. As a result, the demand for these commodities is directly translated into increased demand for raw materials. However, the primary raw materials used for producing energy and products, notably crude oil, and gas, are fossil-based. Fossil-based materials are limited, practically non-renewable, and cannot sustain the growing demand over time. Even more importantly, the fossil carbon sinks should not be utilized and let into the atmosphere. From this premise, a switch to renewable raw materials is imperative.

The use of bio-sourced materials is considered a relevant alternative as a renewable raw material source for energy and chemicals production. Plants represent 80% of all biomasses in the world, and around 450 gigatons of carbon is bound to trees (Bar-On et al., 2018). In regard to the use of biomass, one can classify these resources into different “generations” or groups. Bio-based materials cultivated for human consumption are considered as 1st generation biomass. The concurrence with the food industry limits the use of this type of biomass for the production of energy and materials. Due to this fact, other kinds of biomass should be utilized.

The term 2nd generation biomass refers to lignocellulosic biomass, which comprises of virgin biomass e.g. trees and grass, organic food waste, and agricultural waste which does not compete with the food industry (Yousuf et al., 2020). From these bio-based sources, virgin lignocellulosic biomass has been considered a viable source to produce materials needed in energy production and chemical industries. (Inyang et al., 2022)

Several chemical intermediates and products can be obtained from lignocellulosic biomass; among these compounds, γ -valerolactone is a molecule of high interest, given its properties and uses. This chapter will present relevant information on the general properties of biomass, specifically lignocellulosic biomass, and on obtaining higher added-value compounds, focusing more on the platform molecule γ -valerolactone (GVL). Then, the properties, applications, and products obtained from GVL will be described. The elements needed for obtaining GVL via

the hydrogenation of alkyl levulinates and levulinic acid will be explored from the viewpoints of catalysts, reaction mechanism and kinetics, and mathematical modeling. Finally, the objectives of the thesis are described.

1.2. Platform molecules

Chemical compounds can be considered platform molecules if they are suitable as intermediates for producing several other high-added-value chemicals (Werpy & Petersen, 2004). However, economic and scale-up factors, such as reasonable production cost, should be taken into account when considering a chemical compound as a platform molecule (Bomtempo et al., 2017).

When we consider a platform molecule as “green,” one could be alluding directly to the properties of the raw materials in the production of such molecule or referring to the overall environmental impact related to the use and production of this material. In the current case, we define a green platform molecule as originating from sustainably produced biomass which compounds can be used as a building block to obtain other high-value chemicals.

1.3. Lignocellulosic biomass

Lignocellulosic biomass (LCB) is a complex matrix mainly composed of polysaccharides and phenolic polymers that constitute the essential part of the woody cell walls of plants. (Yousuf et al., 2020). LCB can be used as raw material for energy production by combustion or transformed into combustibles such as synthesis gas by gasification, bio-oils by pyrolysis processes or to fuels and chemicals feedstocks via liquid phase processing. (Raud et al., 2016) LCB is highly resistant to mechanical stress and chemical decomposition, known as recalcitrance. These properties are linked to the different compounds that conform to LCB's properties, such as cellulose's crystalline structure and lignin's hydrophobicity (Isikgor & Becer, 2015). Due to these properties, harsh conditions are generally needed for fractionating LCB, such as strong alkalis and high temperatures. (Démolis et al., 2014; Serrano-Ruiz et al., 2011).

1.3.1. Composition of lignocellulosic biomass

LCB comprises nearly 50% of the world's biomass (Niju et al., 2020). Compared to food and agricultural waste, which have highly variable compositions obtained from a mix of different sources, virgin lignocellulosic biomass is mainly composed of 3 polymers: cellulose (30-50%), hemicellulose (20-34%), and lignin (21-30%) as seen Figure 1-1 (Deivayanai et al., 2022). LCB

is mainly considered a sugar-based compound, as sugars represent 70% of LCB (Arevalo-Gallegos et al., 2017). The study of platform molecules obtained from sugars is the focus in the current study.

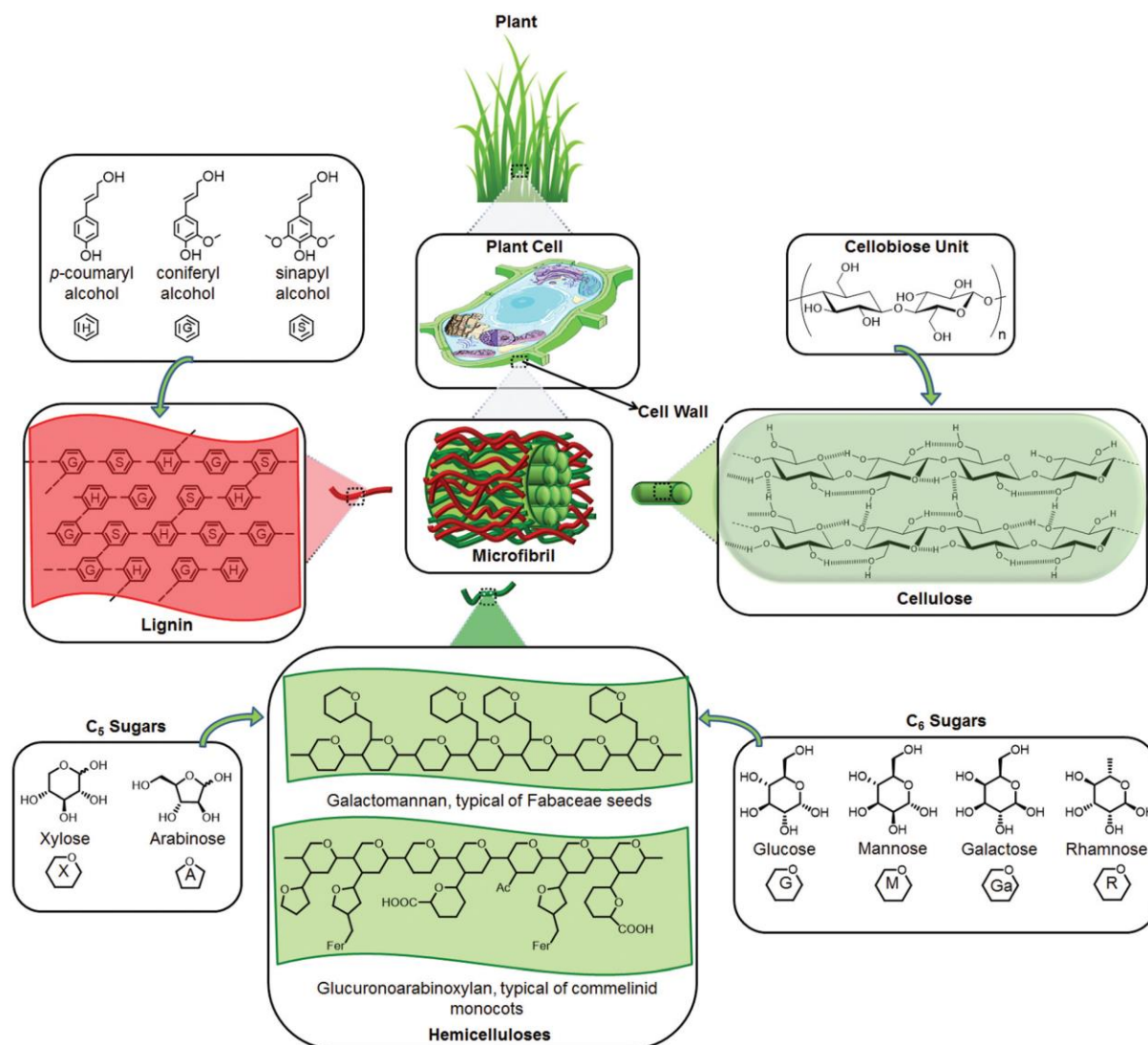


Figure 1-1 - The main components and structure of lignocellulose. “Gl” represents glucuronic acid, and “Fer” represents esterification with ferulic acid. Reproduced from (Isikgor & Becer, 2015) with permission from the Royal Society of Chemistry.

1.3.2. Cellulose

Cellulose is a structured crystalline polymer and the major contributor to lignocellulosic biomass. Cellulose is composed of cellobiose (Deivayanai et al., 2022; Isikgor & Becer, 2015), a D-glucose-based disaccharide structure tightly linked with hydrogen bonds (Isikgor & Becer, 2015). Two different crystalline forms of cellulose are naturally found: I α and I β cellulose.

These forms are present in plants and differ in the stacking arrangements of the hydrogen bonds. For LCB, the I β form is found in higher proportions (Nishiyama, 2009; Zhang et al., 2017).

Cellulose can also be found in non-crystalline forms, notably paracrystalline or fully amorphous cellulose. These forms are found in regions close to hemicellulose and are more prone to depolymerization than crystalline cellulose. (Kulasinski et al., 2014; Zhang et al., 2017).

1.3.3. Hemicellulose

Hemicellulose, compared to cellulose, is a heteropolymer composed of different monosaccharides, from 6-carbon sugars (hexoses) such as D-glucose, D-galactose, and D-mannose, and 5-carbon sugars (pentoses) like D-xylose and L-arabinose. (van Maris et al., 2006). The proportion of 5 and 6-carbon sugars varies with the source, where hardwood possesses a higher quantity of pentoses than hexoses (Isikgor & Becer, 2015). Acidic forms of these sugars, notably glucuronic acid and galacturonic acid, can also be found in hemicellulose (Nechita et al., 2021). As displayed in Figure 1-1, hemicellulose is present in the outer part of the microfibrils, surrounding cellulose, and is intertwined with lignin.

1.3.4. Lignin

Lignin is an aromatic polymer composed of phenols, such as p-trans-coumaryl alcohol, trans-q-coniferyl alcohol, and trans-q-sinapyl alcohol. (Arevalo-Gallegos et al., 2017; Isikgor & Becer, 2015; van Maris et al., 2006). Lignin can be viewed as the material that adheres cellulose and hemicellulose together. Given its hydrophobic properties and recalcitrance, difficulties in processing, lignin has been mainly used as fuel in energy production (van Spronsen et al., 2011; Vishtal & Kraslawski, n.d.). However, as lignin possesses aromatic compounds in the backbone structure, it has particular and interesting applications in producing different materials such as biopolymers (Rajesh Banu et al., 2019). Lignin can be classified based on the sulfur content into lignosulfonates, with 8.5-3.01%, kraft lignin, 3.0-1.0%, hydrolyzed lignin 1.0-0.0%, and sulfur-free lignin (Bajwa et al., 2019).

1.3.5. Extraction of LCB compounds

As LCB presents a highly complex structure, the mixture of the main compounds provides good mechanical and chemical resistance to plants. (Horikawa, 2022; Kulasinski et al., 2014). Depending on the desired use of LCB, different separation processes are needed. Only size

reduction and drying processes are required when LCB is used energy production by combustion, pyrolysis, and gasification. To obtain platform molecules, cellulose, hemicellulose, and lignin must be separated due to their chemical composition differences.

Cellulose and hemicellulose are treated by hydrolysis to obtain sugars from polysaccharides. To break down lignin, harsher conditions are needed due to the recalcitrance properties and poor solubility. Different uses and some possible products obtained from LCB are shown in Figure 1-2

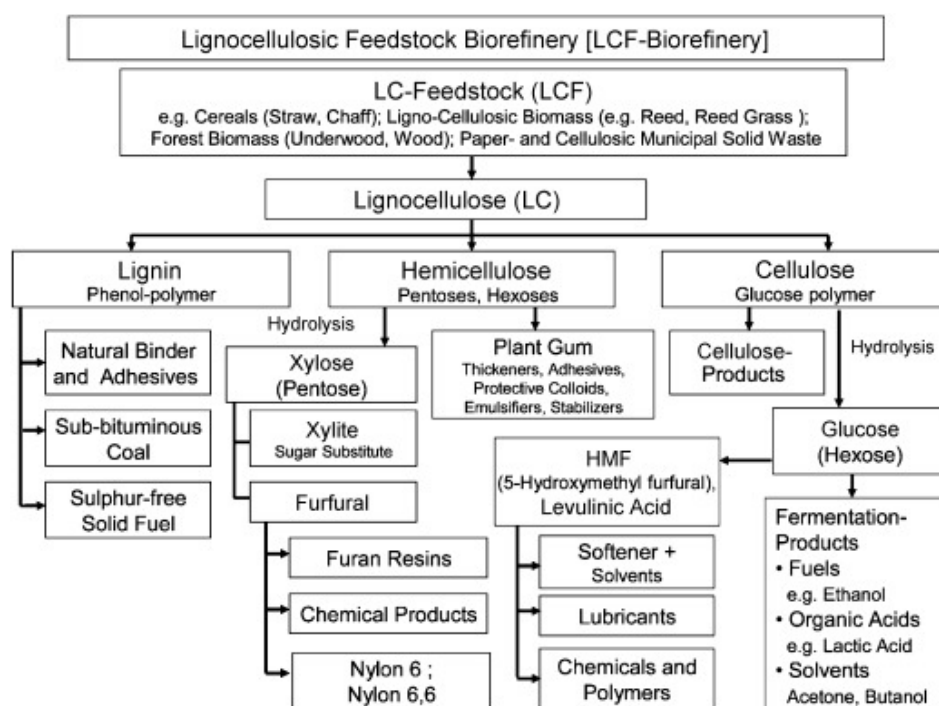


Figure 1-2 - Lignocellulosic Feedstock Biorefinery (LCF-Biorefinery, Phase III) Reproduced with permission from Springer Nature. Licence 5519390807757 (Kamm, 2004)

1.4. Sugars and bio-sourced platform molecules

Cellulose and hemicellulose can be hydrolyzed into sugars as seen in Figure 1-2. Sugars are polyhydroxy aldehydes or ketones, also known as carbohydrates (Bruce, 2010). Hexoses can be obtained from cellulose, whereas hemicellulose provides pentoses and hexoses in different ratios depending on the source. Overall, D-glucose is the most abundant hexose, while xylose is predominant among pentoses.

Sugars can be processed into higher-value chemicals. Some sugar derivatives have been identified as highly important platform chemicals by the USA's Department of Energy (DOE)

shown in Table 1-1. Platform chemicals or “building blocks” are defined as key intermediates in the production of numerous potential chemicals.

Table 1-1 - The top sugar-derived building blocks (Bozell & Petersen, 2010; Werpy & Petersen, 2004)

Platform chemicals	
lactic acid	levulinic acid
2,5 furan dicarboxylic acid	3-hydroxybutyrolactone
3 hydroxy propionic acid	glycerol
aspartic acid	sorbitol
glucaric acid	xylitol/arabinitol
glutamic acid	furfural
itaconic acid	ethanol
1,4 diacids (succinic, fumaric and malic)	

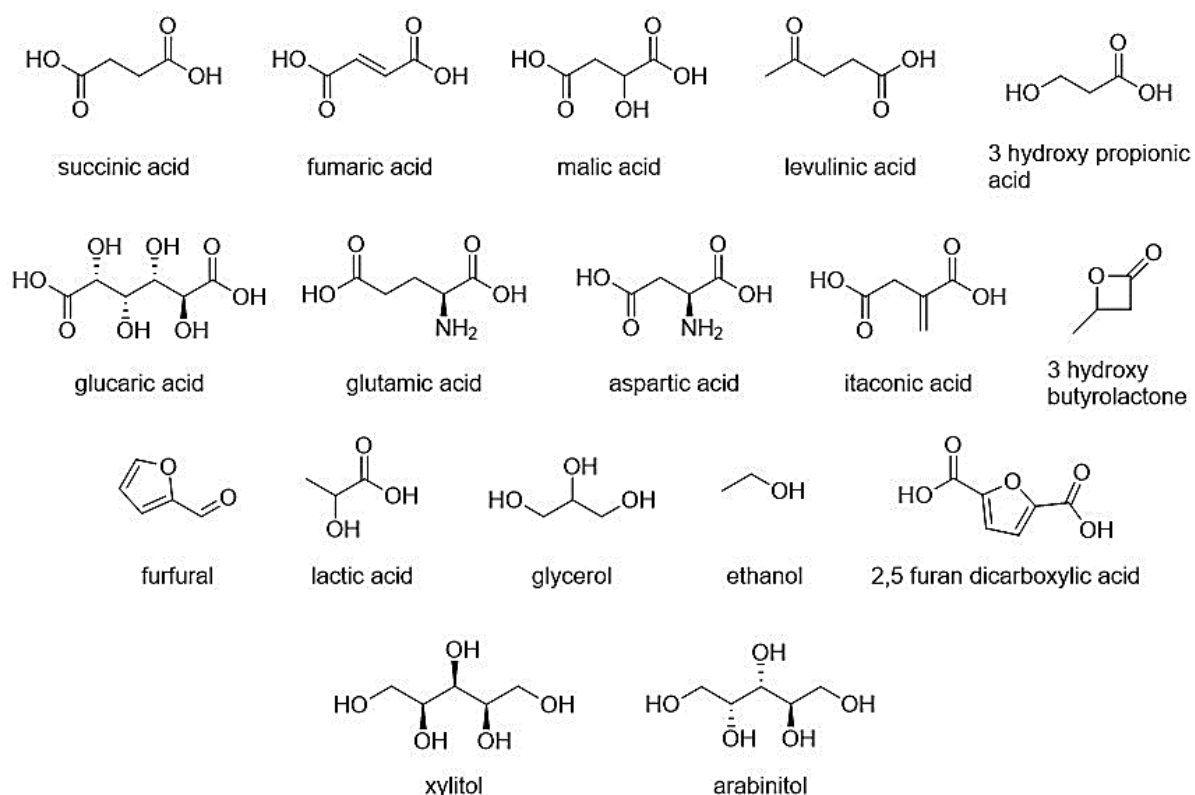


Figure 1-3 – Molecular structure of The Top Sugar-derived Building Blocks. Based on (Bozell & Petersen, 2010; Werpy & Petersen, 2004)

These building blocks can be obtained by fermentation, hydrolysis, oxidative dehydration, amination of hexoses and pentoses, and the transesterification of oils in the case of glycerol. (Werpy & Petersen, 2004).

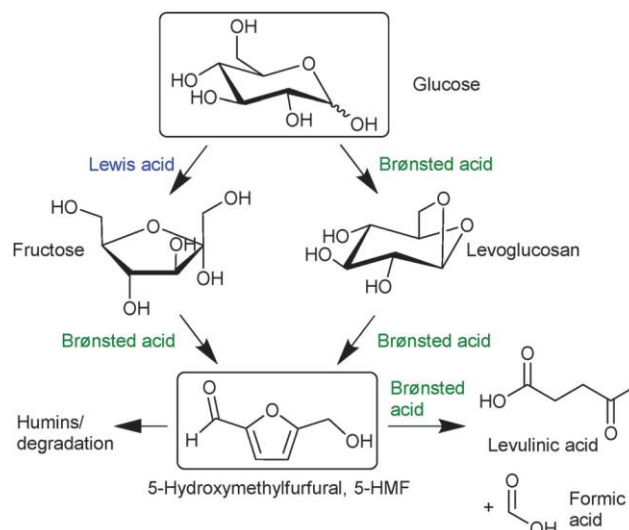


Figure 1-4 - Reaction scheme for 5-HMF production from glucose. Taken from (Herbst & Janiak, 2016) with an CCCN 3.0 licence

According to other references (Isikgor & Becer, 2015; Bozell & Petersen, 2010), other sugar-derived molecules should be considered as building blocks, such as 5-hydroxymethyl furfural and ethanol. While ethanol is mainly produced by the fermentation of sugars, 5-HMF can be obtained from acid dehydration of glucose (Figure 1-4), it is an interesting molecule since the rehydration of this molecule results in the production of levulinic acid (Alonso et al., 2013; Herbst & Janiak, 2016)

1.5. Levulinic Acid

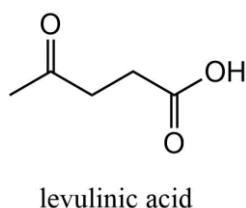


Figure 1-5 - Chemical structure of levulinic acid

Levulinic acid (LA) is a commercially available organic acid and it is considered a promising platform molecule (Isikgor & Becer, 2015). The global levulinic acid market size in 2021 was evaluated to \$26.35 million dollars, and it is expected to advance at a compound annual growth rate (CAGR) of 9.78% during 2021–2030 to reach \$61.04 million by 2030. (*Levulinic Acid Market Global Industry Growth Forecast to 2030*, 2022). LA is a carboxylic acid and it is a white crystalline substance with a strong, disagreeable odor soluble in water (*PubChem*

Compound Summary for CID 11579, Levulinic Acid, 2022). A summary of LA’s chemical and physical properties can be seen in Table 1-2

Table 1-2 – Physical properties of levulinic acid (PubChem Compound Summary for CID 11579, Levulinic Acid, 2022)

Commercial name	Levulinic Acid
IUPAC Name	4-oxopentanoic Acid
CAS #	123-76-2
Molecular weight	116.11
Physical description	Pellets or Large Crystals, Liquid
Boiling point	245 - 246°C @ 760 mm Hg
Melting point	30 - 33°C
Solubility	Soluble in water, alcohol, and oil
Density	1.136 – 1.147
Vapor pressure at 25°C (mmHg)	0.011
Dissociation Constant (pKa)	4.64 @ 18°C

LA can be used for the production of several chemicals, in example, levulinic esters and lactones such as γ -valerolactone and angelica lactones (Isikgor & Becer, 2015; Werpy & Petersen, 2004) and it can be derived from the subsequent processing of LCB, where is directly obtained by the hydration of furfural or 5-HMF. LA can also be produced by the fermentation of plant carbohydrates.(Meinita et al., 2021)

Levulinic acid has a variety of industrial and commercial applications. It may be used as a raw material to make biofuels, polymers, and chemicals. LA is also used in the food industry as flavorings and as an ingredient in cosmetics (A. Kumar et al., 2020; Werpy & Petersen, 2004).

1.6. Alkyl levulinates

Alkyl levulinates (AL) belong to the group of esters. ALs are generally obtained by Fisher esterification in which an alkyl alcohol and levulinic acid react in the presence of an acid (Fernandes et al., 2012). ALs can also be obtained from different alcohols and LCB derived molecules (Démolis et al., 2014). The main precursors for AL production are displayed in Figure 1-6. ALs can be obtained through acid solvolysis processing of cellulose and alcoholysis

of furfuryl alcohol (Di Menno Di Bucchianico et al., 2022; Yamada et al., 2015; Démolis et al., 2014; Fernandes et al., 2012) as well as shorter substituent AL and the desired alkyl alcohol by Fischer transesterification displayed in Figure 1-7 (Melchiorre et al., 2020),

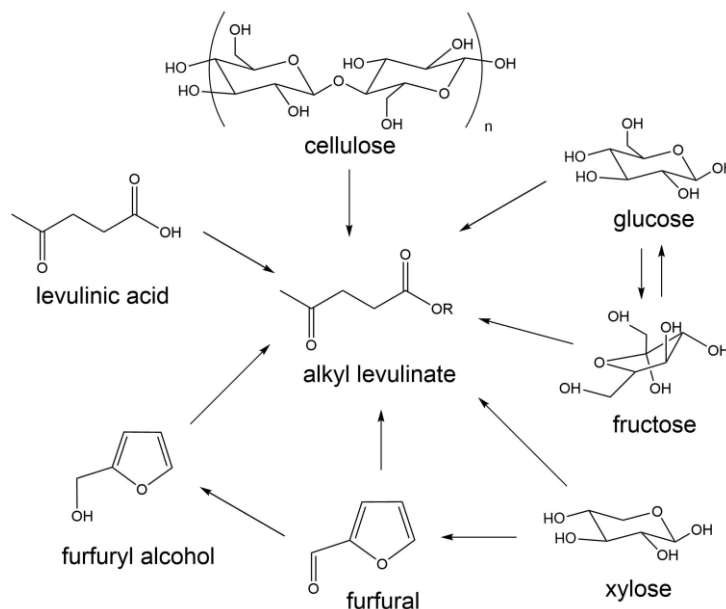


Figure 1-6 - Synthesis of alkyl levulinates from various biomass reactants. Reprinted with permission from (Démolis et al., 2014). Copyright 2014, American Chemical society.

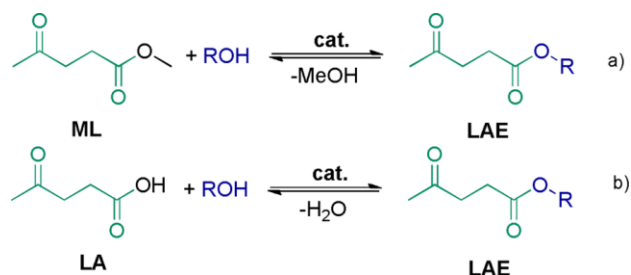


Figure 1-7 - Transesterification of methyl levulinate (a) and esterification of levulinic acid (b) (ML: methyl levulinate, LAE: levulinic acid ester) Reprinted from (Melchiorre et al., 2020) with permission of Elsevier 5519410053276

Alkyl levulinates are typically regarded to be ecologically beneficial and biodegradable compounds with a low toxicity profile. Compared to levulinic acid, levulinic acid esters have lower acidity and higher vapor pressures. Levulinic acid has been linked to corrosion in metal reactors. Compared to levulinic acid, alkyl levulinates present lower solubilities in polar compounds. The lowest chain length n-alkyl levulinates are displayed in Figure 1-8.

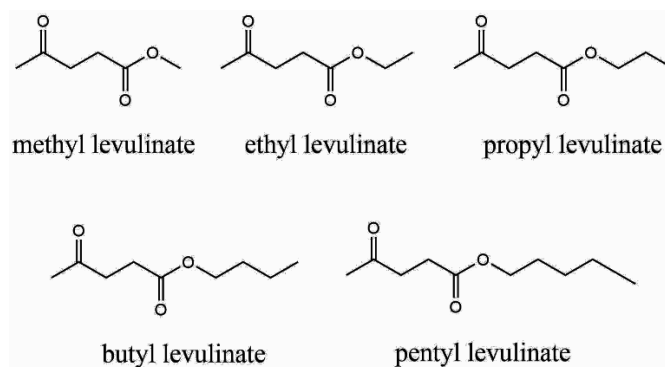


Figure 1-8 – *n*-alkyl levulinates up to 5 chain carbon substituents.

These levulinates were used in the development of this thesis: methyl levulinate, ethyl levulinate, *n*-butyl levulinate, *n*-propyl levulinate and *n*-pentyl levulinate. Some of their properties are summarized in Table 1-3. The properties of each alkyl levulinate mainly differ by the length of their alkyl substituent. Shorter substituent chain levulinates are more accessible due to the availability of short-chain alcohols produced from LCB processing; as such, the properties of shorter substituent AL have been further evaluated in the literature. Short-chain alcohols, lower than six carbons, can be obtained from the catalytic reforming of CO₂ with hydrogen, in the case of methanol, and by fermentation processes from LCB derivatives, especially sugars, for up to 5 carbon alcohols (Birgen et al., 2019). This work focuses on the hydrogenation of *n*-alkyl substituents for levulinates, however, other substituent levulinates would be possible to obtain such as the case of branched alkyl levulinates (i.e., iso-propyl levulinate, sec-butyl levulinate) or aromatic levulinates, (i.e., benzyl levulinate).

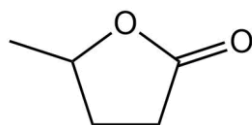
Table 1-3 - Physical properties of alkyl levulinates studied (*N*-Amyl Levulinate | C₁₀H₁₈O₃ | ChemSpider, n.d.; PubChem, n.d.; Registration Dossier - ECHA, n.d.)

Commercial name	Methyl Levulinate	Ethyl Levulinate	Propyl Levulinate	Butyl Levulinate	Pentyl Levulinate
IUPAC Name	methyl 4-oxopentanoate	ethyl 4-oxopentanoate	<i>n</i> -propyl 4-oxopentanoate	<i>n</i> -butyl 4-oxopentanoate	<i>n</i> -pentyl 4-oxopentanoate
Molecular Formula	C ₆ H ₁₀ O ₃	C ₇ H ₁₂ O ₃	C ₈ H ₁₄ O ₃	C ₉ H ₁₆ O ₃	C ₁₀ H ₁₈ O ₃
CAS #	624-45-3	539-88-8	645-67-0	2052-15-5	20279-49-6

Molecular weight (g/mol)	130.14	144.17	158.20	172.22	186.25
Physical description	Colorless liquid; Mild caramelly aroma	colorless to pale yellow liquid with apple odor	colorless transparent liquid with a sweet caramelly odor	colorless or straw-colored liquid	colorless or straw-colored liquid
Boiling point at 760 mmHg (°C)	193-195	205.85	220 - 221	237.50	265 - 268
Melting point at 760 mmHg (°C)	-24	-60	-	-	-
Solubility in water (mg/L @ 25 °C)	1.186e+005	4.566e+004	1.508e+004	4.940e+003	1.61E+003
Vapor pressure at 25°C (mmHg)	0.408	0.2490	0.1100	0.038	0.0305
Relative density to water	1.049 - 1.055	1.009 - 1.014	0.989 - 0.995	0.967 - 0.977	0.959

An interesting molecule obtained from alkyl levulinates is γ -valerolactone (GVL), which can be obtained mainly by the hydrogenation of alkyl levulinates or angelica lactones. GVL possesses many uses and interesting properties which are discussed in the next section.

1.7. Gamma-valerolactone: a green platform molecule



gamma valerolactone

Figure 1-9 - Structure of γ -valerolactone

Gamma valerolactone (GVL), γ -valerolactone, belongs to the family of lactones, cyclic esters that can be formed by the internal esterification of hydroxy acids (Bruice, 2010). It is a bio-based platform molecule derived from renewable resources, such as plant materials or microorganisms and it can also be found in fruits. GVL is a clear, colorless liquid at standard conditions, 25°C and 1 atm pressure, with a pleasant, fruity odor. Some general physical properties of GVL are shown in Table 1-4.

GVL is considered a green platform molecule since it is obtained from renewable resources and has a reduced environmental footprint compared to standard petrochemical-based compounds.(Kerkel et al., 2021). Since GVL is biodegradable and has a low toxicity profile, it may be considered a safe and sustainable alternative.

Table 1-4 - Physical properties of γ -valerolactone (Alonso et al., 2013; Havasi et al., 2016; Kerkel et al., 2021)

Commercial name	Gamma Valerolactone
IUPAC Name	5-methyloxolan-2-one
Molecular Formula (g/mol)	C ₅ H ₈ O ₂
CAS #	108-29-2
Molecular weight	100.12
Physical description	colorless to a pale-yellow clear liquid
Boiling point at 760 mmHg (°C)	207 - 208
Melting point (°C)	-31
Flashpoint (°C)	96
Solubility in water	Soluble
Vapor pressure at 25°C (mmHg)	0.235
Relative density to water	1.047 - 1.054

GVL is miscible in water and does not form an azeotrope; as such, separation processes for a water-GVL mixture are viable by distillation (Havasi et al., 2016). Other separation methods have been observed. After a delignification process using GVL as a solvent, an organic/aqueous biphasic system is obtained, the inclusion of NaCl improved the migration of GVL from the aqueous phase into the organic phase, allowing for better separation of GVL from water (Tabasso et al., 2016). It has also been observed that water tends to open the lactone ring of GVL into 4-hydroxyvaleric acid (4-HVA) in highly acidic conditions, while in basic conditions, salts of 4-HVA are formed. (Wong et al., 2017)

1.8. GVL applications

GVL has several possible applications, such as a solvent, a chemical intermediary (platform molecule), a fuel additive, and as a component of personal care products and fragrances (Alonso et al., 2013; Shokri et al., 2022; K. Yan et al., 2015). These applications are shown below.

1.8.1. Solvent

Since GVL possesses different desirable properties, such as being liquid at a broad temperature range (-31 to 207 °C), having a high flash point (96°C), low toxicity, low vapor pressure, and being soluble in water, it can be used as a suitable solvent for different applications. For example, a binary mixture of GVL-water has been used to improve the solubilization of LCB derivatives, such as lignin and hemicellulose, Figure 1-10 (Shokri et al., 2022; Tabasso et al., 2016; Xue et al., 2016; Alonso et al., 2013; Di Menno Di Bucchianico et al., 2022), GVL has also been used for the solubilization of plastics in recycling processes (W. Chen et al., 2021), for the preparation of membranes (Rasool & Vankelecom, 2019), and as a cleaning agent in various paint and coating formulations as well as a solubilizer in cosmetics, pharmaceuticals, or agrochemicals (Kerkel et al., 2021).

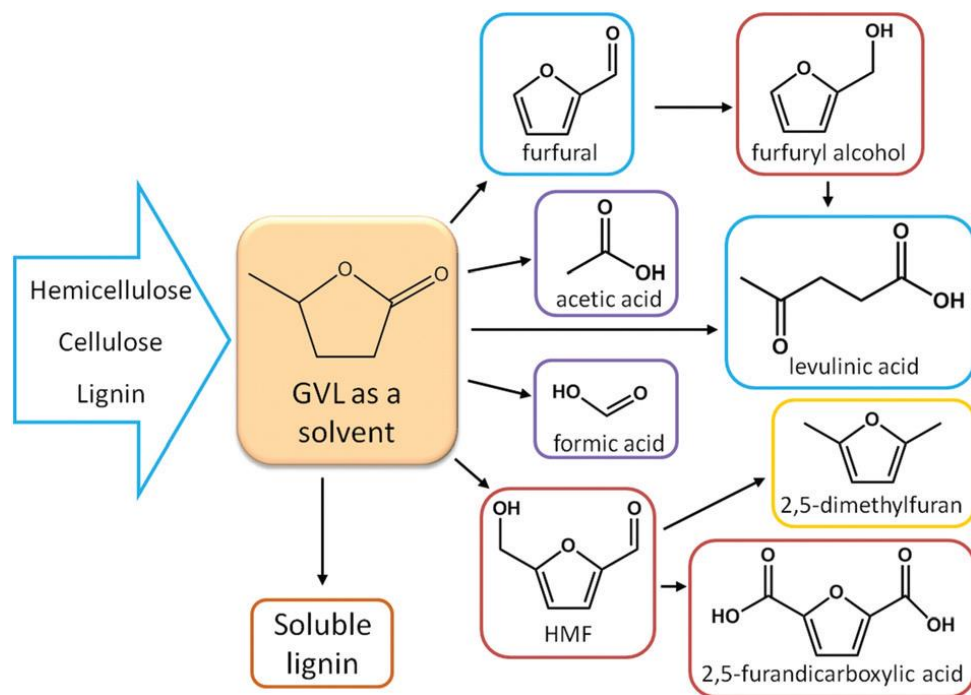


Figure 1-10 – Lignocellulosic biomass-derived products obtained using GVL as solvent. Reproduced from (Alonso et al., 2013) with permission from the Royal Society of Chemistry

1.8.2. Synthesis of chemical compounds

GVL can be used as a precursor for obtaining many interesting compounds, hence its consideration as a platform molecule. Being a lactone, GVL can undergo ring-opening reactions, such as nucleophilic addition. Figure 1-11 and Figure 1-12 display the main compounds obtained from GVL (Alonso et al., 2013; Chalid et al., 2012; Isikgor & Becer, 2015). These compounds are used in the production of polymers or used as fuel additives.

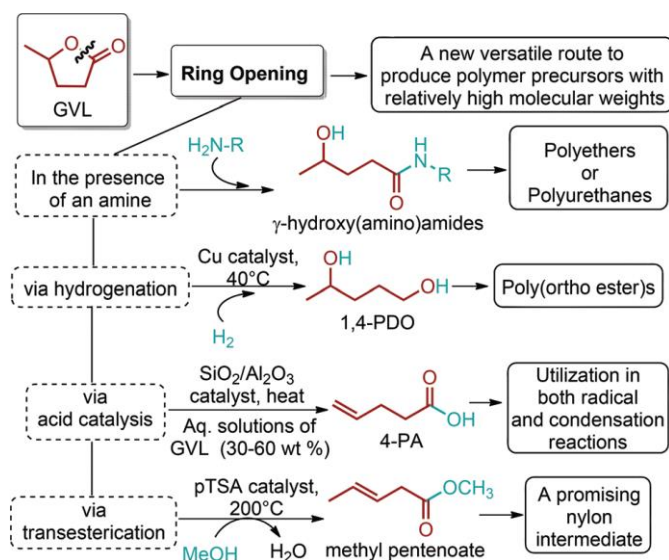


Figure 1-11 - Ring opening of GVL as a new versatile route to produce polymer precursors. Reproduced from (Isikgor & Becer, 2015) with permission from the Royal Society of Chemistry.

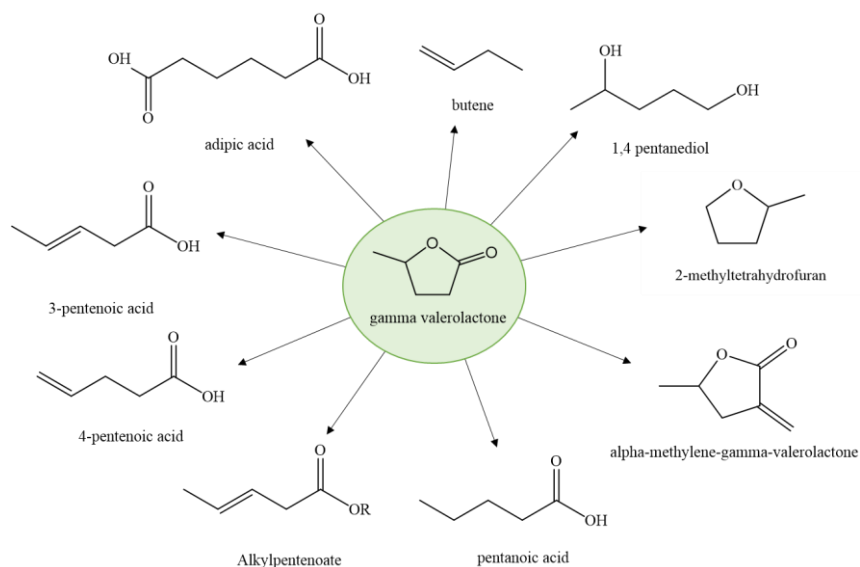


Figure 1-12 – Representation of the leading products obtained from GVL. Synthesized from (Alonso et al., 2013; Chalid et al., 2012; Isikgor & Becer, 2015)

1.8.3. Fuel additive

The use of GVL in a mixture of diesel and biodiesel has been found to reduce CO emissions and smoke production in diesel motors Figure 1-13. (Bereczky et al., 2014). Nevertheless, GVL is poorly soluble in long-chained acyclic hydrocarbons, limiting the dosage used in diesel mixtures. However, no solubilization difficulties have been observed for gasoline (Bereczky et al., 2014; Bruno et al., 2010; Falcchi Corrêa et al., 2019).

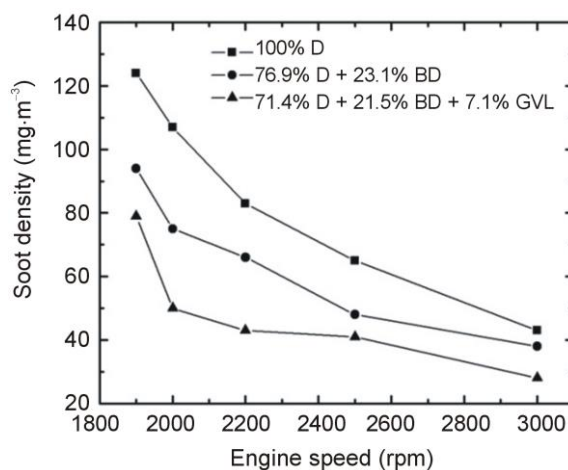


Figure 1-13 - Emitted smoke concentration at full load as a function of engine speed. (Bereczky et al., 2014) Public licence CCCN 4.0

1.9. Production methods

In the production of GVL from LCB, GVL has been mainly obtained via the hydrogenation of levulinic acid and alkyl levulinates, as shown in Figure 1-14. Although Figure 1-14 shows the main pathway to obtain GVL from LCB, the reaction pathway from AL or LA produces different intermediates which must be taken into account, such as angelica lactones and pseudo-levulinic acid. (A. Kumar et al., 2020; Tabanelli et al., 2019).

GVL can also be synthesized from other non-bio-sourced, and bio-sourced molecules e.g. through the hydroalkoxylation or intramolecular additions of carboxylic acids with unsaturated hydrocarbons Figure 1-15 (C.-G. Yang et al., 2005; Zhou et al., 2007), oxidative cyclization of diols (Jung et al., 2002), or by reduction of oxiranes using methyl metal compounds, Figure 1-16 (Mitani et al., 1990). However, these reactions require certain conditions, costly special

catalysts, or other complex molecules to obtain GVL, which would present more challenges than the LCB route shown in Figure 1-14.

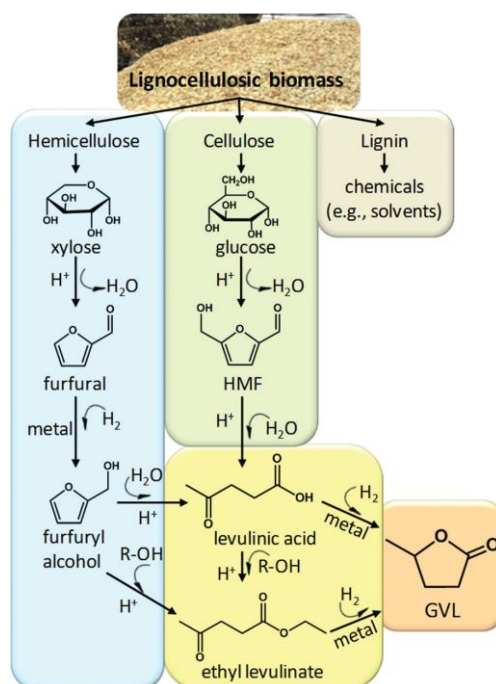


Figure 1-14 - Fractionation of lignocellulosic biomass and reaction pathways to produce GVL from hemicellulose and cellulose. Reproduced from (Alonso et al., 2013) with permission from the Royal Society of Chemistry

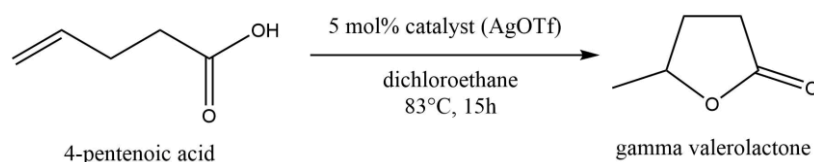


Figure 1-15 - Intramolecular Hydroalkoxylation of olefins. Reprinted with permission from (C.-G. Yang et al., 2005). Copyright 2005, American Chemical Society.

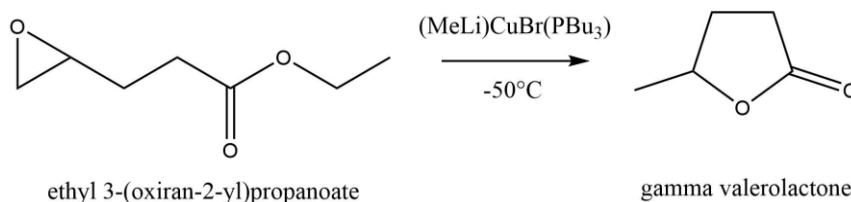


Figure 1-16 – Reaction of epoxide with (MeLi)CuBr(PBu₃) complex. Adapted with permission from (Mitani et al., 1990), Copyright 1990, American Chemical Society.

1.10. Reaction pathways

The estimated reaction pathways for the production of GVL from LA are shown in Figure 1-17, where two reaction pathways are viable with two reaction steps, hydrogenation and cyclization/lactonization. These pathways differ by the order in which hydrogenation or cyclization steps take place. The precursors for GVL can be 4-hydroxyvaleric acid (4-HVA) or the α - β angelica lactones (Putrakumar et al., 2015). These reaction pathways are also equivalent and applicable to alkyl levulinates. Depending on the reaction conditions, such as acidity and the presence of specific catalysts, one of these reaction paths would be performed faster.

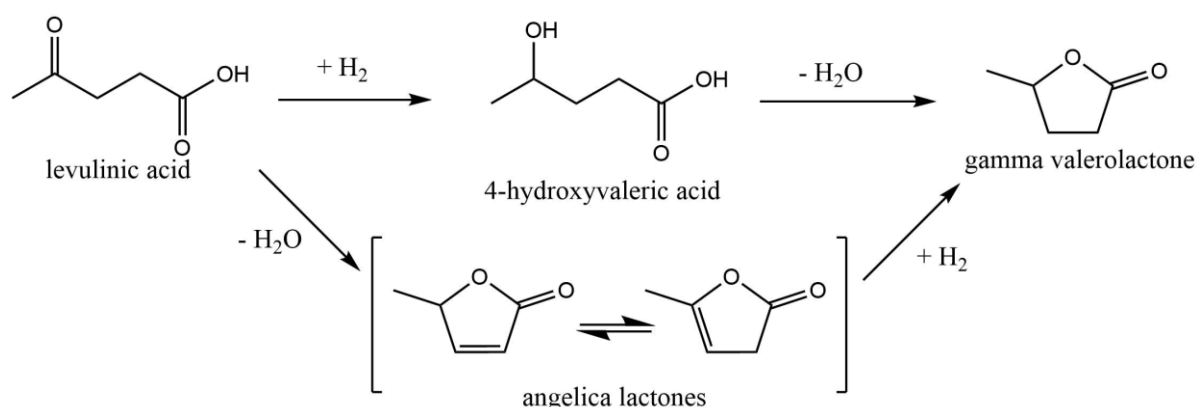


Figure 1-17 - Reaction scheme: Reaction pathway of hydrogenation of LA to GVL Reprinted from (Putrakumar et al., 2015) with permission from Elsevier.

1.10.1. Hydrogenation

This reaction step can be performed in liquid or vapor phases with the help of different catalysts. Based on the source of hydrogen, three methods have been described in the literature: hydrogenation by molecular hydrogen, catalytic transfer hydrogenation (CTH), and hydrogenation by in situ generation of hydrogen.

Catalytic transfer hydrogenation (CTH)

Catalytic transfer hydrogenation is thought to be based on the Meerwein-Schmidt-Ponndorf-Verley (MSPV) reduction of carbonyl groups into alcohols (Polshettiwar & Varma, 2009). In this mechanism, an alcohol group-containing molecule is oxidated by “donating” hydrogen to the carbonyl group. Figure 1-18.

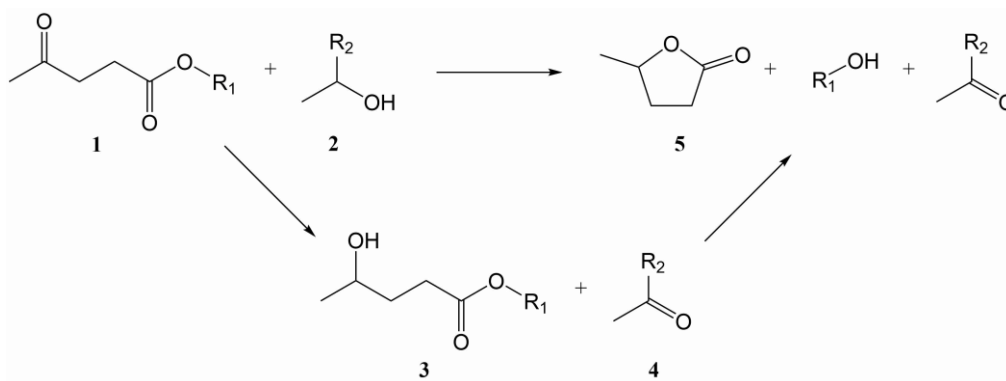


Figure 1-18 - Catalytic transfer hydrogenation of levulinic acid (1, R₁ = H) and its esters (1, R₁ = C_xH_{2x+1}) to γ -valerolactone (5) using a secondary alcohol as the hydrogen donor (2, R₂ = C_yH_{2x+1}). Used with permission of Royal Society of Chemistry, from (Chia & Dumesic, 2011), permission conveyed through Copyright Clearance Center, Inc.

Secondary alcohols have been more often used as hydrogen donors compared to primary alcohols, with which low selectivities have been observed (Chia & Dumesic, 2011). Other LCB-derived molecules have also been used as hydrogen donors, such as hydroxy-ethyl-furan, glyceraldehyde and ethyl lactate. (Assary et al., 2013).

In situ hydrogen production

Another hydrogen source is in situ hydrogen production. The decarboxylation of formic acid (FA) into molecular hydrogen and carbon dioxide, known as dehydrogenation (He & Li, 2016) is a good example of this method. Differently from transfer hydrogenation, the decomposition of formic acid releases molecular hydrogen that would be available for the hydrogenation reaction as seen in Figure 1-19. This reaction can be performed with the use of noble metal catalysts such as Pt and Pd. (Feng et al., 2018).

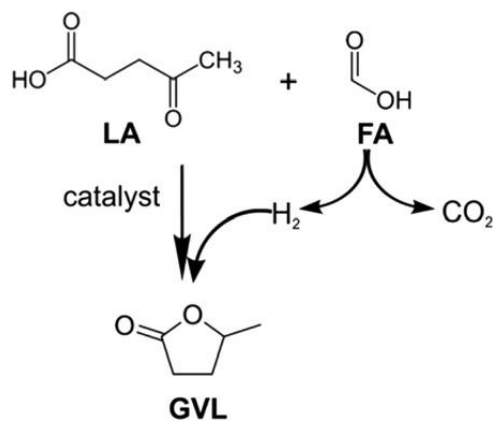


Figure 1-19 – γ -valerolactone production from levulinic acid with formic acid as a hydrogen source. Used with permission of Royal Society of Chemistry from (Ruppert et al., 2016); permission conveyed through Copyright Clearance Center, Inc.

However, FA decomposition can also undergo dehydration producing CO and water, Figure 1-20. The selectivity to dehydration or decarboxylation is highly influenced by the operating conditions and the solvent used. (Chauhan et al., 2022; Goddard et al., 1992; He & Li, 2016). Catalyst poisoning by CO has been observed with this method, where the CO molecule binds strongly onto the active surface of the catalyst, limiting the available sites for the hydrogenation reaction Figure 1-21 (Assary et al., 2013; Dey & Dhal, 2020; Ruppert et al., 2016; S. Xu et al., 2020).

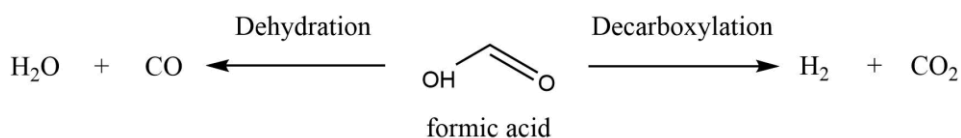


Figure 1-20 - Decomposition reactions for formic acid. Reproduced from (Goddard et al., 1992), with the permission of AIP Publishing.

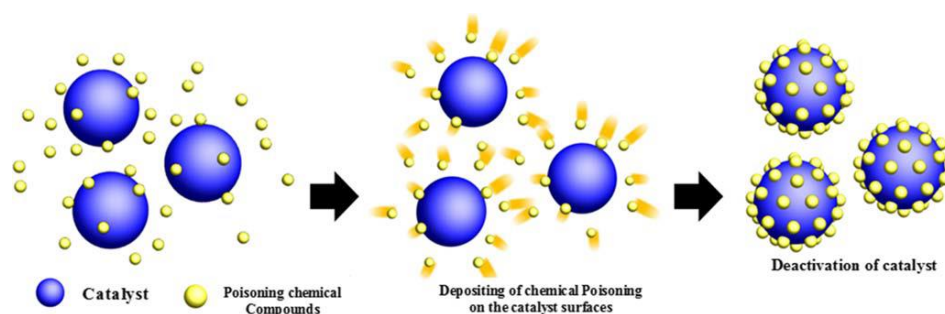


Figure 1-21 – Graphic representation of deactivation of rhodium and ruthenium catalysts by contacting with poisoning compounds. Reproduced from (Dey & Dhal, 2020) with permission from Springer

The use of high-temperature water (HTW) has also been found to enable the hydrogenation of levulinic acid. This method relies on a surface reaction with Zinc reducing water generating molecular hydrogen and ZnO in batch conditions. This hydrogen is then available to perform the hydrogenation reaction obtaining 4-HVA (Zhong et al., 2017).

Molecular hydrogen (H_2)

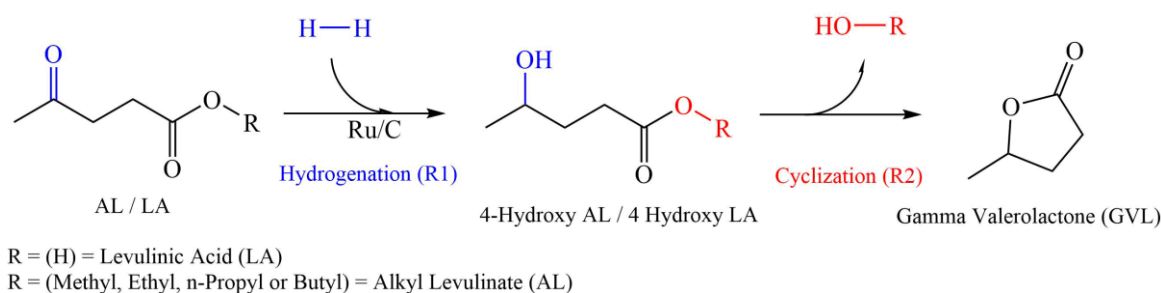


Figure 1-22 - Production of GVL by hydrogenation of alkyl levulinate and levulinic acid with molecular hydrogen.

Molecular hydrogen has been used as a source for hydrogenation reactions. In the literature, several references have used this source for the hydrogenation of levulinic acid and its esters (Abdelrahman et al., 2014; Bonrath et al., 2016; Kasar et al., 2019). Molecular hydrogen can be obtained from fossil-based sources such as steam reforming of natural gas and coal gasification, but it can also be obtained from non-fossil-based sources such as water electrolysis and biomass conversion (R. Kumar et al., 2022; Registration Dossier - ECHA, n.d.). The use of this hydrogen source requires high pressures to increase the availability of this

reagent in the bulk of the reaction media and, in some cases, the adsorption on heterogeneous catalyst surfaces.

Each hydrogen source has different advantages and disadvantages. Transfer hydrogenation avoids using high pressures, but costly separation methods are required downstream to remove the hydrogen donor's products. Formic acid decomposition can also produce CO, which needs to be considered for some catalytic systems as it can cause catalyst deactivation. Water as a hydrogen donor requires high-temperature conditions, over 200°C. Molecular hydrogen requires high pressures, for which safety measures need to be considered, but molecular hydrogen produced can be obtained from non-renewable sources.

1.10.2. Cyclization / Lactonization

Following the reaction paths in Figure 1-17, two paths of cyclization are possible. The cyclization or lactonization reaction is considered an internal Fischer esterification reaction. Here a hydroxyl group and a carboxylic/ester group within the molecule react forming the lactone. This reaction has been catalyzed by the presence of acidic conditions, as seen in Figure 1-23.

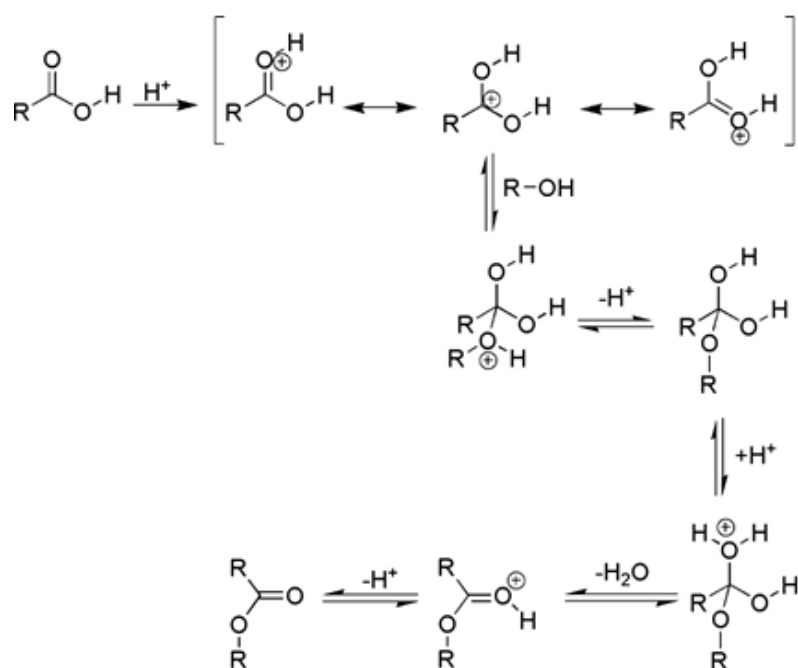


Figure 1-23 - Classic mechanism for acid-catalyzed Fischer esterification. Reprinted from (Vafaezadeh & Fattahi, 2015) with permission of Elsevier.

In this case, γ -valerolactone can be obtained from the intermediates produced in the hydrogenation step, hydroxy alkyl levulinates or 4-hydroxyvaleric acid. Alkyl alcohol or water are byproducts obtained for each intermediate. This is a reaction known as dehydration, for 4-hydroxyvaleric acid, and de-alcoholization in the case of hydroxy alkyl levulinates.

Enol Cyclization

The ketone group in levulinic acid and its esters can undergo isomerization. The ketone group rearranges into a carbon-carbon double bond and a hydroxyl group, to form a structure known as an enol (Figure 1-24) (Bruice, 2010). This isomerization allows the cyclization reaction due to the presence of hydroxy group and the ester/carboxylic groups.

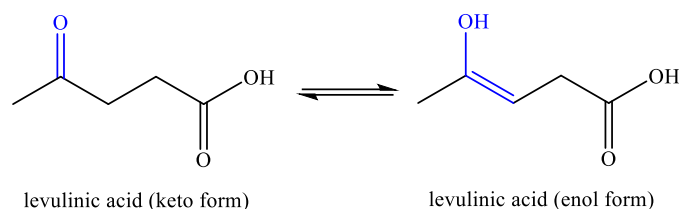


Figure 1-24 - Levulinic acid keto and enol forms. Representation made from (Bruice, 2010)

Both, keto and enol forms, can coexist in a mixture. Nevertheless, the ratio of enol-keto form present is influenced on the structure of the molecule and the acid/base conditions of the solution. Commonly, the keto form would be more stable for aliphatic compounds and enols form would be more predominant for aromatic compounds (Bruice, 2010). Once the enol form is present, a dehydration/dealcoholizing reaction would be plausible where α -angelica lactone and water or alcohol are obtained (Lomate et al., 2018).

1.11. Catalysis

In general, catalysis is the process by which a material called a catalyst accelerates a chemical reaction without being consumed. As catalysts operate by giving an alternate pathway for the reaction to occur which requires a lower activation energy, so the reaction is faster. Catalysts can be classified by their physical structure, such as the physical state of matter, solid, liquid, and gaseous and their miscibility in the reaction media, such as homogeneous (one phase with the reaction media) or heterogeneous (different phases with the reaction media).

The kinetics in homogeneous catalytic systems is faster compared to heterogeneous systems due to mass transfer limitations but the use of homogeneous catalysts requires costly separation operations after production. As such, the use of heterogeneous catalysts has been preferred over homogeneous systems. Within this thesis, heterogeneous catalysts will be considered as catalytically active material dispersed on a solid support.

As catalysts directly influence the reaction pathway, operational conditions, conversion, and selectivity, the choice of catalyst is quite important. In the literature, several catalysts have been explored for the obtention of GVL from levulinic acid and alkyl levulinates, focusing more on the hydrogenation reaction step.

1.11.1. Noble metals

The use of noble metals as catalytically active surfaces on different supports has been greatly explored in the literature. Noble metals such as Au, Pt, Pd, Rh, Ir, Re, Ag and Ru have shown good reactivity in hydrogenation reactions, however, selectivity and conversion vary among the studied metals (Abdelrahman et al., 2014; Alonso et al., 2013; Bonrath et al., 2016; B. Chen et al., 2018; Dutta et al., 2019; Feng et al., 2018; Li et al., 2017; Lomate et al., 2018; Luo et al., 2013; Tabanelli et al., 2019; Tan et al., 2016). For example, the use of Pt has been observed to produce 1,4 pentanediol, a product obtained from the hydrogenation of GVL (Mizugaki et al., 2015). Some relevant noble metal catalytic systems used in alkyl levulinates and levulinic acid hydrogenation, summarized by R. Xu et al, are displayed in Table 1-5.

Table 1-5 - Preparation of GVL catalyzed by noble metal catalysts. Used with permission of WILEY - VCH VERLAG GMBH & CO. KGAA, from (R. Xu et al., 2020) permission conveyed through Copyright Clearance Center, Inc.

Catalyst	Substrate	Solvent	H ₂ sources	T [°C]	t [h]	Yield GVL [%]	Ref.
5% Ru/ZrO ₂ + Al ₂ (SO ₄) ₃	Cellulose	2-Propanol	–	180	1.2	51.2	(Huang et al., 2018)
5% Ru/C	Ethyl levulinate	H ₂ O	10 MPa H ₂	100	3.6	52.6	(Tukacs et al., 2019)

CNT-Ru-1	Ethyl levulinate	methanol	3 MPa H ₂	60	6	93	(Shen et al., 2019)
ZSM+Au/ZrO ₂	furfural	2-Propanol	–	120	24	77.5	(Zhu et al., 2016)
Au/ZrO ₂ +ZSM-5	furfural	2-Propanol	–	120	30	80.4	
5% Ru/C	LA	triethylamine	formic acid	160	3	80.75	(Feng et al., 2018)
Ru/TiO ₂	LA	dioxane	4.5 MPa H ₂	150	4	96	(Piskun et al., 2018)
2% Ru/TiO ₂	LA	H ₂ O	4 MPa H ₂	130	0.5	99.9	(Tan et al., 2015)
1% Ru-Pd/TiO ₂	LA	dioxane	4 MPa H ₂	200	0.5	99	(Luo et al., 2015)
Ru/HAP	LA	H ₂ O	–	275	48	88.8	(Sudhakar et al., 2016)
r-Ru-NH ₂ - γ -Al ₂ O ₃	LA	H ₂ O	4 MPa H ₂	25	13	99.1	(Tan et al., 2016)
Ru-NHC complexes	LA	H ₂ O	1.2 MPa H ₂	130	2.7	96	(Tay et al., 2016)
Ru/OMS	LA	–	3 MPa H ₂	100	1	99.8	(Molleti et al., 2018)
Ru/FLG	LA	H ₂ O	4 MPa H ₂	25	12	99.7	(Xiao et al., 2016)
Ru-Ni/Meso-C	LA	–	4.5 MPa H ₂	150	2	96	(Y. Yang et al., 2014)
AgPd g-C ₃ N ₄	LA	H ₂ O	formic acid	50	12	98	(Verma et al., 2016)
Au-Pd/TiO ₂	LA	dioxane	4 MPa H ₂	200	5	97.5	(Luo et al., 2015)
Pd@UiO-66-NH ₂	LA	H ₂ O	2 MPa H ₂	140	2	98.2	(Feng et al., 2020)

5% Pd/AlMCM-41	LA	octane	6 MPa H ₂	240	10	88.5	(A. Wang et al., 2018)
Pd/MCM-41	LA	H ₂ O	6 MPa H ₂	240	10	96.3	(K. Yan et al., 2014)
H ₂ SO ₄ +Shvo catalyst	LA	–	formic acid	100	2	55	(Qi & Horváth, 2012)

1.11.2. Non-noble metals

The use of non-noble metals has been noticeable in the production of GVL from levulinic acid and alkyl levulinates. In the literature, several researchers have focused on the use of non-noble metals in the catalytic transfer hydrogenation from secondary alcohols. Common non noble catalysts are Ni, Cu, Fe, Co, Zr and Sn where good selectivities and conversions were observed. (Dutta et al., 2019; R. Xu et al., 2020).

Among the different noble metals, Ru has been observed to present a better catalytic effect, presenting a higher selectivity to GVL (Hsiao et al., 2021). From the non-noble metals, Fe/Ni have shown better conversions for this reactive system. Although the use of non-noble catalytic systems is preferred for the lower cost for production, the catalytic effect of these non-noble catalysts is much lower, requiring a higher mass of catalyst per reactive media and the requirements to reduce catalysts beforehand. For the estimation of the kinetics in the production of GVL from levulinic acid and alkyl levulinates, the use of a commercially available Ru catalyst was chosen.

1.12. Mathematical modeling

In the development of mass balances and kinetic equations that would describe the reaction system, high-order differential equations are commonly present. The differential order of these equations is directly linked to the complexity of the reaction system estimated, considerations such as reactions involved, reversibility, reaction mechanisms or mass and thermal transfer. In addition, these equations possess crucial parameters, such as activation energy or rate constants, that can be difficult to determine.

A kinetic model can be considered as the ensemble of equations and parameters used to describe the reaction mechanism of a reaction system. To solve these equations and determine these parameters, different mathematical approaches are needed. Computational software is used for this task. The structure of the kinetic models can lead to a high correlation between some parameters which can lead to uncertainties, which can be assessed by the use of probability determination methods.

1.12.1. Bayesian inference

An interesting method to evaluate parameter reliability for kinetic models and to evaluate the probability of the obtained values is Bayesian inference. Bayesian inference is based on an a priori estimation of parameters, estimating a likelihood or probability distribution that the model would predict such value at different conditions and later estimating the posterior probability to infer an updated value of the parameter. Bayes theorem can be seen in equation (1), (Matera et al., 2019).

$$P(\theta|D) = \frac{P(D|\theta) \cdot P(\theta)}{P(D)} \quad (1)$$

“Where D represents the observed data (typically a vector of dimensionality > 1), and θ represents a vector of all the parameters that would be required to simulate the data (e.g., activation energies, preexponential factors, adsorbate interaction terms, etc.)”. (Matera et al., 2019)

1.13. Objectives

Based on an extensive literature study, the production of GVL has been studied in a broad range of experimental conditions. levulinic acid being the most common substrate (Alonso et al., 2013; Hengst et al., 2015; Kluson & Cervený, 1995; Zhou et al., 2007). The hydrogenation of different levulinates into GVL has not gained as much attention, even though there are very potential alternatives. The current thesis is focused on the production of GVL by the hydrogenation of different levulinates with emphasis on the following aspects:

- Study of the kinetics of isothermal hydrogenation of butyl levulinate: Use of Bayesian inference and the effect of levulinic acid on reaction mixture and the effect of a dual catalyst system.
- Calorimetric study of alkyl levulinates hydrogenation: Method development and correlation between enthalpy and chain length.

In Chapter 3 - , a Bayesian inference approach was used to evaluate and compare different kinetic model expressions for producing GVL by hydrogenation of BL under isothermal conditions. Given that the overall reaction proceeds in two consecutive steps, hydrogenation, and cyclization, the evaluation for both reaction steps was considered (Y. Wang et al., 2018). Isothermal experiments were carried out in a Parr batch reactor by taking samples to follow the concentration profiles of the reagents and products as a function of time. The model fitting and kinetic parameters estimation for each kinetic model was performed with Athena Visual Studio.

In Chapter 4 - , we evaluate different kinetic models for BL hydrogenation in the presence of LA and an acidic catalyst. These experiments investigated the effect of LA concentration on BL hydrogenation and cyclization kinetics (Capecchi, Wang, Delgado, et al., 2021). The experiments were performed in an isothermal mode with a Parr batch reactor and samples were taken to observe the concentration profiles of reagents, intermediates, and products as a function of time. Athena Visual Studio was used to estimate the kinetic parameters, model fitting and simulations. Finally, a cross-validation method, K fold, was used to estimate the predictive power of the models by making a regression from several experiments and using it to predict experimental data.

In Chapter 5 - , we focused on determining reaction enthalpies for different alkyl levulinates and levulinic acid to observe the possible effect of the substituent chain length on these properties. The isothermal hydrogenation of levulinic acid (LA), methyl levulinate (ML), ethyl levulinate (EL), n-propyl levulinate (n-PrL), and n-butyl levulinate (n-BL) to produce GVL was performed in a 1.6 L calorimeter, Mettler Toledo RC1Mx. Here the overall energy released in the reaction system was observed. Since the second reaction step also occurs in the RC1Mx calorimeter, a micro-calorimeter, Setaram C80 Tian-Calvet, was used to measure the heat flow on the cyclization reaction. The reaction enthalpies can be obtained by observing the change in concentrations and the heat flows in the calorimeters.

Chapter 2 - Materials and Equipments

2.1. Materials

Table 2-1 shows the reagents and materials used for analytical identification and experiments. Most were obtained from different providers and used without further purification. Other chemicals were synthesized.

Table 2-1 - Materials bought for analysis and experiments.

Material	Purity	CAS #	Provider
Hydrogen gas (H_2)	99.99% v/v	1333-74-0	Linde
γ valerolactone (GVL)	99% wt	108-29-2	Sigma Aldrich
Levulinic acid (LA)	99% wt	123-76-2	Acros Organics
Methyl levulinate (ML)	99% wt	624-45-3	Sigma-Aldrich
Ethyl levulinate (EL)	99% wt	539-88-8	Sigma-Aldrich
n-Propyl levulinate (PrL) ^c	95% wt	645-67-0	Sigma-Aldrich
n-Butyl levulinate (BL)	98% wt	2052-15-5	Alfa-Aesar
Methanol (MeOH)	99% wt	67-56-1	Fischer Scientific
Ethanol (EtOH)	99% wt	64-17-5	Carlo Erba
1-Propanol (PrOH)	99% wt	71-23-8	Carlo Erba
1-Butanol (BuOH)	99% wt	71-36-3	Lab Line
1-Pentanol (PeOH)	99% wt	71-41-0	Carlo Erba
Acetone	99% wt	67-64-1	Carlo Erba
Furfural	99% wt	98-01-1	Sigma Aldrich
*Ru/C ^a	5% Ru	7440-18-8	Alfa-Aesar
*Amberlite IR-120 ^b	-	67-64-1	Acros Organics

* Catalyst

^a Powder, reduced, 50% nominally wet

^b Ion-exchange resin, H-Form

^c Sample bought for analysis.

Some intermediates used were obtained from experiments since they were not stable: methyl 4-hydroxy pentanoate (MHP), ethyl 4-hydroxy pentanoate (EHP), n-propyl 4-hydroxy pentanoate (PrHP), n-butyl 4-hydroxy pentanoate (BHP), n-pentyl hydroxy pentanoate (PeHP). According to Melchiorre et al, longer chain alkyl levulinates can be obtained from the transesterification of methyl levulinate in the presence of acidic catalysts, as such, propyl levulinate and pentyl levulinate were obtained by this method (Melchiorre et al., 2020)

2.2. Equipment

2.2.1. Kinetic experiments

Parr Autoclave

A high-pressure 300 mL autoclave reactor from Parr was used in the experiments. To regulate temperature, the reactor was equipped with an electric heating jacket and an internal water-cooling coil. A gas entrainment stirrer was used to improve the gas dispersion in the liquid phase. A PI-controller was used to regulate the temperature and stirring conditions. A schematic representation of the experimental setup is displayed in Figure 2-1.

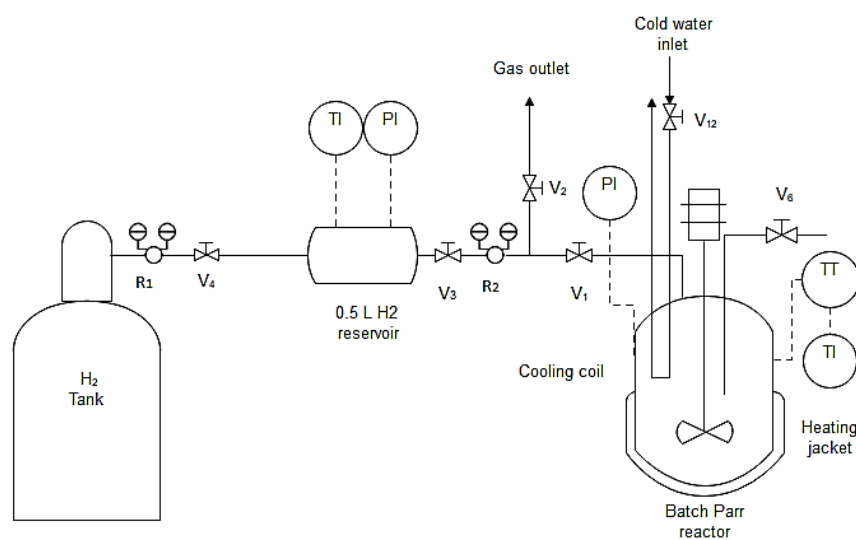


Figure 2-1 – Scheme of the experimental setup for kinetic experiments by autoclave. (Capecci, Wang, Delgado, et al., 2021)

2.2.2. Calorimetry

Mettler Toledo RC1Mx Calorimeter

The Mettler Toledo RC1mx reactor has a split heating and cooling loop, allowing it to regulate the temperature of the reaction media quickly. An external cooling system is attached to the calorimeter. The calorimeter was coupled with a HP100-SS reactor, a Hastelloy C22 metal vessel with 1500mL capacity and 100 bar pressure tolerance, an overhead gassing stirrer (internal diameter: 46mm), a temperature sensor and a calibration heater in direct contact with the reaction media.(*Figure 2-2*). Calibration of the reactor is performed by inducing a known amount of energy via a heating rod to estimate the transfer coefficient between the reaction media and the heating fluid.

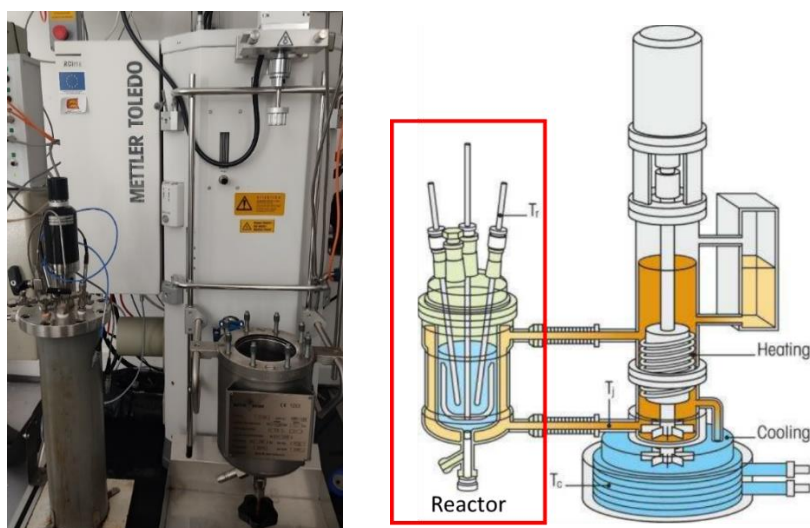


Figure 2-2 - Mettler Toledo RC1 Mx calorimeter. Picture of reactor (left) and schema of heating mechanism (right) from Mettler Toledo.

Tian Calvet – C80 calorimeter

The Tian Calvet microcalorimeter, shown in Figure 2-3, is used for the estimation of the cyclization reaction enthalpies. The equipment measures the heat signal by comparing the tension difference between two 12.5 mL cells, one with the reaction mixture and another as the reference. The reference cell must be filled with a mixture with similar thermodynamical properties but without chemical reactions. The equipment has a resolution of 0.10 μ W and a sensitivity of 30 μ V/mW. Hastelloy reversal mixing cells were used for all experiments due to their corrosion resistance Figure 2-4).

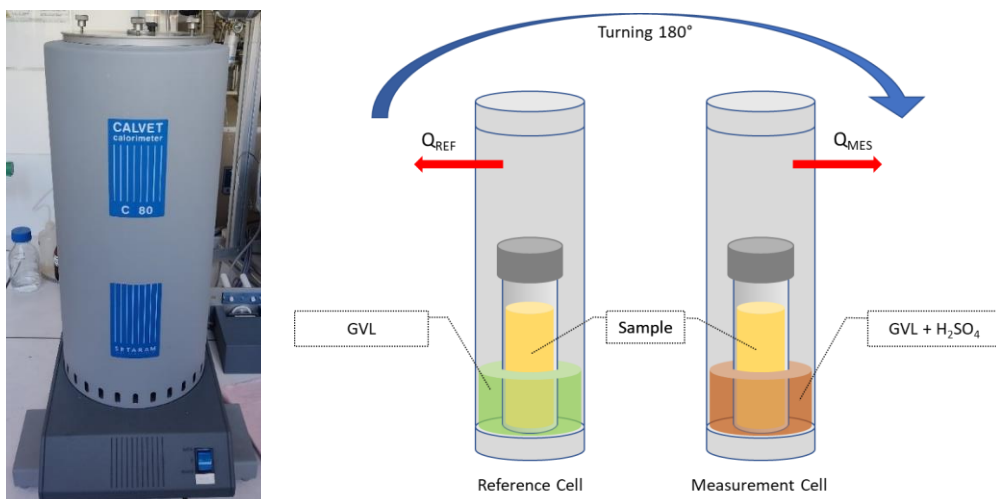


Figure 2-3 - Tian Calvet C80 micro-calorimeter. Picture (left) and schema for cells (right)

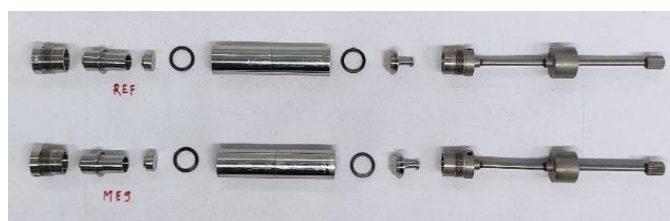


Figure 2-4 - Hastelloy reversal mixing cells in C80 microcalorimeter.

2.2.3. Transesterification

Batch Reactor

A 300 mL jacketed batch reactor coupled with a paddle agitator, thermocouple and a condenser were used for the transesterification reactions. Water was used as heat carrier in the jacket connected to a thermostat.



Figure 2-5 - Batch reactor used for transesterification reactions.

Rotavapor

An IKA RV 10 digital V-C rotavapor was used to separate the levulinates obtained in transesterification reactions from the remaining alcohols. A mineral oil, 47V100, was used as heating media to attain temperatures higher than water's boiling point.

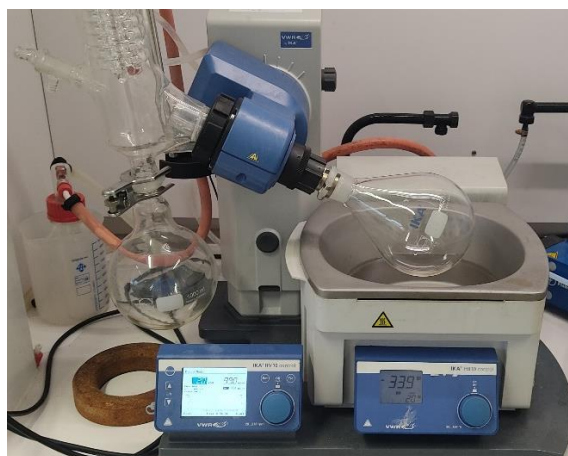


Figure 2-6 - IKA RV 10 digital rotavapor.

2.2.4. Analytical equipment

Gas chromatography – Flame Ionization Detector

Samples were analyzed by gas chromatography (GC) supplied by Scion Instruments. A Bruker Scion GC436 gas chromatography device. The GC was equipped with a flame ionization detector (FID) and a low polarity capillary column, ZB-5. This column is comprised by 95% dimethylpolysiloxane and 5% phenyl groups and is 30m in length, 0.32 mm in diameter, and has a 0.25 μm internal film coating. Helium (99.99%) was employed as the carrier gas, with a constant flow rate of 1.2 mL/min.



Figure 2-7 - GC FID used for experiments.

In Chapter 3 - , the injector and detector were both run at 270°C. The following sequence was used to set the oven temperature: 35°C (3 min) with 15°C min ramping to 300°C. The split ratio was 30:1, and the injection volume was 0.2 μL . Internal standards were set up using furfural, and acetone was used as a solvent to dilute the samples from the experiments. For experiments in Chapter 4 - , the injector and detector temperature were set to 250°C, the temperature ramp was of 50°C (2 min) – 20°C/min – 260°C, the injection volume, 1 μL and the split ratio 1:20 using acetone as solvent. For Chapter 5 - the injector and detector temperature were set to 250°C, the temperature ramp was 1 min (50°C) – 7,5 min (20°C.min⁻¹) – 1 min (200°C), and methanol was used as solvent to observe propanol peaks. Figure 2-8.

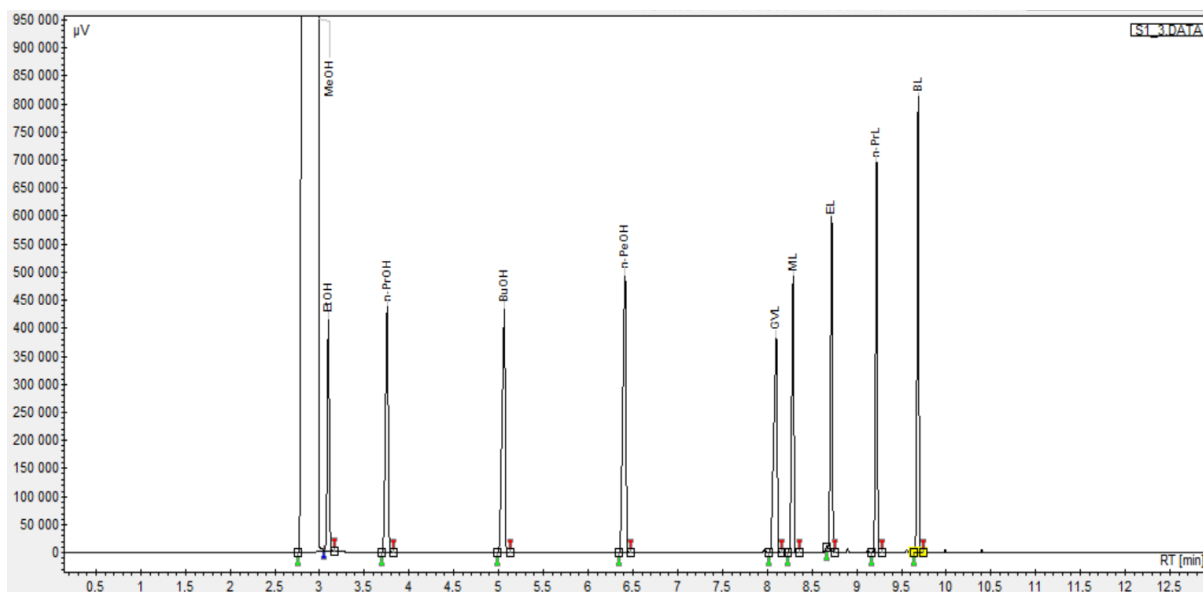


Figure 2-8 – Chromatogram on GC-FID with methanol as solvent. From left to right: methanol, ethanol, *n*-propanol, *n*-butanol, *n*-pentanol, γ -valerolactone, and alkyl levulinates (methyl, ethyl, *n*-propyl and *n*-butyl levulinate) studied.

Gas chromatography – Mass spectrometer

For chemicals synthesized in experiments, a gas chromatography coupled with mass spectrometer (GC-MS) method was employed. GC-MS Specs GC: System: (Perkin Elmer Clarus 580); Mass Spectrometer: (SQ8S); Column (Phenomenex ZB-5MS plus (Length: 30 m, internal diameter: 0,25 mm, internal coating width: 0,25 μ m composed of 95% Dimethylpolysiloxane and 5% Phenyl-Arylene); Carrier gas: He (99.99%), gas flow: 1 mL/min; Injector temperature: 250°C; Split Ratio: 1:20; Ramp: 50°C (1 min) – 10°C/min – 245°C (1 min); Source Temperature: 150°C, Transfer line temperature: 170°C; Ionization mode: EI 70eV; Identification method: Mode SCAN, with database NIST 03 from 40 to 600 m/z.

2.2.5. Catalyst characterization

Nitrogen Physisorption

The determination of the surface area for the Ru/C catalyst was performed in a Micrometrics 3Flex, shown in Figure 2-9 left. The equipment is used for microporous and mesoporous measurements and allows the measurement of three samples simultaneously. A Micromeritics VacPrep 061 Sample Degas System, Figure 2-9 right, was used for ex-situ pretreatment,

removing the adsorbed gases on the catalyst surface *in vacuo* at 180°C. Adsorption-desorption isotherms and pore volume distribution graphs are shown in Figure 2-10.

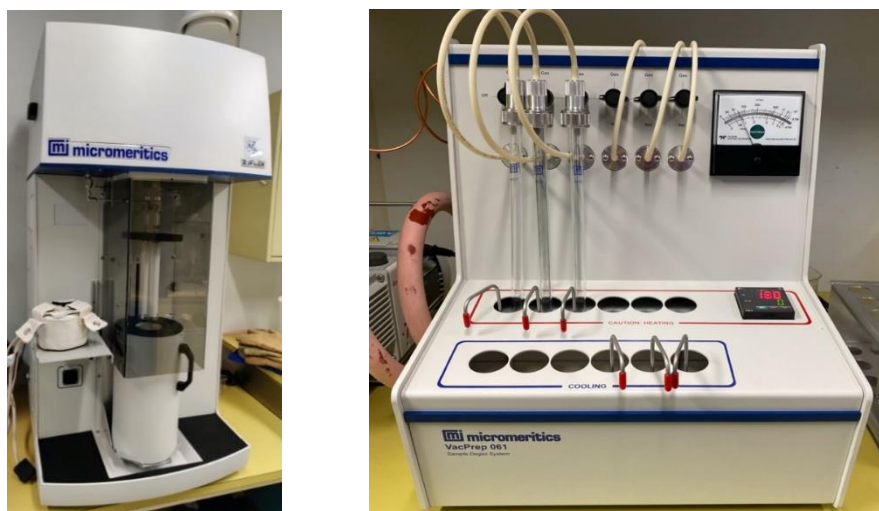


Figure 2-9 - Micromeritics 3 Flex used (left) and VacPrep 061 sample degasser system (right)

The determination of the surface area was performed where a surface area of 915 m²/g and a mean pore size radius of around 6.0 Å were obtained after 18 hours of measurement. Surface area (Dubinin), DFT pore size and micropore volume were obtained. These values are summarized on Table 2-2.

Table 2-2 - Surface area and pore size volume values of Ru/C catalyst

Textural Properties	5% Ru/C
BET Specific Surface Area (m ² /g)	952
Micropore Volume (cm ³ /g)	0.259
Mesopore Volume (cm ³ /g)	0.962
Main Pore Size (Å)	6.0

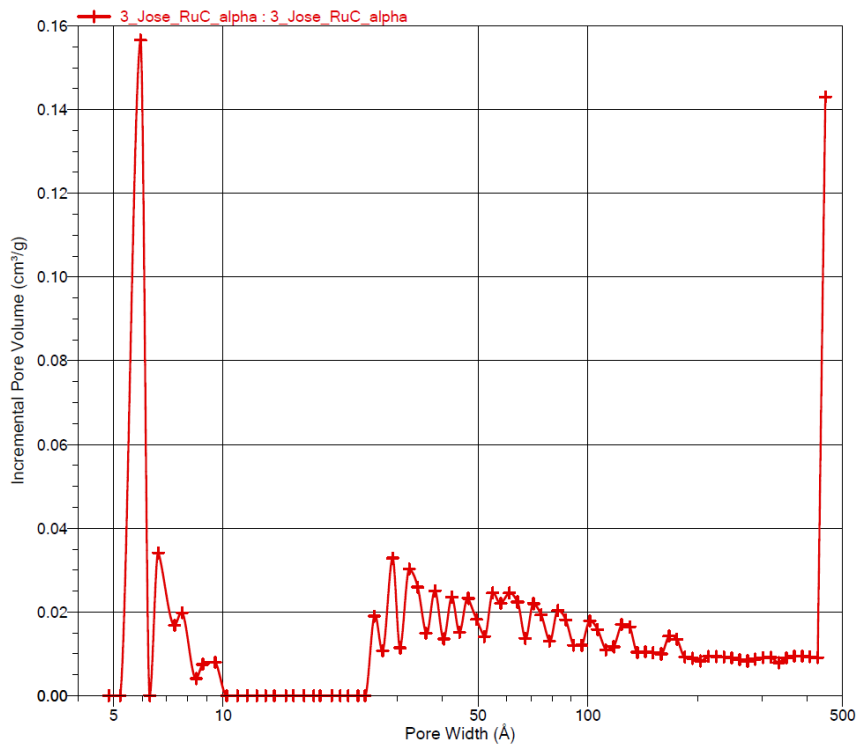
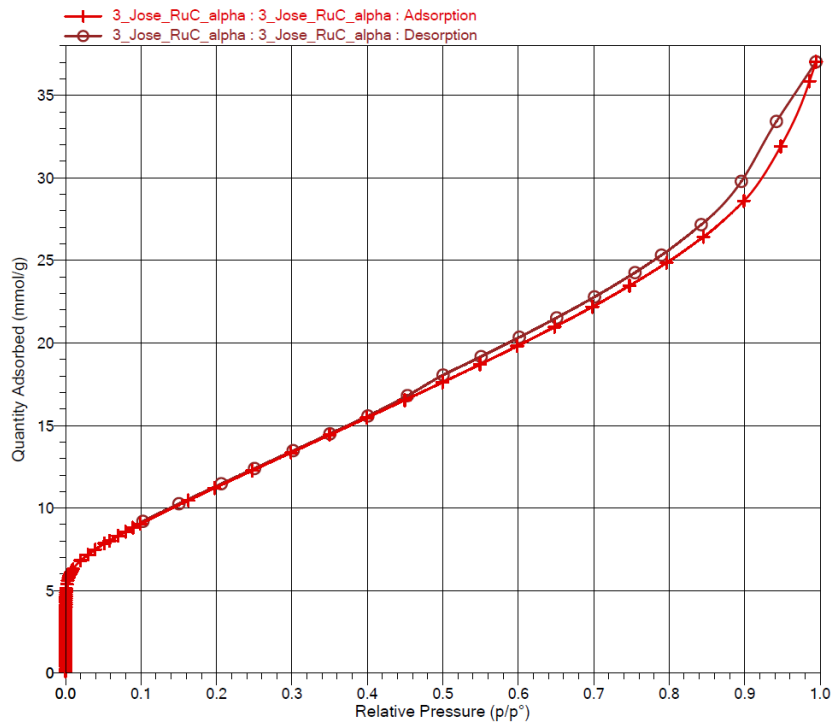


Figure 2-10 – Adsorption and Desorption isotherms (up) and DFT Pore size distribution (down) for Ru/C catalyst.

2.3. Reaction pathway

From the different possibilities observed for the hydrogenation and cyclization reactions, we have focused on the reaction system describing a molecular hydrogenation of alkyl levulinates or levulinic acid to obtain hydroxy valerates, followed by the cyclization reaction into the production of γ -valerolactone and the side products as shown in Figure 2-11. This reaction pathway is used over the cyclization of alkyl levulinates or levulinic acid into angelica lactones as the analytical results of the experiments performed showed no presence of angelica lactones.

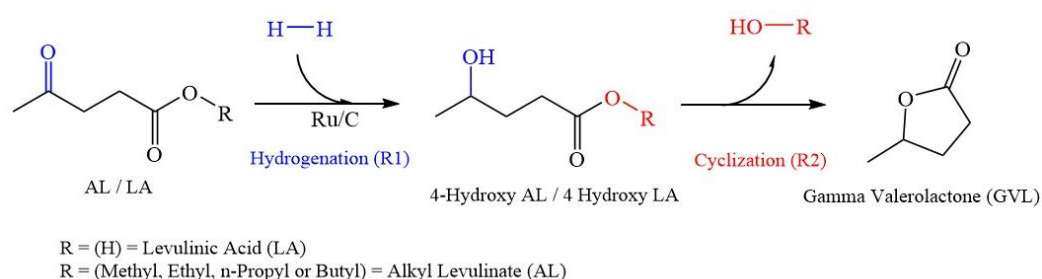


Figure 2-11 - Reaction scheme of Hydrogenation of alkyl levulinates into GVL

For the kinetic experiments, GVL was used as a solvent based on the fact that all reagents and products generated in the reactions were soluble in the mixture. In the work of Capecci et al, (Capecci, Wang, Casson Moreno, et al., 2021), the use of GVL as solvent provided better yields of GVL compared to using of butanol or pure reagent as solvents. For the calorimetric studies, GVL was also used as solvent when needed.

In the presence of a heterogeneous catalyst, the selectivity for the hydrogenation of the ketone group over the ester group is linked to different factors, such as the surface of the dispersed metal on the catalyst, the choice of metal, the support and operational conditions (Mäki-Arvela et al., 2005). Based on the intrinsic properties of the functional groups, the mesomeric effect (resonance) would support the ketone group to be more easily reduced than the ester group. The carboxylic oxygen in the ester group, increases the electrophilic property of the group. (Bruice, 2010)

An acidic environment is favorable for the cyclization reaction of the intermediates, as found in the literature. Here, the available protons attack the carboxylic group in the ester by protonation, thus creating a substituent able to react with the hydroxyl group by nucleophilic attack. The hydroxyl group is generated by the hydrogenation of the carbonyl group in the

hydrogenation step (Siengalewicz et al., 2014; Thompson & Wolfrom, 1957; Vafaezadeh & Fattahi, 2015). This is expected given that the lactonization/cyclization reaction is considered as an internal Fischer esterification. Authors such as Piskun and Brenna, have also observed that the presence of acidic environments improves the cyclization step. (Brenna et al., 2017; Piskun et al., 2016)

Chapter 3 - Bayesian statistic evaluation for kinetic models on butyl levulinate hydrogenation to γ -valerolactone

Part of this chapter is adapted from the post print of the following articles: J. Delgado et al., “Bayesian Statistics to Elucidate the Kinetics of γ -Valerolactone from n-Butyl Levulinate Hydrogenation over Ru/C.” *Industrial & Engineering Chemistry Research* 2021 60 (31), 11725-11736 DOI: 10.1021/acs.iecr.1c02107

Further permissions related to the material excerpted should be directed to ACS Publications. Copyright © 2020 American Chemical Society.

3.1. Introduction

The development and estimation of a kinetic model that is able to describe the generation of γ -valerolactone (GVL) from alkyl levulinates (AL) was explored in this chapter. The use of Power law relationships to describe the production of GVL has been reported in literature. The use of Bayesian inference to evaluate the different parameters in the modeling of the system is explored in this chapter. The aim is to predict the behavior of reaction kinetics, observe the different factors that affect the generation of GVL and optimize the experimental conditions .

GVL can be obtained from different sources and methods already explored in the Context of the study, here we focus on the production of GVL by direct hydrogenation of alkyl levulinates. The use of alkyl levulinates is preferred over to levulinic acid to avoid corrosion issues related to using high concentrations of levulinic acid. In the experimental section, butyl levulinate (BL) was chosen over other levulinates due to its high vapor pressure.

3.2. Experimental procedure

In each experiment, the reagents were introduced into the Parr reactor, Figure 2-1, and then it was tightly closed. A vacuum pump was used to remove the gases in the head of the reactor up until 50 mbars. Stirring was then set to 400 rpm and temperature was increased to the desired value. Once the temperature was reached, stirring was stopped for 2 minutes. Hydrogen was allowed into the reactor from a reservoir through a pressure regulator. Stirring was then set to 1000 rpm and samples were taken in pre-determined time intervals. The samples were filtered to remove the solid catalyst prior to the analysis.

An experimental matrix was followed to study systematically the effect of different parameters in the reaction system. Temperature, hydrostatic pressure, reagent concentration, and catalyst loading were varied in the experiments. To better observe the effect of temperature in the cyclization reaction step, a mixture of highly concentrated intermediate without solid catalyst was studied. The experimental matrix is presented in Table 3-1

Table 3-1 - Experimental matrix for kinetic experiments

Exp.	H ₂ press. bar	Temp K	m _{cat} * g	[BL] ₀ mol/L	[Interm] ₀ mol/L	[GVL] ₀ mol/L	[BuOH] ₀ mol/L
1	23.4	403.15	2.80	1.834	0	6.833	0
2	23.3	413.15	2.80	0.866	0	8.831	0
3	22.3	423.15	1.80	0.807	0	8.515	0
4	22.3	407.15	2.80	0.839	0	8.877	0
5	22.3	427.15	2.80	0.619	0	8.827	0
6	20.3	403.15	2.80	0.868	0	8.755	0
7	23.8	373.20	0.50	1.821	0	6.851	0
8	23.3	423.15	0.00	0.059	1.586	6.884	0.189
9	16.3	373.15	0.50	1.893	0	6.719	0
10	11.4	373.15	0.50	1.821	0	6.675	0
11	5.2	393.15	1.00	1.885	0	6.720	0
12	23.7	413.15	0.00	0.056	1.411	7.120	0.168

*(50% wt moisture)

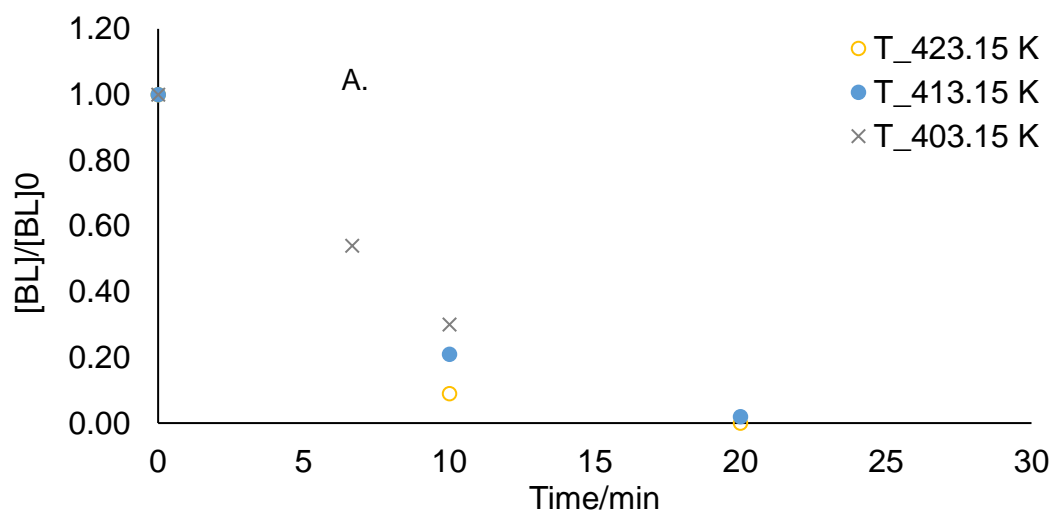
3.3. Experimental results

The concentrations of BL and the intermediate were used to the reactions progress. The conversion of BL and BHP as a function of time was used to compare the experimental results.

Conversions were expressed as $\frac{[BL]}{[BL]_0}$ and $\frac{[BHP]}{[BL]_0}$. According to the work of Wang (Y. Wang et al., 2019), mass transfer limitations are negligible for this reaction system either under the employed conditions. No mass transfer limitations were observed in the current work. The consumption of hydrogen would be interesting to track as the reaction progresses in order to better discriminate the proposed models. However, a better pressure regulator would be needed to quantify the exact volume of gases injected into the reactor.

3.3.1. Effect of temperature

The effect of temperature on the kinetics was studied comparing experiments at 403.15K, 413.15K and 423.15K, data from experiments 2, 5 and 6. The results are displayed in Figure 3-1. From these graphs, one can observe an increase of kinetics with an increase of temperature for both reaction steps. It can be clearly seen that the hydrogenation step is very rapid, while the cyclization step is much slower.



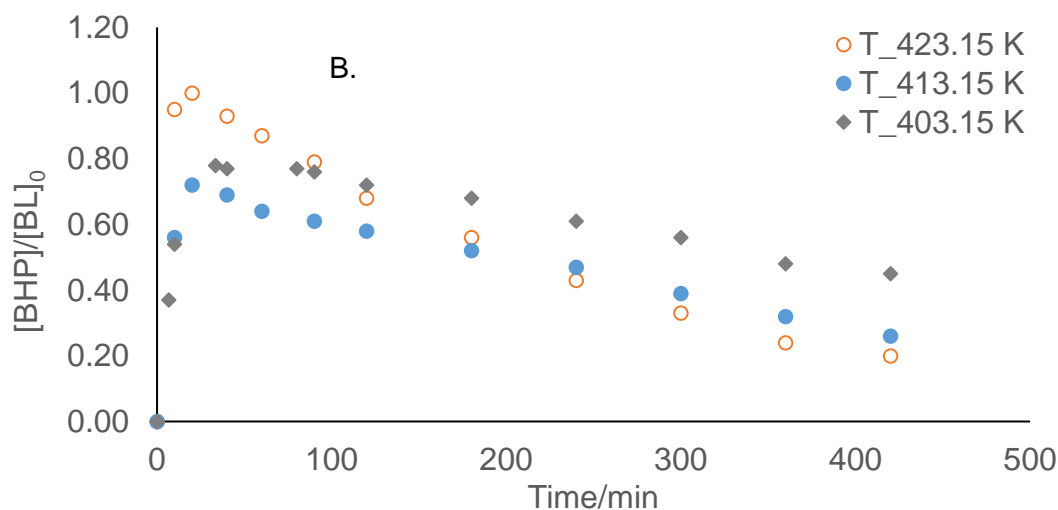


Figure 3-1 - Temperature effect on BL(A) and BHP (B) conversion at 20 bars. Experiments 2, 5, and 6.

3.3.2. Effect of pressure

The effect of the hydrostatic pressure in the reactor is displayed in Figure 3-3 for 11.4, 16.3 and 23.8 bars comparing experiments 7, 9, and 10. As observed for similar conditions and reactive systems, higher hydrogen pressure is expected to increase the availability of this molecule in the liquid phase and onto the surface of the catalyst which would then increase the kinetics of the hydrogenation step (Brunner, 1985; Capecci, Wang, Casson Moreno, et al., 2021; Grilc & Likozar, 2017; Y. Wang et al., 2019). As seen from the figure, this behavior is observed. The experiments were limited, below 25 bars, for a great increase of hydrogen pressure could affect the selectivity of the reaction by further hydrogenation of GVL into other products, such as 1,4 pentanediol. (Bababrik et al., 2017).

From Figure 3-3, one might observe an apparent stagnation on the concentrations of BHP after 2h. One would compare the effect of catalyst loading for this matter as for higher catalyst loading and same pressures, 23 bar H₂ and 100°C, the reaction is able to continue, lowering BHP concentration. The presence of acidic sites on the catalyst's support would influence this behavior. Another possible cause would be an increase in acidic conditions due to hydrogen dissociation on the catalyst surface, being able to donate protons and allow the cyclization reaction.

According to Grilc et al., an increase of pressure would proportionally increase hydrogen solubility for a binary mixture of levulinic acid – H₂ (Grilc & Likozar, 2017). This behavior

would suggest that hydrogen solubility on LA would follow Henry’s law where the concentration of hydrogen would be proportional to the gas pressure. As such, reaction rate would be increased for higher hydrogen pressure.

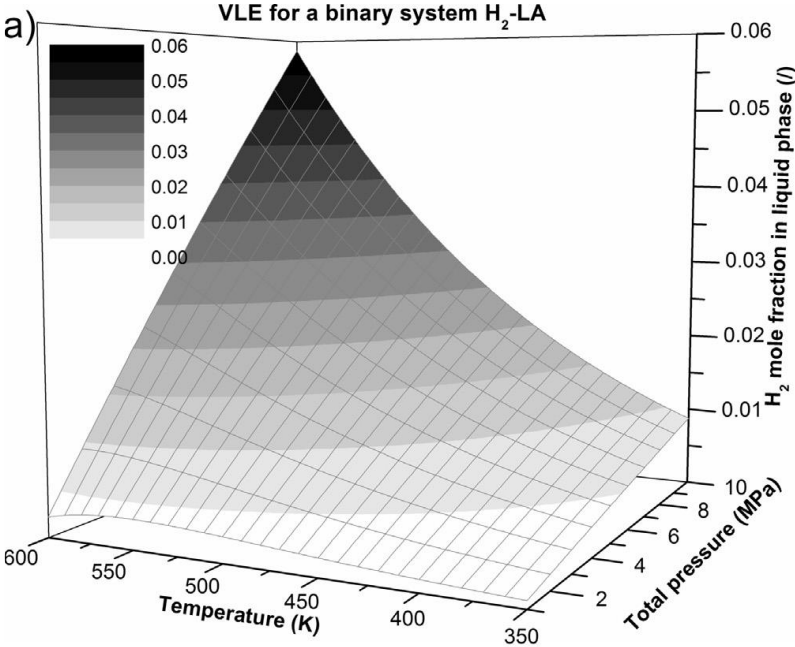
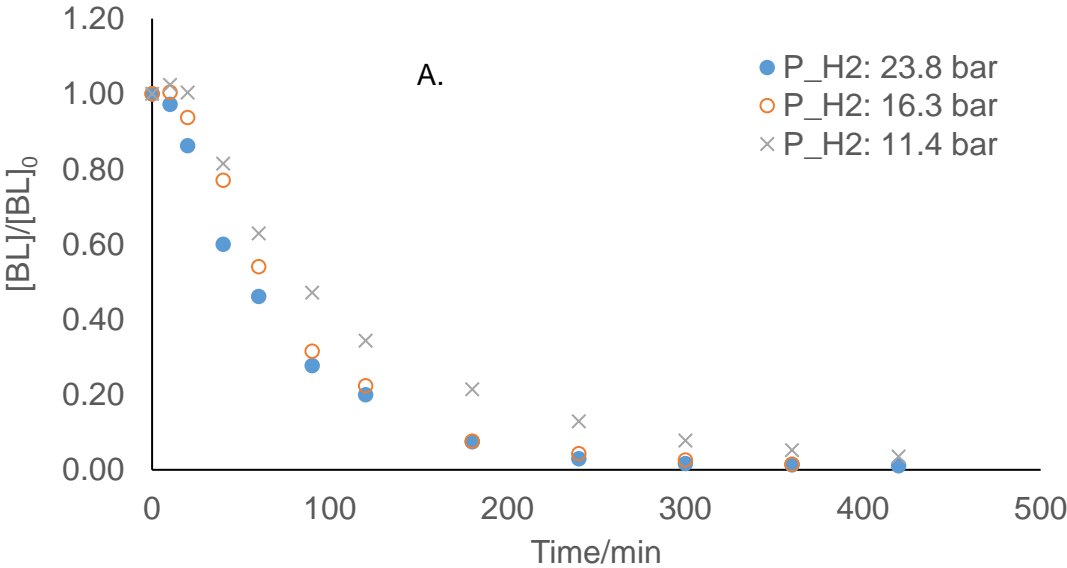


Figure 3-2 - The effect of temperature and total pressure on the vapor–liquid equilibria for a binary system hydrogen–levulinic acid; equilibrium mole fraction of H2 in the liquid phase. Used with permission of Elsevier Science & Technology Journals, from (Grilc & Likozar, 2017) permission conveyed through Copyright Clearance Center, Inc



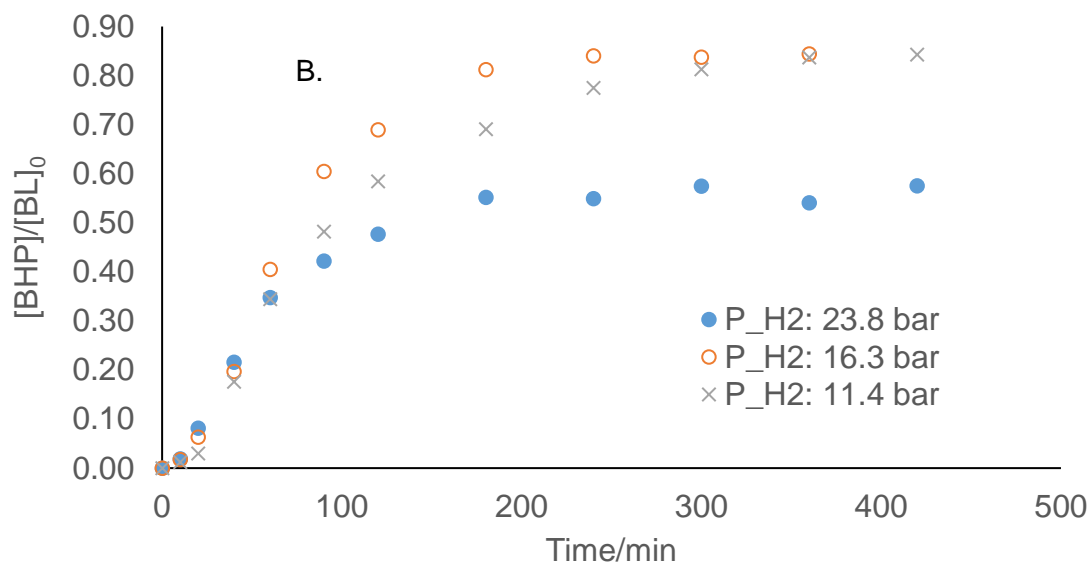


Figure 3-3 - Hydrostatic pressure effect in BL (A) and BHP (B) at 100°C with a Ru catalyst loading of 0.5g. Experiments 7, 9, and 10.

3.3.3. Catalyst loading

It would be expected to observe a faster conversion of the compounds when the catalyst loading is increased, given that the number of available sites for the reaction increases however, besides conversion, selectivity is also an important issue and increased catalyst load has been observed in some cases to negatively affect the selectivity of LA hydrogenation to GVL to further hydrogenation of GVL into side products such as 1,4 pentanediol (Upare et al., 2011).

The effect of catalysts concentration on the reaction kinetics was studied with two different catalyst amounts, 1.8 g and 2.8 g. The results are displayed in Figure 3 4. An increase of the catalyst loading indicates that the kinetics are improved for the hydrogenation and the cyclization step. Only GVL and butanol were observed as products.

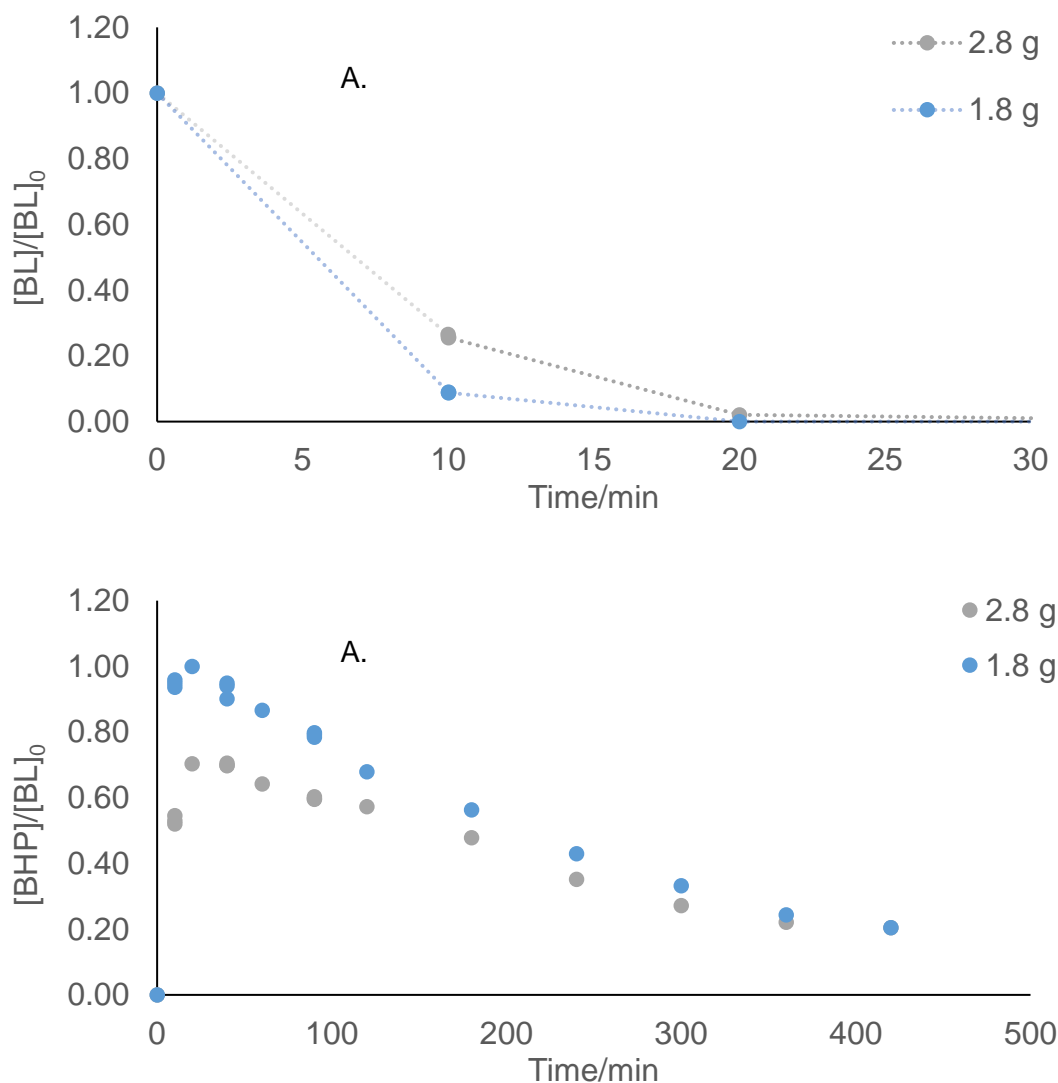


Figure 3-4 - Catalyst loading effect on BL (1) and BHP (B) at 150°C and 20 bars. Experiments 3 and 5.

3.4. Kinetic models

As shown before, the reaction pathway for the production of GVL from BL by hydrogenation comprises of two reaction steps, hydrogenation of the ketone group to produce an intermediate, butyl hydroxy pentanoate (BHP), which then undergoes cyclization with the alkyl carboxylic group. No other compounds or secondary reactions were observed in the analysis of the samples, the modeling of this reaction system is focused solely on these two reaction steps.

Mechanistically based models is explored to describe the kinetics. Compared to power law expressions, which have been used for evaluating and modelling kinetics for this reaction system (Y. Wang et al., 2019), mechanistic based models consider the interactions of the

catalyst surface with the reagents. The estimated reaction models are based on variations of the Langmuir Hinshelwood and Eley-Rideal reaction mechanisms expressions.

For the hydrogenation step, different reaction pathways are considered. The models differ in how the reactants interact with each other and with the catalyst surface. Here, we explore the possibility of non-competitive and competitive adsorption of reactants and the hydrogen dissociation on the catalyst surface according to the Langmuir Hinshelwood mechanism. Moreover, we explore the possibility of hydrogen reacting without adsorption on the catalyst surface according to the Eley-Rideal mechanism. Figure 3-5.

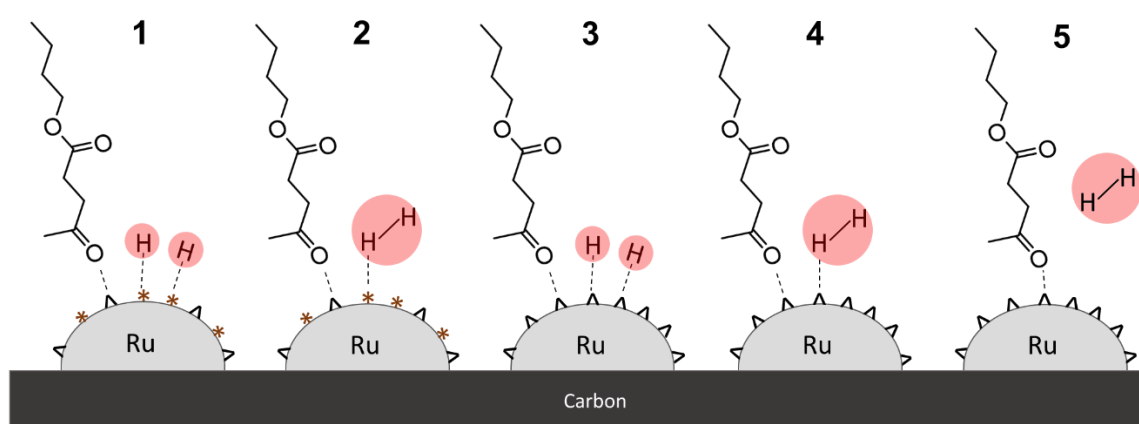


Figure 3-5 – Schema for hydrogenation step adsorption models based on Langmuir Hinshelwood non-competitive mechanism with (1) and without (2) dissociation of hydrogen; competitive with (3) and without (4) dissociation of hydrogen and (5) Eley-Rideal mechanisms. (Sites for adsorption: * and ^)

As shown by Piskun et al. (Piskun et al., 2016), the presence of acidic sites influences positively the kinetics of the cyclization reaction. The possibility of a catalyzed and non-catalyzed reaction pathway for the cyclization reaction is considered. This consideration assumes that the activated carbon support possesses low but not negligible acidity.

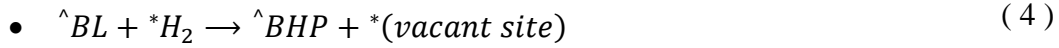
For the hydrogenation step, the considered rate expressions are expressed in Table 3-2, where the terms K_{BL} , K_{H_2} , K_H , K_{BL^\wedge} , K_{BHP^\wedge} and K_{BHP} are adsorption constants for the corresponding compound. The term K_i and K_C are equilibrium constants for the active sites and the term ω_{cat} refers to the catalyst loading (mass on dried basis per reaction volume).

Table 3-2 - Rate expressions for the hydrogenation step of the reaction system.

MODELS	Rate expression (R)
Langmuir Hinshelwood with molecular adsorption of H ₂ (LH1)	$\frac{k_1 * K_{H_2} * [H_2] * K_{BL} * [BL] * \omega_{Cat.}}{(K_{H_2} * [H_2] + K_{BL} * [BL] + K_{BHP} * [BHP] + 1)^2}$
Langmuir Hinshelwood with hydrogen dissociation (LH2)	$\frac{k_1 * K_H * [H_2] * K_i * K_{BL} * [BL] * \omega_{Cat.}}{(\sqrt{K_H * [H_2]} + K_{BL} * [BL] + K_{BHP} * [BHP] + K_i * K_{BL} * [BL] * \sqrt{K_H * [H_2]} + 1)^2}$
Eley-Rideal with no adsorption of hydrogen (ER1)	$\frac{k_1 * [H_2] * K_{BL} * [BL] * \omega_{Cat.}}{(K_{BL} * [BL] + K_{BHP} * [BHP] + 1)}$
Non-competitive Langmuir Hinshelwood with no dissociation of hydrogen (NCLH1)	$\frac{k_1 * K_{H_2} * [H_2]}{(1 + K_{H_2} * [H_2])} * \frac{K_{BL^{\wedge}} * [BL]}{(1 + K_{BHP^{\wedge}} * [BHP] + K_{BL^{\wedge}} * [BL])} * \omega_{Cat.}$
Non-competitive Langmuir Hinshelwood with hydrogen dissociation (NCLH2)	$\frac{k_1 * K_H * K_C * K_{BL^{\wedge}} * [H_2]}{\sqrt{K_H * [H_2]} + 1} * \frac{[BL] * \omega_{Cat.}}{K_{BL^{\wedge}} * [BL] + K_C * \sqrt{K_H * [H_2]} * K_{BL^{\wedge}} * [BL] + K_{BHP^{\wedge}} * [BHP] + 1}$

The derivation of these rate expressions can be found in the supporting information for the referred article (Capecci, Wang, Delgado, et al., 2021), however, the derivation of NCLH1 model is presented below as an example. In this model, hydrogen and BL are adsorbed on different sites and there's no dissociation of hydrogen Figure 3-5:





We observe the adsorption of the species on the active sites in equations (2) and (3), the hydrogenation reaction of the ketone group into the intermediate in equation (4) and the desorption of the intermediate (5) to enable the cyclization step in the liquid phase (6).

The adsorption and desorption steps are considered to be rapid and in equilibrium (Murzin & Salmi, 2005). Thus, we can assume that the following equilibria are valid and can be expressed by the following adsorption constants:

- $K_{BL\hat{}} = \frac{\theta_{\hat{BL}}}{[BL] \cdot \theta_{\hat{}}}$ (7)

- $K_{H_2} = \frac{\theta_{H_2}}{[H_2] \cdot \theta_*}$ (8)

- $K_{BHP\hat{}} = \frac{\theta_{\hat{BHP}}}{[BHP] \cdot \theta_{\hat{}}}$ (9)

Where, $\theta_{\hat{}}$ refers to the coverage or fraction of available active sites for BL species, and $\theta_{\hat{BL}}$ refers to the fraction of sites occupied by BL species.

Reaction (4) is assumed to be as the rate determining step in the hydrogenation step, given that the adsorption and desorption steps are considered rapid. These assumptions allow us to express the overall rate as:

$$R = k_1 * \theta_{H_2} * \theta_{\hat{BL}} * \omega_{Cat.} = k_1 * K_{H_2} * [H_2] * \theta_* * K_{BL\hat{}} * [BL] * \theta_{\hat{}} * \omega_{Cat.} \quad (10)$$

The ratio of the different available active sites leads to the following:

- $1 = \theta_{\hat{BL}} + \theta_{\hat{BHP}} + \theta_{\hat{}}$ (11)

- $1 = \theta_{H_2} + \theta_*$ (12)

From the adsorption constant, equations (8) and (9); and material balances of active sites, equations (11) and (12)(10):

$$\bullet \theta_* = \frac{1}{K_{H_2} * [H_2] + 1} \quad (13)$$

$$\bullet \theta_{\wedge} = \frac{1}{K_{BL^{\wedge}} * [BL] + K_{BHP^{\wedge}} * [BHP] + 1} \quad (14)$$

And after introduction to the rate equation (10), we obtain the rate equation:

$$\bullet R_1 = k_1 * K_{H_2} * [H_2] * \frac{1}{(1 + K_{H_2} * [H_2])} * K_{BL} * [BL] * \frac{1}{(1 + K_{BHP^{\wedge}} * [BHP] + K_{BL^{\wedge}} * [BL])} * \omega_{Cat}. \quad (15)$$

In the cyclization step, there were two different reaction pathways considered, a catalytic pathway (17) by the presence of acid sites in the solid catalyst and a non-catalytic (16) pathway. These reactions are considered to be of first order as the concentrations of the intermediates would not follow a constant rate of consumption, taking from the experimental data:

$$\bullet R_{2,non-cat.} = k_{2,non-cat.} * [BHP] \quad (16)$$

$$\bullet R_{2,Heterogeneous} = k_{2,Heterogeneous} * [BHP] * \omega_{Cat}. \quad (17)$$

Based on these assumptions, 10 different overall models were considered for the kinetics. The tested models are depicted in Table 3-3:

Table 3-3 - Tested models for the hydrogenation of BL to GVL

	Hydrogenation step					Cyclization step	
	LH1	LH2	ER1	NCLH1	NCLH2	Non-catalyzed	Heterogeneous catalyst
Model 1	X					X	
Model 2	X					X	X
Model 3		X				X	
Model 4		X				X	X
Model 5			X			X	
Model 6			X			X	X
Model 7				X		X	
Model 8				X		X	X
Model 9					X	X	
Model 10					X	X	X

3.5. Material balances

Based on the changes in concentrations, material balances were derived for the reaction system. Isothermal and isobaric conditions were used in the experiments. The material balances in the batch reactor are expressed as follows:

$$\frac{dC_{BL}}{dt} = -R_1 \quad (18)$$

$$\frac{d[H_2]_{liq}}{dt} = k_L \cdot a * ([H_2]_{liq}^* - [H_2]_{liq}) - R_1 \quad (19)$$

$$\frac{dC_{BHP}}{dt} = R_1 - R_{2,non-cat} - R_{2,Heterogeneous} \quad (20)$$

$$\frac{dC_{BuOH}}{dt} = R_{2,non-cat} + R_{2,Heterogeneous} \quad (21)$$

$$\frac{dC_{GVL}}{dt} = R_{2,non-cat} + R_{2,Heterogeneous} \quad (22)$$

Equation (18) displays the changes of hydrogen dissolved in the liquid phase. Here, $[H_2]_{liq}^*$ refers to the hydrogen concentration at the gas-liquid interphase, and $[H_2]_{liq}$ is the hydrogen concentration in the liquid phase, estimated by Henry's constant in GVL(Y. Wang et al., 2019). The volumetric gas to liquid mass transfer coefficient, $k_L \cdot a$, was expressed as a function of density, viscosity and temperature according to the findings of Wang et al. (Y. Wang et al., 2019)

3.6. Bayesian statistical method

The concentrations of BL and BHP were used as observables during the reaction to estimate the parameters described in the kinetic models. The parameter estimation was evaluated via Bayesian inference, given that the use of this approach has shown better results compared to the non-linear least squares method. (Kopyscinski et al., 2012; Stewart et al., 1992). To perform these tasks, the commercial program Athena Visual Studio was used. (Stewart & Caracotsios, 2008)

To solve the ordinary differential equations, ODEs, expressed in the mass balances, a solver known as DDAPLUS was used. This solver is incorporated in Athena Visual Studio to solve nonlinear initial-value problems comprising of stiff implicit systems. For the parameter estimation, a package GREGPLUS was used, which estimates the model parameters, their inference intervals and covariance, using single-response or multi-response data. (Stewart & Caracotsios, 2008)

The estimation was performed by calculating the probability of each model (M_ω) being able to describe the experimental values (Y), within the error range (Σ) (Stewart & Caracotsios, 2008). This probability is known as the posterior distribution, expressed in equation (23):

$$p(M_\omega|Y, \Sigma) = \frac{L(Y, \Sigma|M_\omega) \cdot p(M_\omega)}{C} \quad (23)$$

In equation (23), the term $L(Y, \Sigma|M_\omega)$ represents the likelihood function. The likelihood function evaluates the probability of the model (M_ω) to generate the experimental concentrations (Y) using a parameter vector (θ). This equation is normalized with a constant C. The experimental results provide information to estimate the probability of the model $p(M_\omega)$, known as the prior distribution. The boundary conditions are set and known for the different parameters and the experiments are replicated to evaluate the error space.

The normalized posterior probabilities are allowed to discriminate between the different models, so that the best fitting model would be determined. The probabilities were obtained with equation (24):

$$\pi(M_k|Y, \Sigma) = \frac{p(M_k|Y, \Sigma) * 100}{\sum_k p(M_k|Y, \Sigma)} \quad (24)$$

The package GREGPLUS performs the minimization of the objective function $S(\theta)$, shown in equation (25) and it also allows to calculate the maximum posterior probability density for the estimated parameters φ and the values of the posterior distribution for the tested models. (*AthenaVisual, Inc., n.d.; Computer-Aided Modeling of Reactive Systems / Wiley, n.d.*)

$$S(\theta) = (n + m + 1) \cdot \ln|v(\theta)| \quad (25)$$

$$v_{ij}(\theta) = \sum_{u=1}^n [Y_{iu} - f_{iu}(\xi_u, \theta)] \cdot [Y_{ju} - f_{ju}(\xi_u, \theta)] \quad (26)$$

In equation (25), the objective function $S(\theta)$ the number of events in response (n), the number of responses (m) and the determinant of the covariance matrix of the responses ($|v(\theta)|$) are used. The elements in the covariance matrix were obtained with equation (26), where the covariances between the experimental (Y) and estimated concentrations ($f_{iu}(\xi_u, \theta)$) are calculated. Here, Y_{iu} corresponds to the experimental concentration and $f_{iu}(\xi_u, \theta)$ to the

estimated value for the response i and event u ; Y_{ju} the experimental concentration and $f_{ju}(\xi_u, \partial)$ the estimated value for response j and event u .

To evaluate the precision of the estimated parameters, the marginal highest posterior density (HPD) was used. GREGPLUS allowed to calculate the 95% HPD.

The parameters to estimate, ∂ , are the activation energies, the rate constants, and the adsorption constants shown in Table 3-2. To decrease the correlation between the pre-exponential factor and the activation energy, the modified Arrhenius equation was used:

$$k_i(T_R) = k_i(T_{ref}) \cdot \exp \left(-\frac{E_{a_i}}{R} \left(\frac{1}{T_R} - \frac{1}{T_{ref}} \right) \right) \quad (27)$$

In equation (27), the reference temperature (T_{ref}) was set to 403.15K considering the experimental temperature range.

The Akaike information Criterion (AIC) was used to observe the effect of the number of estimated parameters in the model (28). Based on this criterion, the model with the lower AIC would be more reliable (McDonald et al., 2018).

$$\begin{aligned} AIC = & \text{Number of independent events} \\ & \cdot \ln \left([Y_{ju} - f_{ju}(\xi_u, \partial)]^2 / \text{number of independent event} \right) + 2 \\ & \cdot \text{Number of estimated parameters} \end{aligned} \quad (28)$$

3.7. Modeling results

From preliminary results of the modeling, the adsorption constant of the intermediate BHP and the activation energy for the cyclization step always approached the value 0, and that the value of K_{BHP} and $E_{a2, \text{heterogeneous}}$ were set to zero. It was also observed that the cyclization reaction, catalyzed by the Ru/C, did not show any dependence with temperature.

The results of the posterior probability for each model are shown in Table 3-4.

Table 3-4 - Modeling results from Bayesian statistics

Model	Objective function $S(\theta)$	Posterior probability $\text{Log}_{10} p(M_k Y, \Sigma)$	Posterior probability share $\pi(M_k Y, \Sigma)$ in%	Number of estimated parameters	AIC
1	6497.91	-1.25 10 ⁺²	0.08	6	4.27 10 ⁺³
2	6430.30	-1.22 10 ⁺²	31.80	7	4.16 10 ⁺³
3	6451.40	-1.25 10 ⁺²	0.06	7	4.26 10 ⁺³
4	6386.27	-1.22 10 ⁺²	22.26	7	4.15 10 ⁺³
5	6647.54	-1.27 10 ⁺²	0.00	4	4.42 10 ⁺³
6	6602.22	-1.26 10 ⁺²	0.01	5	4.35 10 ⁺³
7	6464.54	-1.25 10 ⁺²	0.09	6	4.26 10 ⁺³
8	6417.32	-1.22 10 ⁺²	41.35	6	4.15 10 ⁺³
9	8114.67	-1.50 10 ⁺²	0.00	1	5.77 10 ⁺³
10	6434.52	-1.23 10 ⁺²	4.35	5	4.19 10 ⁺³

From this table, the normalized posterior probability share denotes that the models 2, 4 and 8 are the more probable models to accurately describe experimental data as they display the lowest AIC values. It is good to notice that these models consider the catalyzed path for the cyclization reaction. The estimated parameters, covariance matrix and parity plots are shown in the sections below.

3.7.1. Model 4 – LH2 with catalyzed cyclization step

In Table 3-5, the estimated values of parameters are displayed for Model 4. It can be seen that the estimation was not quite accurate, as the higher posterior density (HPD) intervals for $k_1(T_{ref})$, K_{H2} and K_{BL} are higher than 100%.

Table 3-5 - Estimated values at T_{ref} (403.15K) and statistical data for Model 4.

Parameters	Units	Bayesian approach	
		Estimated	HPD Intervals %
$k_1(T_{ref})$	mol/m ³ /s/kg _{dry basis cat}	40.4	>100%
Ea_1	J/mol	3.05 10 ⁺⁴	12.88
K_{H2}	m ³ /mol	29.0	>100%
K_{BL}	m ³ /mol	4.31 10 ⁻³	>100%
K_i	-	nd	nd
$k_{2,Het}(T_{ref})$	m ³ /s/kg _{dry basis cat}	3.67 10 ⁻⁶	24.19
$k_{2,non-cat}(T_{ref})$	1/s	2.20 10 ⁻⁵	17.46
$Ea_{2,non-cat}$	J/mol	2.86 10 ⁻⁴	43.83

Parity plots for this model are shown in Figure 3-6 and the covariances are shown in Table 3-6.

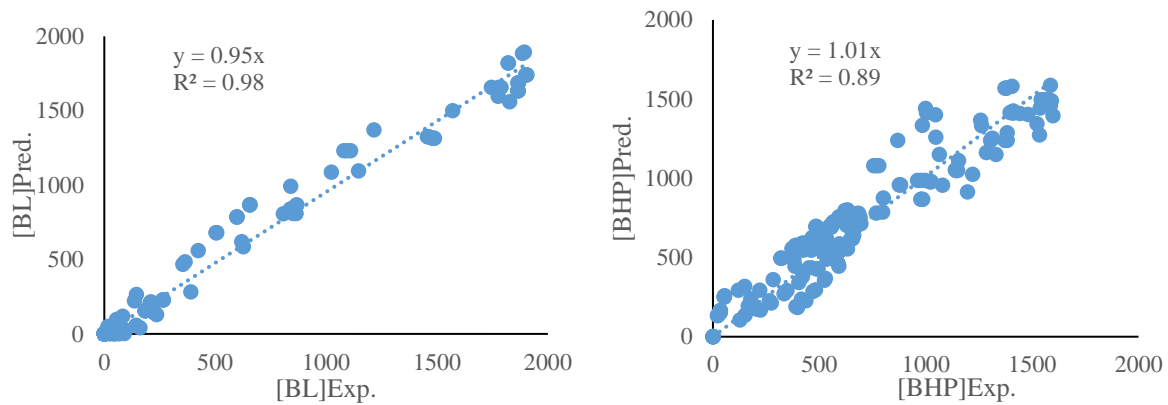


Figure 3-6 - Parity Plots for Model 4

From the parity plots Figure 3-6 one can see that the predicted values display an overestimation for the concentrations for BL and a high dispersion for BHP. This would be due to the uncertainty of the estimation of parameters estimated, the adsorption constants are not possible to define, meaning that the model might not describe the adsorption mechanism.

Table 3-6 - Normalized parameter covariance matrix for Model 4

	$k_1(T_{ref})$	Ea_1	K_{H_2}	K_{BL}	K_{BHP}	K_i	$k_{2,Het}(T_{ref})$	$Ea_{2,Het}$	$k_{2,non-cat}(T_{ref})$	$Ea_{2,non-cat}$
$k_1(T_{ref})$	1									
Ea_1	0.585	1								
K_{H_2}	-0.998	-0.567	1							
K_{BL}	-0.999	-0.569	0.995	1						
K_{BHP}	-	-	-	-	-					
K_i	nd	nd	nd	nd	nd	nd				
$k_{2,Het}(T_{ref})$	0.018	0.014	-0.016	-0.019	-	nd	1			
$Ea_{2,Het}$	-	-	-	-	-	nd	-	-		
$k_{2,non-cat}(T_{ref})$	-0.076	-0.066	0.073	0.079	-	nd	-0.641	0.000	1	
$Ea_{2,non-cat}$	0.092	0.081	-0.088	-0.095	-	nd	0.501	0.000	-0.670	1

From the covariance matrix, one can observe a high correlation between the rate constant $k_1(T_{ref})$, and adsorption constants for hydrogen and BL (K_{H_2} and K_{BL}). This could imply that the determination of the adsorption constants is difficult given the available kinetic data or other rate mechanisms should be explored.

From these results, Model 4 displays significant uncertainties in the parameter estimations and other models should be explored.

3.7.2. Model 2 – LH1 with catalyzed cyclization step

The values of the estimated parameters and HPD intervals are shown in Table 3-7. The HPD intervals are more reliable compared to Model 4, but some uncertainty is observed for the adsorption constant for BL and the rate constant.

Table 3-7 - Estimated values at T_{ref} 403.15K and statistical data for Model 2

Parameters	Units	Bayesian approach	
		Estimated	HPD Intervals %
$k_1(T_{ref})$	mol/s/kg_dry basis cat	3.57	68.18
Ea_1	J/mol	33094.04	13.42
K_{H2}	m ³ /mol	0.0439	29.65
K_{BL}	m ³ /mol	$2.78 \cdot 10^{-4}$	80.23
$k_{2,Het}(T_{ref})$	m ³ /s/kg_dry basis cat	$3.72 \cdot 10^{-6}$	23.80
$k_{2,non-cat}(T_{ref})$	1/s	$2.15 \cdot 10^{-5}$	18.14
$Ea_{2,non-cat}$	J/mol	$3.07 \cdot 10^4$	43.12

The parity plots for this model can be seen in Figure 3-7 and Table 3-8 shows the covariance matrix for the estimated parameters.

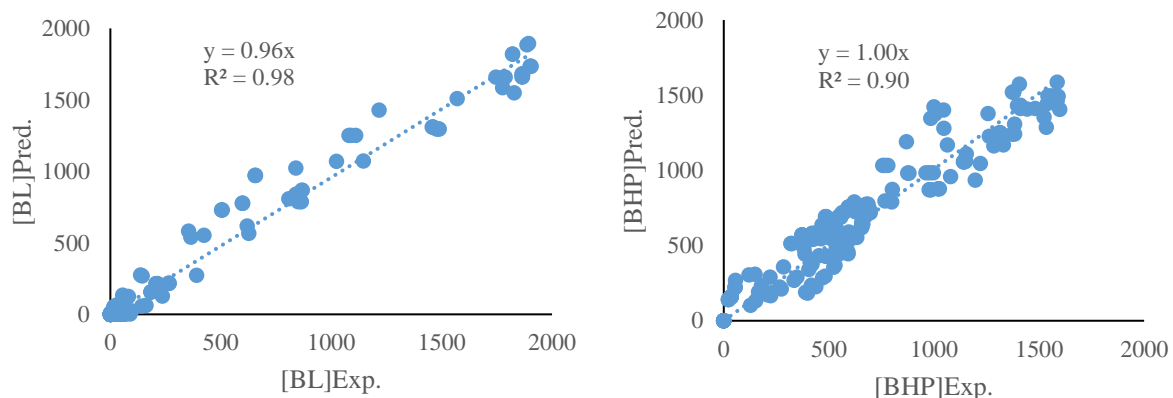


Figure 3-7 - Parity plots for Model 2

From Figure 3-7, one can observe that the over estimation of BL concentration is still noticeable and that the dispersion in BHP concentration is slightly reduced but still relevant. This improvement in the predictability would not also be related to a higher confidence in the parameter estimations but also for the initial assumptions in the model where molecular adsorption of hydrogen on the catalyst would be more probable.

Table 3-8 - Normalized parameter covariance matrix for Model 2

o	$k_1(T_{ref})$	Ea_1	K_{H2}	K_{BL}	K_{BHP}	$k_{2,Het}(T_{ref})$	$Ea_{2,Het}$	$k_{2,non-cat}(T_{ref})$	$Ea_{2,non-cat}$
$k_1(T_{ref})$	1								
Ea_1	0.655	1							
K_{H2}	-0.867	-0.555	1						
K_{BL}	-0.992	-0.574	0.849	1					
K_{BHP}	-	-	-	-	-				
$k_{2,Het}(T_{ref})$	0.032	0.022	-0.019	-0.034	-	1			
$Ea_{2,Het}$	-	-	-	-	-	-	-		
$k_{2,non-cat}(T_{ref})$	-0.111	-0.086	0.079	0.115	-	-0.646	0.000	1	
$Ea_{2,non-cat}$	0.132	0.103	-0.094	-0.138	-	0.517	0.000	-0.704	1

3.7.3. Model 8 – NCLH1 with catalyzed cyclization step

The results for the parameter estimation of Model 8 are shown in Table 3-9. Based on the HPD intervals; it can be noticed that the uncertainty of the estimated parameters in Model 8 is lower compared to the previous models.

Table 3-9 - Estimated values at Tref=403.15K and statistical data for Model 8

Parameters	Units	Bayesian approach	
		Estimated	HPD Intervals %
$k_1(T_{ref})$	mol/m ³ /s/kg_dry basis cat	0.711	52.72
Ea_1	J/mol	29472.46	14.69
K_{H2}	m ³ /mol	0.264	39.59
K_{BL}^{\wedge}	m ³ /mol	3.94 10 ⁻⁰⁴	63.86
$k_{2,Het}(T_{ref})$	m ³ /s/kg_dry basis cat	3.67 10 ⁻⁰⁶	24.05
$k_{2,non-cat}(T_{ref})$	1/s	2.20 10 ⁻⁰⁵	9.38
$Ea_{2,non-cat}$	J/mol	28661.77	43.65

Parity plots for Model 8 are displayed in Figure 3-8. It can be noticed that the parity plots for models 2, 4 and 8 have similar behavior, as such, one cannot discriminate which model better fits the data by parity plots only.

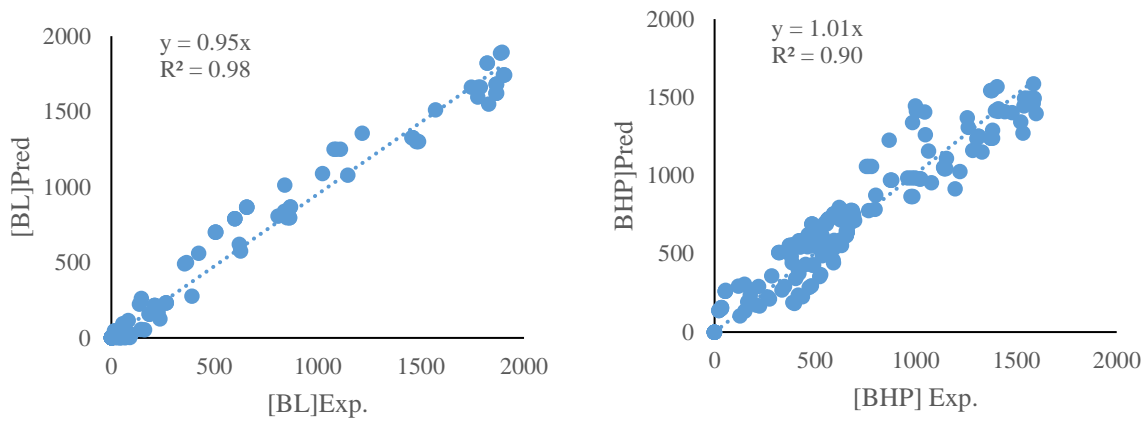


Figure 3-8 - Parity plots for Model 8.

The covariance matrix for Model 8 is displayed in Table 3-10. Model 8 presents lower correlation between the estimated parameters than the other evaluated models. However, a strong relationship between the adsorption constant for BL and the rate constant is still present.

Table 3-10 - Normalized parameter covariance matrix for Model 8

	$k_1(T_{ref})$	Ea_1	K_{H2}	K_{BL}	K_{BHP}	$k_{2,Het}(T_{ref})$	$Ea_{2,Het}$	$k_{2,non-cat}(T_{ref})$	$Ea_{2,non-cat}$
$k_1(T_{ref})$	1								
Ea_1	0.718	1							
K_{H2}	-0.435	-0.410	1						
K_{BL}	-0.979	-0.608	0.295	1					
K_{BHP}	-	-	-	-	-				
$k_{2,Het}(T_{ref})$	0.031	0.022	0.001	-0.036	-	1			
$Ea_{2,Het}$	-	-	-	-	-	-	-		
$k_{2,non-cat}(T_{ref})$	-0.106	-0.085	0.021	0.112	-	-0.641	-	1	
$Ea_{2,non-cat}$	0.130	0.104	-0.025	-0.137	-	0.502	-	-0.673	1

The fit of the model to experimental data (Runs 5, 7, 8, 9 and 11) for Model 8 are shown in Figure 3-9. Here, a good fitting of the predicted values is observed for BL. However, overestimation on the concentration of BHP is noticeable.

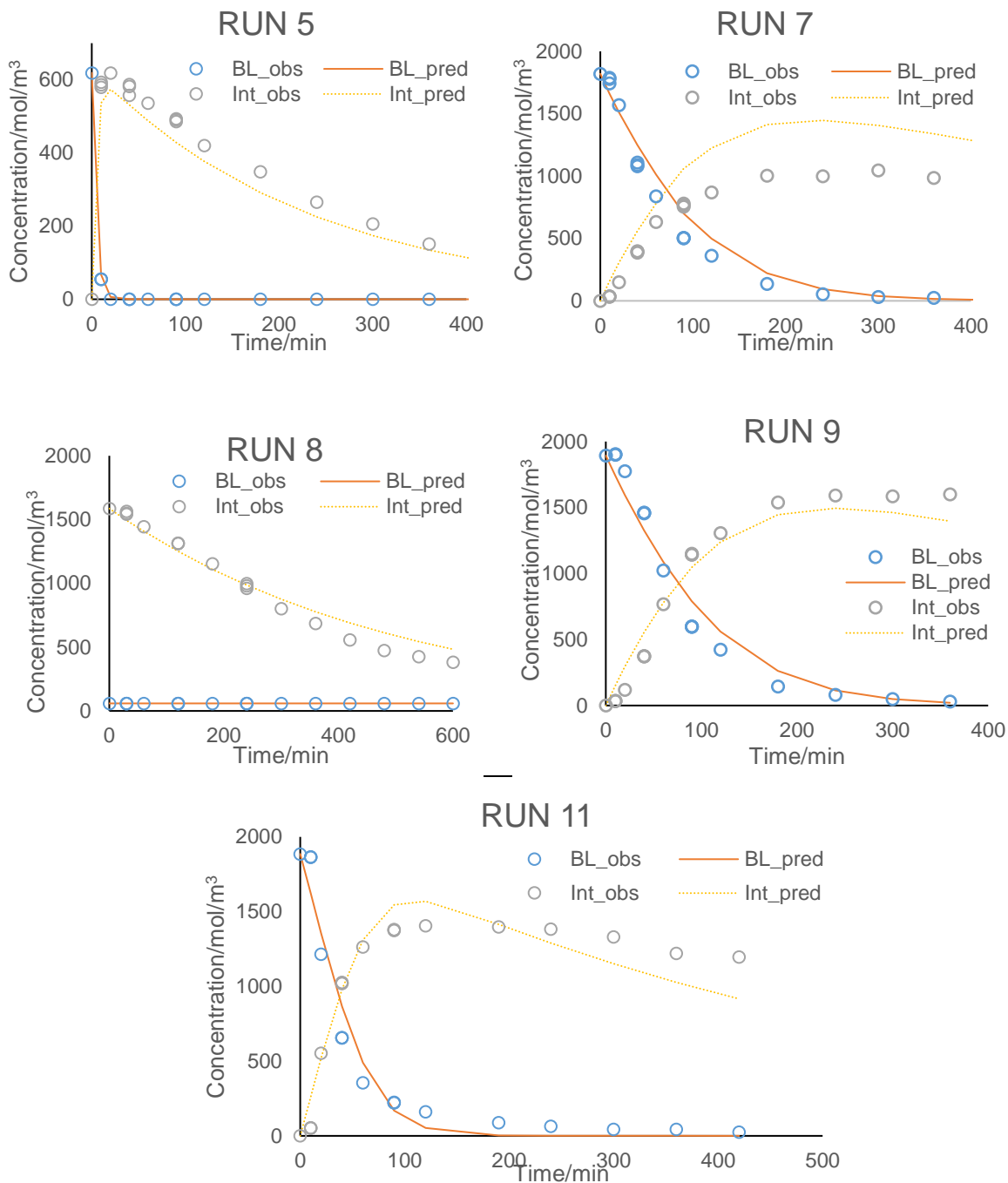


Figure 3-9 - Fit of Model 8 (Non-competitive Langmuir-Hinshelwood with no dissociation of Hydrogen) to the experimental data.

All three models presented significant correlation between the hydrogenation kinetic constant and the adsorption constants. The estimation of these parameters from kinetic experiments was difficult for models 2 and 4, as high posterior density intervals were obtained making the confidence on the estimation less reliable. The obtention of these parameters from solely kinetic experiment is difficult and quantum calculation such as DFT is needed. The estimation of BHP

is troublesome for the models, which would be based on the pressure effect on the cyclization reaction.

Taking from these factors, the more fitting model would be model 8 as it better estimates the experimental data, as observed from the parity plots, has a more reliable estimation of parameters from the lower HPD intervals and lower correlation between the estimated constants. Meaning that a Langmuir Hinshelwood model with no competition for adsorption sites and molecular adsorption of hydrogen would be more probable to represent the kinetics.

3.8. Conclusions

An experimental study on the hydrogenation of butyl levulinate over heterogeneous catalyst was performed. Model fits and discrimination of various mechanistically based models was performed with Bayesian inference with Athena Visual Studio. The reaction system comprised two reaction steps, hydrogenation of BL, and cyclization of BHP to obtain GVL. Ten kinetic models were derived and evaluated, based on the mechanistic approaches from Langmuir Hinshelwood and Eley-Rideal with and without hydrogen dissociation on adsorption. Also, the influence of solid catalyst on the cyclization reaction was considered. Bayesian inference was used to estimate the different kinetic parameters and their intervals of confidence.

The evaluation of the kinetic models was performed considering the AIC and the model posterior probability, where the more probable model to correctly describe the reaction kinetics was the non-competitive Langmuir Hinshelwood Hydrogenation with molecular adsorption of hydrogen and catalytic effect of the Ru/C catalyst over the cyclization step.

Chapter 4 - Kinetic model assessment for butyl levulinate and levulinic acid hydrogenation over dual catalysts

Part of this chapter is adapted from the post print of the following articles: J. Delgado et al., “Kinetic model assessment for the synthesis of γ -valerolactone from n-butyl levulinate and levulinic acid hydrogenation over the synergy effect of dual catalysts Ru/C and Amberlite IR-120.” *Chemical Engineering Journal*, vol. 430, p. 133053, Feb. 2022, DOI: 10.1016/j.cej.2021.133053.

Further permissions related to the Mass retrieved should be directed to Elsevier. Copyright © 2021 Elsevier B.V.

4.1. Introduction

In the production of alkyl levulinates from fructose alcoholysis, levulinic acid (LA) is generated as a side product at equilibrium with the levulinate shown in Figure 4-1 (Démolis et al., 2014; Di Menno Di Bucchianico et al., 2022; Ramírez et al., 2021). Given that GVL can be obtained from the hydrogenation of LA (Hsiao et al., 2021), Figure 2-11, a combination of BL-LA as a reagent mixture would be plausible to use. The effect of LA on the kinetics of the hydrogenation of BL is explored in this chapter.

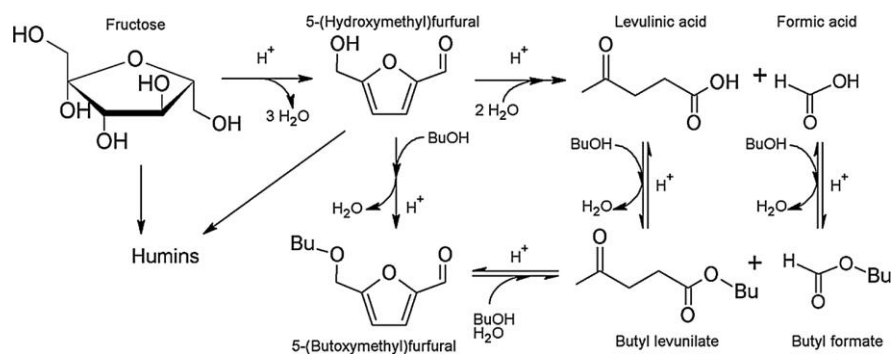


Figure 4-1 - Reaction scheme for butyl levulinate production from fructose alcoholysis (Ramírez et al., 2021; Démolis et al., 2014; Di Menno Di Bucchianico et al., 2022)

According to the literature and mentioned in previous chapters, an acidic environment is favorable for the cyclization reaction as the reaction is considered as a Fischer esterification (Russo et al., 2020; Piskun et al., 2016; Abdelrahman et al., 2014). The presence of hydrogen ions, formed from the dissociation of levulinic acid, would improve the kinetics of the cyclization reaction between the hydroxyl group and the ester group of the hydroxy-valerates formed from BL and LA hydrogenation. To improve the kinetics of this reaction, an acidic solid catalyst Amberlite IR-120, was added. Amberlite IR-120 is a cation exchange resin with sulphonic groups that showed great catalytic activity for esterification reactions (Russo et al., 2020). Using a heterogeneous catalyst over a homogeneous catalyst allows an easier separation process from the product mixture.

This chapter also explores a method to assess the predictive power of the different proposed models, known as the K-fold method (Slotboom et al., 2020). In the K-fold method, different sets of experiments are first used in the regression and other data is then used to compare the model prediction.

4.2. Experimental procedure

An experimental matrix was developed to better observe the influence of different parameters on the reaction kinetics. A set of fourteen experiments were performed, and their initial conditions are shown in Table 4-1. The reaction in focus were butyl levulinate's hydrogenation and cyclization of the formed intermediates to obtain GVL. GVL was used as a solvent in all the experiments, and they were performed under isothermal and isobaric conditions.

The studied parameters were temperature, hydrostatic pressure, initial concentrations of reagents, and catalyst loading. The presence of levulinic acid and Amberlite IR120 in the

reaction mixture and their influence on the kinetics were also studied. Since the sulfonic groups in Amberlite can leach at 120°C, experiments performed with this catalyst were kept below this temperature threshold.

Table 4-1 - Experimental matrix

Run	Pressure bar	Temp K	mcat_Ru g (50% weight moisture)*	mcat_A mb g (dried)*	m ₀ GVL g*	m ₀ BL g*	m ₀ LA g	BL ₀ mol/L*	GVL ₀ mol/L*	LA ₀ mol/L*
1	20.6	404.15	0.500	0	83	27	15	1.27	7.70	1.11
2	20	403.15	0.500	0	83	42	0	1.91	6.31	0.00
3	20.6	404.15	0.500	0	83	27	15	1.25	6.61	1.03
4	22	383.15	0.500	0	83	27	15	1.25	6.61	1.03
5	10.9	403.15	0.500	0	83	27	15	1.35	7.17	1.03
6	21.5	402.15	0.500	0	83	22	20	1.06	6.83	1.37
7	21.4	374.15	0.500	0	83	27	15	1.45	6.61	1.30
8	21.6	373.15	1.000	0	83	27	15	1.31	6.84	1.08
9	21.7	383.15	1.500	0	83	22	20	0.88	5.95	0.72
10	21.3	385.15	1.500	10.48	83	22	20	1.09	6.82	1.39
11	9.7	375.15	1.200	10.00	83	22	25	1.12	6.77	1.60
12	9.5	414.15	1.000	0	83	27	10	1.42	7.43	0.58
13	10.5	391.15	1.200	10.00	83	22	25	1.06	6.59	1.71
14	15.4	394.15	1.200	6.00	83	30	15	1.34	6.52	1.15

*Values used in kg and mol/m³ for modeling stages.

Experiments were performed in a Parr stirred autoclave shown in Figure 2-1. In an experiment, the reactor was filled with the reagents and the catalysts and then closed. The gases in the reactor were evacuated with a vacuum pump until a pressure of 50 mbar was reached. The stirring was then set to 400 rpm and the heating was initiated. Hydrogen was then passed from the pressurized tank into a reservoir. From the reservoir, the gas was dosed into the reactor at the

desired pressure through a pressure gauge. When the reactor reached the desired temperature, the stirring was stopped for two minutes. Hydrogen was allowed to flow into the reactor and an initial sample was taken. Stirring was set to 1000 rpm and samples were taken at predetermined times and analyzed with GC-FID (Figure 2-7). The experiments were performed under isobaric and isothermal conditions. The samples were analyzed three times in order to calculate the uncertainty in the concentration measurement, replicate measurements and their standard deviation was then calculated.

4.3. Experimental results

The effect of different parameters on the reaction kinetics is shown in this section. All experiments contain butyl levulinate as the main initial reagent and GVL as the solvent (Capecci, Wang, Casson Moreno, et al., 2021; Capecci, Wang, Delgado, et al., 2021). The studied parameters were temperature, hydrogen hydrostatic pressure, catalyst loading, and initial concentration of levulinic acid.

Estimated ratios of concentrations were used as observables to compare and evaluate the effect of all parameters. These ratios were obtained from the reagent's highest concentration. In the hydrogenation step, the ratios of $[BL]/[BL]_0$ and $[LA]/[LA]_0$ were used, and for the cyclization step, the ratios $[BHP]/[BL]_0$ and $[HPA]/[LA]_0$ were used. As previously mentioned, each sample was measured three times, and their average standard deviations were found lower than 3.64%.

4.3.1. Effect of temperature

The effect of temperature on the kinetics was evaluated by comparing experiments 3 and 4 in Table 4-1. The results for these experiments are shown in Figure 4-2. In the hydrogenation step, the consumption rate of BL and LA increased with temperature an increase in the kinetics. Regarding the cyclization step, an increase in temperature correlates to the consumption of intermediates, which is more noticeable for HPA.

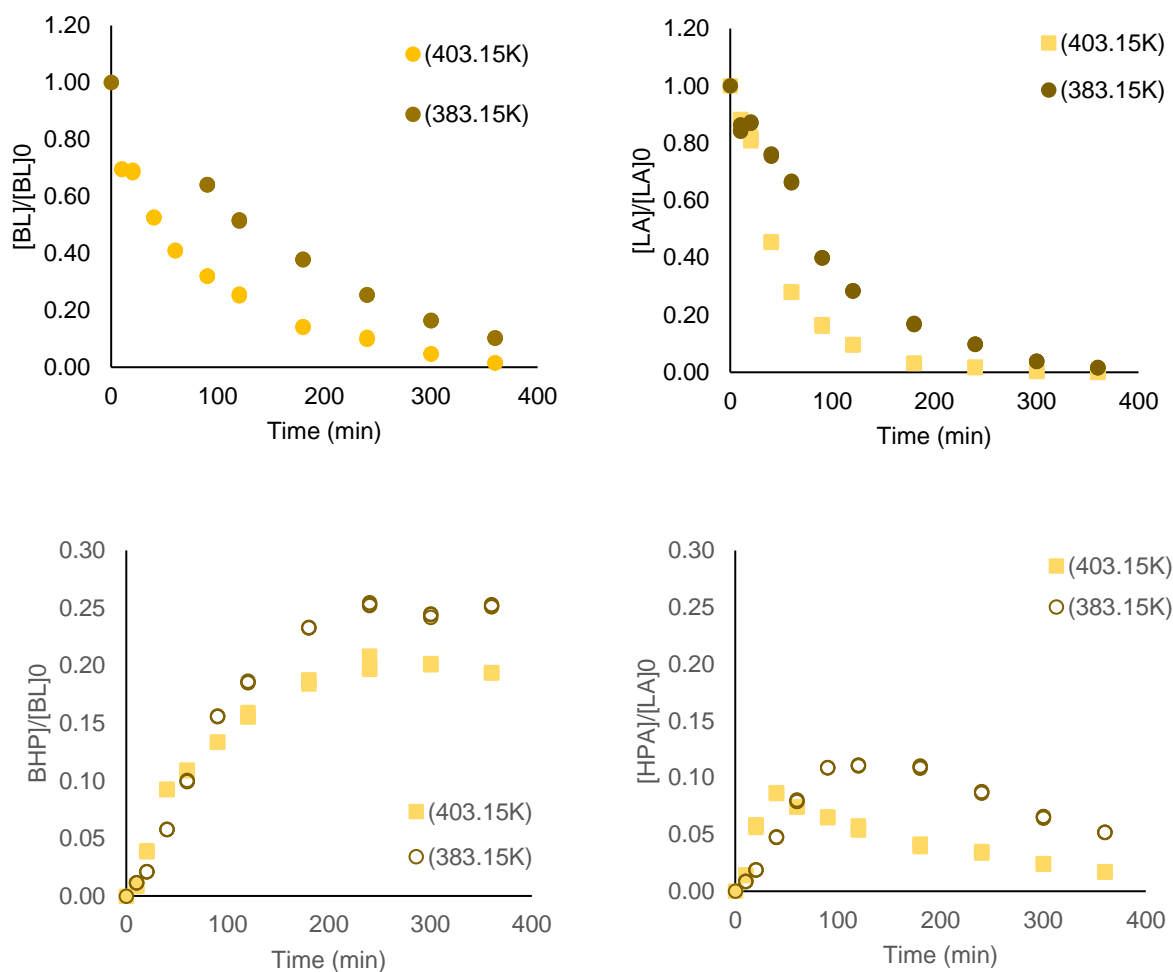


Figure 4-2 - Effect of Temperature: Comparison between exp 3&4. Hydrogenation and Cyclization reaction steps. (P:20bar, 0.5g Ru/C, 0g Amberlite)

4.3.2. Effect of hydrogen hydrostatic pressure

The influence of hydrogen pressure on the kinetics can be seen in Figure 4-3. Increasing the hydrostatic pressure, increases the kinetics for the hydrogenation reaction step. Consequently, this also increases the intermediates concentrations (BHP and HPA) as one can notice a faster accumulation of BHP and HPA.

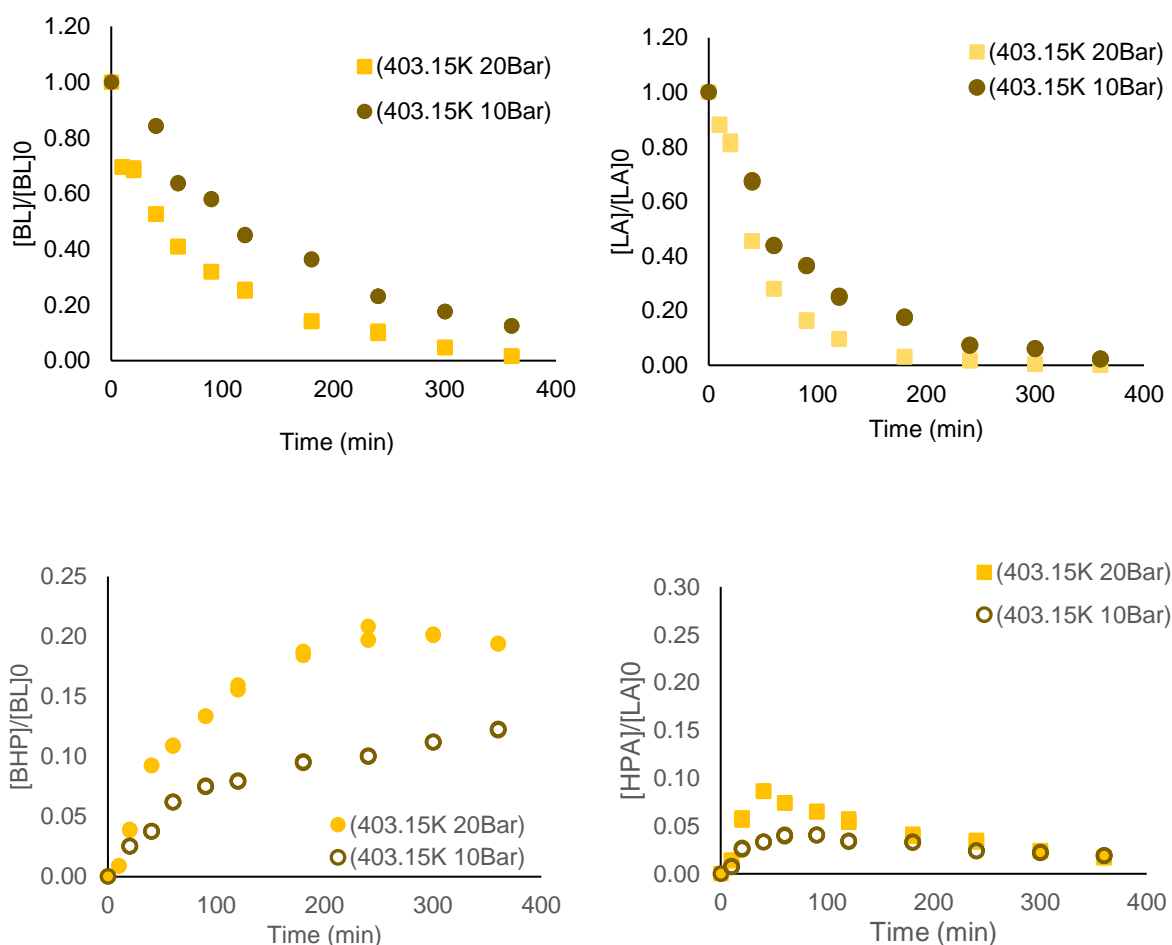


Figure 4-3 - Effect of pressure: Comparison between exp 3&5. Hydrogenation and Cyclization reaction steps.(0.5g Ru/C, 0g Amberlite)

4.3.3. Effect of ruthenium catalyst loading

Figure 4-4 displays the effect of Ru/C loading on the kinetics. From the results, one can observe that the increase in Ru/C catalyst loading increases the hydrogenation kinetics. Regarding the cyclization step, an increase in intermediate concentration was observed. This increase would be correlated to the acceleration in the kinetics of the hydrogenation step.

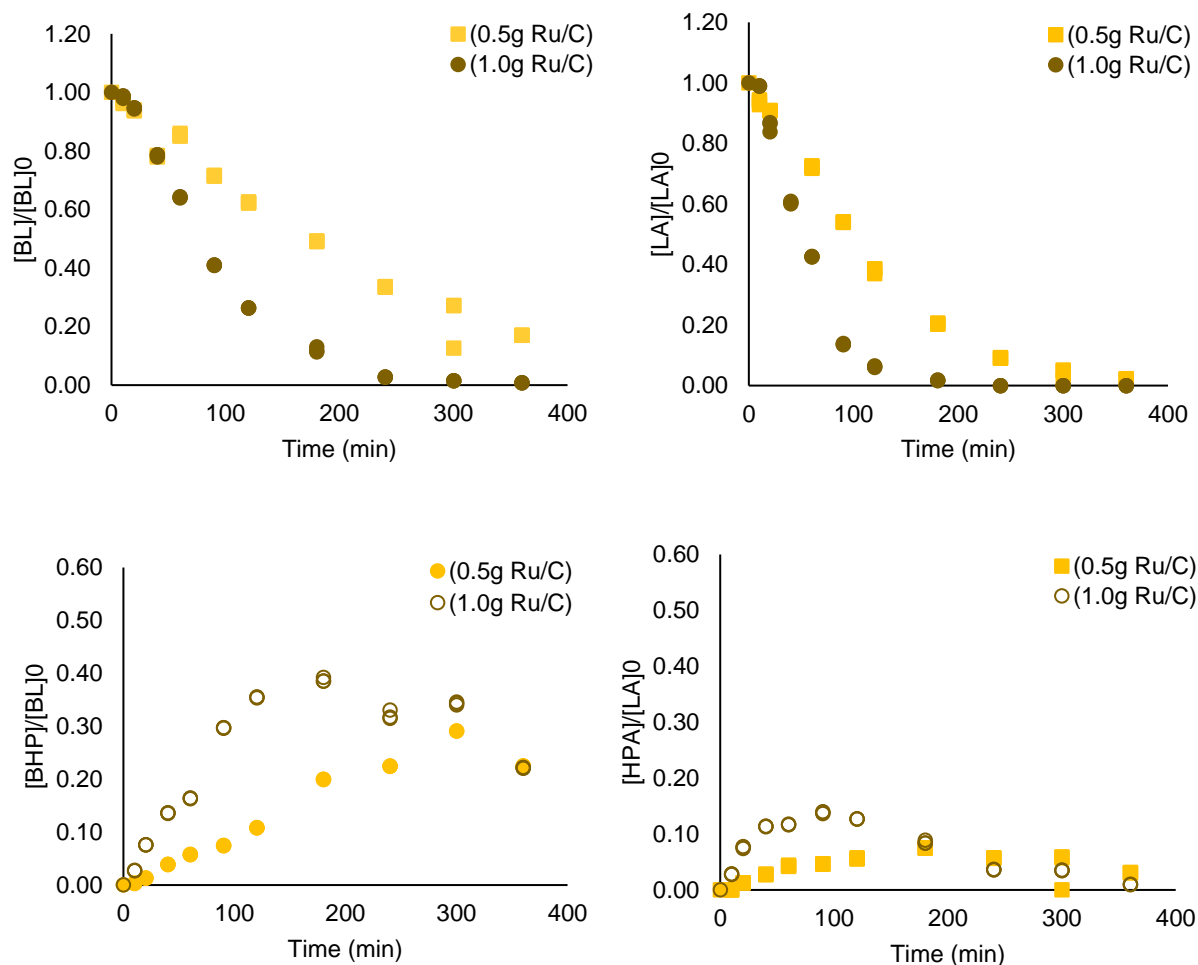


Figure 4-4 - Effect of Ru/C loadings: Comparison between exp 7&8. Hydrogenation and Cyclization reaction steps. ($T: 403.15K$, $P: 20$ bar, $0g$ Amberlite)

4.3.4. Effect of Amberlite IR120 loading

The influence of Amberlite IR120 on the reaction kinetics is displayed in Figure 4-5. For the hydrogenation step, one can see that the impact of this catalyst on the kinetics is negligible. However, the kinetics in the cyclization step is significantly influenced. The concentration of BHP was noticeably lower in the presence of the catalyst, and the HPA concentration was not detected in the analysis. It can be concluded that the presence of this acidic catalyst improves the conversion of the intermediates to the product, GVL. According to the manufacturer, Amberlite is able to exchange up to ≥ 1.80 eq/L of protons.

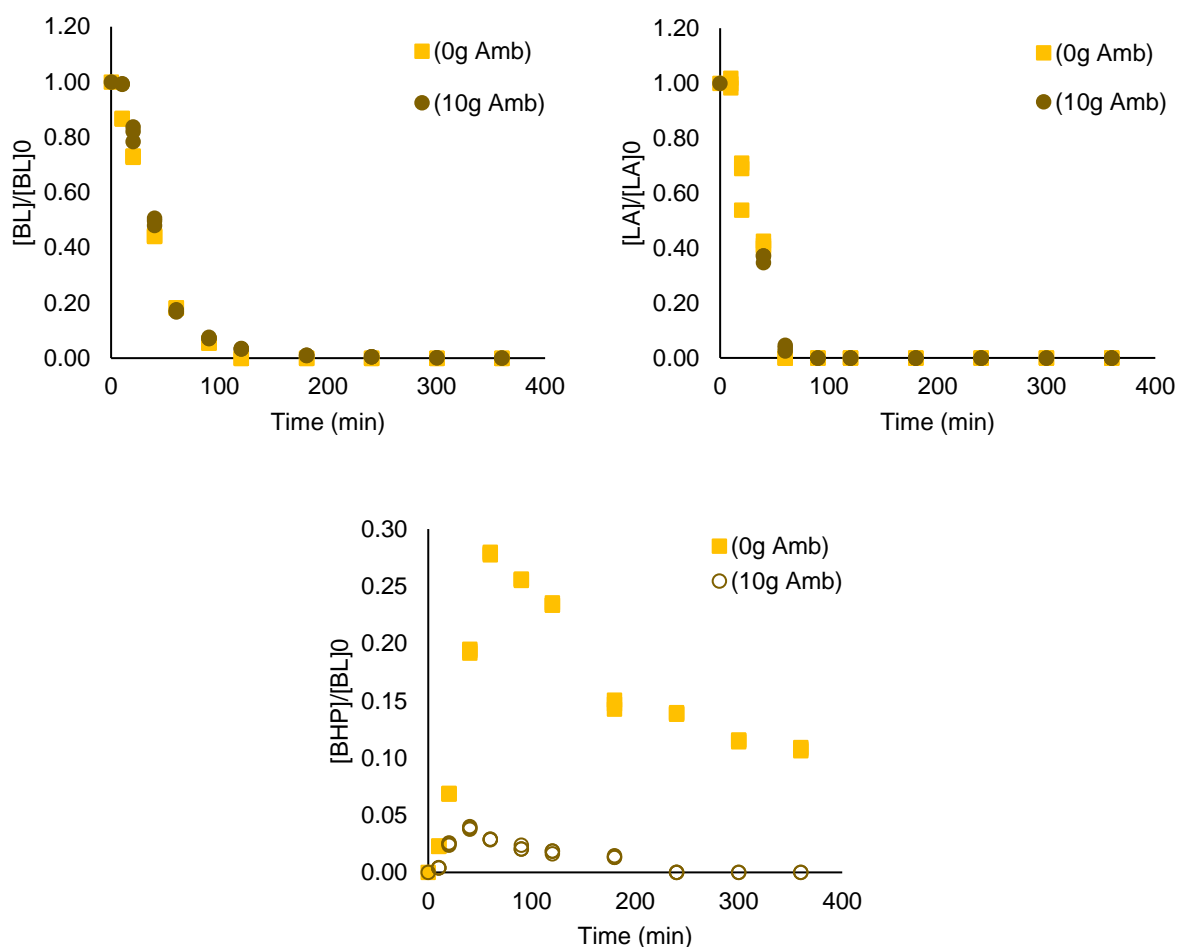


Figure 4-5 - Effect of Amberlite IR120 concentration on the kinetics: Comparison between exp 9&10. Hydrogenation and Cyclization reaction steps. (T: 403.15K, P:20 bar, 0.5g Ru/C)

4.3.5. Effect of levulinic acid (LA) concentration

When levulinic acid dissociates in the reaction mixture, protons are formed. These protons should catalyze the second reaction step i.e. the GVL production (Tejero et al., 2016). Figure 4-6 displays that the kinetics of BL hydrogenation are very similar with the different LA concentrations. One can observe that the kinetics of LA hydrogenation is somewhat faster when the concentration of LA is higher. A noticeable observation is that the increase in LA concentration accelerates the cyclization of the intermediates BHP and HPA.

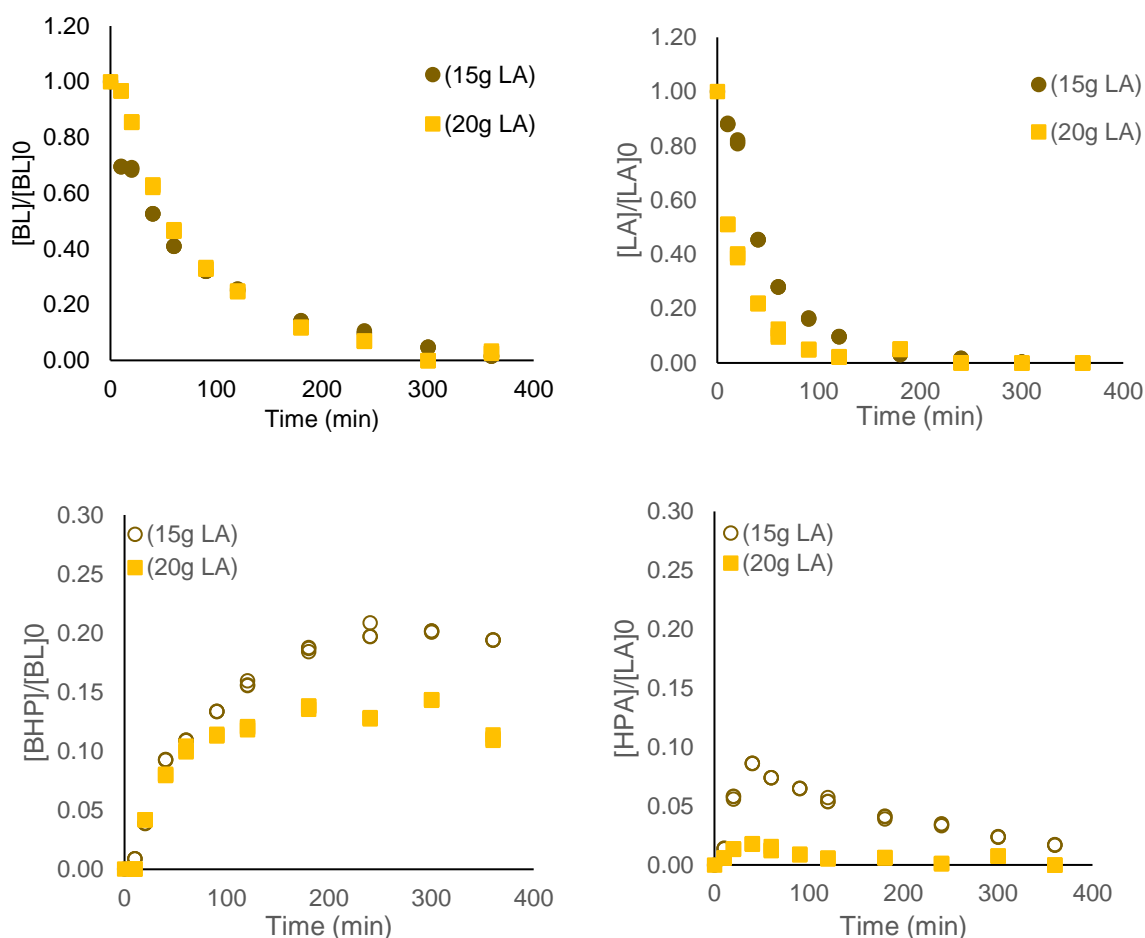


Figure 4-6 - Effect of LA concentration: Comparison between exp 3&6. Hydrogenation and Cyclization reaction steps. (T:403.15K, P:20 Bar, 0.5g Ru/C, 0g, Amberlite)

4.4. Kinetic modeling

Several reaction mechanisms are possible for the hydrogenation and cyclization steps in the overall reaction to produce GVL from BL and LA. Based on the possible reaction mechanisms, several mathematical models can be derived for explaining the kinetics. As mentioned in Chapter 3 - , it was observed that the surface reaction for the hydrogenation of BL would follow a non-competitive Langmuir-Hinshelwood kinetic model with no dissociation of molecular hydrogen. In the case where hydrogen does not dissociate, the carbonyl carbon would be hydrogenated first, and a subsequent hydrogenation on the oxygen would occur. From this result, one would infer that there are two kinds of ruthenium sites for the adsorption of molecules. In this mechanism, different adsorption sites exist in the catalyst where the hydrogen molecule and the carbonyl group can adhere without interfering with one another. In our previous work, it was observed that even the Ru/C catalyst could improve the kinetics of the cyclization step.

Both reagents (BL and LA) were thought to follow similar reaction pathways in this reaction system, where BL and LA are first hydrogenated to produce the intermediates (BHP and HPA) which then form the GVL, butanol and water. The presence of levulinic acid as a reagent and alcohols produced in the reaction system would be a plausible environment to allow the esterification of LA as a side reaction (Tejero et al., 2016). However, based on the experimental results, this side reaction is not favored, given the fast conversion of LA into HPA,

4.4.1. Rate expressions for the hydrogenation step

Seven kinetic models were evaluated for the hydrogenation step:

Mechanistic expressions for compound adsorption and desorption. These mechanisms were expressed based on Langmuir Hinshelwood and Eley-Rideal surface mechanism models. These mechanisms were considered as they have been used to describe adsorption mechanism in liquid-solid-gas phase systems and the initial assumption fast adsorption-desorption at the catalyst surface.

- (LH1) Competitive Langmuir-Hinshelwood with no dissociation of hydrogen.
- (LH2) Competitive Langmuir-Hinshelwood with dissociation of hydrogen.
- (NCLH1.1) Non-competitive Langmuir-Hinshelwood with no dissociation of Hydrogen. LA and BL are in competitive adsorption on the same site. hydrogen adsorbs in a different site.
- (NCLH1.2) Non-competitive Langmuir-Hinshelwood with no dissociation of Hydrogen. LA, BL, and H₂ are adsorbed on different sites.
- (ER) Eley-Rideal with no adsorption of hydrogen on the active sites.
- (NCLH2.1) Non-competitive Langmuir-Hinshelwood with dissociation of hydrogen. LA and BL are in competitive adsorption on the same site. Hydrogen adsorbs in a different site.
- (NCLH2.2). Non-competitive Langmuir-Hinshelwood with dissociation of hydrogen. LA, BL, and H₂ are adsorbed on different sites.

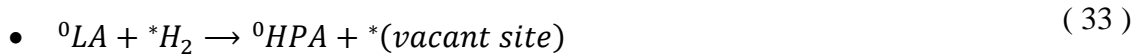
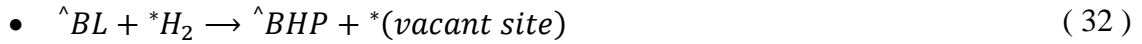
The rate expressions for the reaction system in an NCLH1.2 scenario are derived below. In this case, BL, LA, and molecular Hydrogen are adsorbed in different sites. These sites are denoted as \wedge , 0 , and $*$, respectively:

Estimated reaction mechanism steps in an NCLH1.2 kinetic model:

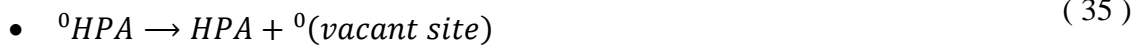
1) Adsorption of species on the catalytic sites:



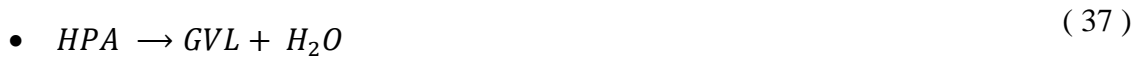
2) Hydrogenation reaction step of adsorbed compounds:



3) Desorption of intermediates obtained:



4) Cyclization reaction step of intermediates producing GVL:



It is considered that the adsorption and desorption steps are fast. Such an assumption is observed for heterogeneous reactions (Murzin & Salmi, 2005). Thus, we obtain the following:

$$\bullet \quad K_{BL\wedge} = \frac{\theta_{\wedge BL}}{[BL] \cdot \theta_{\wedge}} \quad (38)$$

$$\bullet \quad K_{LA0} = \frac{\theta_{{}^0LA}}{[LA] \cdot \theta_0} \quad (39)$$

$$\bullet \quad K_{H_2} = \frac{\theta_{H_2}}{[H_2] \cdot \theta_*} \quad (40)$$

$$\bullet \quad K_{BHP\wedge} = \frac{\theta_{\wedge BHP}}{[BHP] \cdot \theta_{\wedge}} \quad (41)$$

$$\bullet \quad K_{HPA0} = \frac{\theta_{{}^0HPA}}{[HPA] \cdot \theta_0} \quad (42)$$

Here, θ_{\wedge} refers to the coverage or fraction of available active sites for BL species, and $\theta_{\wedge BL}$ refers to the fraction of sites occupied by BL species. Given that the adsorption and desorption steps are estimated to be very fast, the hydrogenation reactions (4) are considered rate-determining steps. These steps are considered direct reactions, given the non-reversibility observed in the performed experiments.

From the adsorption constants, the reaction rates for the hydrogenation of BL and LA would be expressed as follows:

$$\begin{aligned} R_{BL_{hyd}} &= k_{BL_h} * \theta_{*H_2} * \theta_{\wedge BL} * \omega_{Cat}. \\ &= k_{BL_h} * K_{H_2} * [H_2] * \theta_* * K_{BL\wedge} * [BL] * \theta_{\wedge} * \omega_{Cat}. \end{aligned} \quad (43)$$

$$\begin{aligned} R_{LA_{hyd}} &= k_{LA_h} * \theta_{*H_2} * \theta_{0LA} * \omega_{Cat}. \\ &= k_{LA_h} * K_{H_2} * [H_2] * \theta_* * K_{LA0} * [LA] * \theta_0 * \omega_{Cat}. \end{aligned} \quad (44)$$

From these equations, ω_{Cat} refers to the dry weight of the Ru/C catalyst. Given that the coverage or fraction of empty active sites cannot be directly measured, the rate equations are expressed as a function of kinetic constants and concentrations.

Mass balances on the different active sites lead to the following:

$$\bullet \quad 1 = \theta_{\wedge BL} + \theta_{\wedge BHP} + \theta_{\wedge} \quad (45)$$

$$\bullet \quad 1 = \theta_{0LA} + \theta_{0HPA} + \theta_0 \quad (46)$$

$$\bullet \quad 1 = \theta_{H_2} + \theta_* \quad (47)$$

By substitution and rearrangements of the adsorption constant equations (8), (9), and (42); with the mass balances of active sites equations (11), (46), and (12), we get equations:

$$\bullet \quad \theta_* = \frac{1}{K_{H_2} * [H_2] + 1} \quad (48)$$

$$\bullet \quad \theta_{\wedge} = \frac{1}{K_{BL\wedge} * [BL] + K_{BHP\wedge} * [BHP] + 1} \quad (49)$$

- $$\theta_0 = \frac{1}{K_{LA^0}[LA] + K_{HPA^0}[HPA] + 1} \quad (50)$$

From these equations, we can express the rate of the hydrogenation reaction to be

- $$R_{BL_{hyd}} = k_{BL_h} * K_{H_2} * [H_2] * \frac{1}{(1 + K_{H_2}[H_2])} * K_{BL} * [BL] * \frac{1}{(1 + K_{BL}[BL] + K_{BHP}[BHP])} * \omega_{Cat.} \quad (51)$$

- $$R_{LA_{hyd}} = k_{LA_h} * K_{H_2} * [H_2] * \frac{1}{(1 + K_{H_2}[H_2])} * K_{LA} * [LA] * \frac{1}{(1 + K_{LA}[LA] + K_{HPA}[HPA])} * \omega_{Cat.} \quad (52)$$

By expressing $k_{BL_h} * K_{H_2} * K_{BL}$ as $k_{BL_{hyd}}$, and $k_{LA_h} * K_{H_2} * K_{LA}$ as $k_{LA_{hyd}}$, we obtain the rate equations :

- $$R_{BL_{hyd}} = k_{BL_{hyd}} * [H_2] * \frac{1}{(1 + K_{H_2}[H_2])} * [BL] * \frac{1}{(1 + K_{BL}[BL] + K_{BHP}[BHP])} * \omega_{Cat.} \quad (53)$$

- $$R_{LA_{hyd}} = k_{LA_{hyd}} * [H_2] * \frac{1}{(1 + K_{H_2}[H_2])} * [LA] * \frac{1}{(1 + K_{LA}[LA] + K_{HPA}[HPA])} * \omega_{Cat.} \quad (54)$$

The rate expressions for the hydrogenation step for all the considered reactions mechanisms, are shown in Table 4-2. The derivation of the rate expressions is presented in the supplementary information of the referenced article (Delgado et al., 2022).

Table 4-2 - Rate expressions for hydrogenation steps

MODELS	Rate expression for BL, $R_{BL, Hyd}$	Rate expression for LA, $R_{LA, Hyd}$
(LH1)	$\frac{k_1 * [H_2] * [BL] * \omega_{cat.}}{\left(K_{H_2} * [H_2] + K_{BL} * [BL] + K_{BHP} * [BHP] \right)^2 + K_{LA} * [LA] + K_{HPA} * [HPA] + 1}$	$\frac{k_1 * [H_2] * [LA] * \omega_{cat.}}{\left(K_{H_2} * [H_2] + K_{BL} * [BL] + K_{BHP} * [BHP] \right)^2 + K_{LA} * [LA] + K_{HPA} * [HPA] + 1}$
(LH2)	$\frac{k_1 * [H_2] * [BL] * \omega_{cat.}}{\left(K_H * \sqrt{[H_2]} + K_{BL} * [BL] + K_{BHP} * [BHP] + K_i * [BL] * \sqrt{[H_2]} \right)^2 + K_{LA} * [LA] + K_{HPA} * [HPA] + K_{i_2} * [LA] * \sqrt{[H_2]} + 1}$	$\frac{k_1 * [H_2] * [LA] * \omega_{cat.}}{\left(\sqrt{K_H} * [H_2] + K_{BL} * [BL] + K_{BHP} * [BHP] + K_i * [BL] * \sqrt{[H_2]} \right)^2 + K_{LA} * [LA] + K_{HPA} * [HPA] + K_{i_2} * [LA] * \sqrt{[H_2]} + 1}$
(ER1)	$\frac{k_1 * [H_2] * [BL] * \omega_{cat.}}{\left(K_{BL} * [BL] + K_{BHP} * [BHP] + K_{LA} * [LA] \right) + HPA * [HPA] + 1}$	$\frac{k_1 * [H_2] * [LA] * \omega_{cat.}}{\left(K_{BL} * [BL] + K_{BHP} * [BHP] \right) + K_{LA} * [LA] + HPA * [HPA] + 1}$
(NCLH1.1)	$\frac{k_1 * [H_2]}{(1 + K_{H_2} * [H_2])^*} * \frac{[BL] * \omega_{cat.}}{\left(1 + K_{BHP} * [BHP] + K_{BL} * [BL] \right) + K_{HPA} * [HPA] + K_{LA} * [LA]}$	$\frac{k_1 * [H_2]}{(1 + K_{H_2} * [H_2])^*} * \frac{[LA] * \omega_{cat.}}{\left(1 + K_{BHP} * [BHP] + K_{BL} * [BL] \right) + K_{HPA} * [HPA] + K_{LA} * [LA]}$
(NCLH1.2)	$\frac{k_1 * [H_2]}{(1 + K_{H_2} * [H_2])^*} * \frac{[BL] * \omega_{cat.}}{(1 + K_{BHP} * [BHP] + K_{BL} * [BL])}$	$\frac{k_1 * [H_2]}{(1 + K_{H_2} * [H_2])^*} * \frac{[LA] * \omega_{cat.}}{(1 + K_{HPA} * [HPA] + K_{LA} * [LA])}$
(NCLH2.1)	$\frac{k_1 * [H_2]}{K_H * \sqrt{[H_2]} + 1} * \frac{[BL] * \omega_{cat.}}{\left(K_{BL} * [BL] + K_{C1} * \sqrt{[H_2]} * [BL] + K_{BHP} * [BHP] + K_{LA} * [LA] \right) + K_{C2} * \sqrt{[H_2]} * [LA] + K_{HPA} * [HPA] + 1}$	$\frac{k_1 * [H_2]}{\sqrt{K_H} * [H_2] + 1} * \frac{[LA] * \omega_{cat.}}{\left(K_{BL} * [BL] + K_{C1} * \sqrt{[H_2]} * [BL] + K_{BHP} * [BHP] + K_{LA} * [LA] \right) + K_{C2} * \sqrt{[H_2]} * [LA] + K_{HPA} * [HPA] + 1}$
(NCLH2.2)	$\frac{k_1 * [H_2]}{K_H * \sqrt{[H_2]} + 1} * \frac{[BL] * \omega_{cat.}}{\left(K_{BL} * [BL] + K_{C1} * \sqrt{[H_2]} * [BL] + K_{BHP} * [BHP] + 1 \right)}$	$\frac{k_1 * [H_2]}{\sqrt{K_H} * [H_2] + 1} * \frac{[LA] * \omega_{cat.}}{\left(K_{LA} * [LA] + K_{C2} * \sqrt{[H_2]} * [LA] + K_{HPA} * [HPA] + 1 \right)}$

4.4.2. Rate expressions for the cyclization step

Four reaction pathways were considered to affect this reaction step independently from each other. The pathways are:

- Non-catalytic cyclization of intermediate.
- Reaction catalyzed by the acid sites on the support of Ru/C.

- Reaction catalyzed by the acidic groups on Amberlite IR120.
- Reaction catalyzed by the protons from the dissociation of levulinic acid.

The rate equations for the cyclization steps are shown below:

Non-catalytic pathway:

$$\bullet \quad R_{BHP_noncat} = k_{BHP_noncat} \cdot [BHP] \quad (55)$$

$$\bullet \quad R_{HPA_noncat} = k_{HPA_noncat} \cdot [HPA] \quad (56)$$

Catalytic cyclization due to active sites in Ru/C:

$$\bullet \quad R_{BHP_RuC} = k_{BHP_RuC} \cdot [BHP] \cdot \frac{1}{(K_{\blacksquare}HPA \cdot [HPA] + K_{\blacksquare}BHP \cdot [BHP] + 1)} \cdot \omega_{Cat.RuC} \quad (57)$$

$$\bullet \quad R_{HPA_RuC} = k_{HPA_RuC} \cdot [HPA] \cdot \frac{1}{(K_{\blacksquare}HPA \cdot [HPA] + K_{\blacksquare}BHP \cdot [BHP] + 1)} \cdot \omega_{Cat.RuC} \quad (58)$$

Catalytic cyclization due to Amberlite IR-120:

$$\bullet \quad R_{BHP_SO3H} = k_{BHP_SO3H} \cdot [BHP] \cdot \frac{1}{(K_{SO3H-HPA} \cdot [HPA] + K_{SO3H-BHP} \cdot [BHP] + 1)} \cdot \omega_{Cat.Amb} \quad (59)$$

$$\bullet \quad R_{HPA_SO3H} = k_{HPA_SO3H} \cdot [HPA] \cdot \frac{1}{(K_{SO3H-HPA} \cdot [HPA] + K_{SO3H-BHP} \cdot [BHP] + 1)} \cdot \omega_{Cat.RuC} \quad (60)$$

Catalytic cyclization due to LA dissociation:

$$\bullet \quad R_{BHP_diss} = k_{BHP_diss} \cdot [BHP] \cdot [LA] \quad (61)$$

$$\bullet \quad R_{HPA_diss} = k_{HPA_diss} \cdot [HPA] \cdot [LA] \quad (62)$$

4.5. Material balances

The mass balances for the various compounds in the liquid phase are presented below, considering the reaction rates for the hydrogenation and cyclization reaction steps. Given the operating circumstances for the tests, it is assumed that the reaction occurs in the liquid phase.

Furthermore, given the applied turbulence and the results displayed by Wang (Y. Wang et al., 2019), internal and external mass transfer limitations may be regarded as negligible.

The mass balances in the liquid phase can be expressed as:

$$\bullet \frac{dC_{BL}}{dt} = -R_{BL_hyd} \quad (63)$$

$$\bullet \frac{d[H_2]_{liq}}{dt} = k_L \cdot a * ([H_2]_{liq}^* - [H_2]_{liq}) - R_{BL_hyd} - R_{LA_hyd} \quad (64)$$

$$\bullet \frac{dC_{BHP}}{dt} = R_{BL_hyd} - R_{BHP_noncat} - R_{BHP_RuC} - R_{BHP_SO_3H} - R_{BHP_diss} \quad (65)$$

$$\bullet \frac{dC_{BuOH}}{dt} = R_{BHP_noncat} + R_{BHP_RuC} + R_{BHP_SO_3H} + R_{BHP_diss} \quad (66)$$

$$\bullet \frac{dC_{LA}}{dt} = -R_{LA_hyd} \quad (67)$$

$$\bullet \frac{dC_{HPA}}{dt} = R_{LA_hyd} - R_{HPA_noncat} - R_{HPA_RuC} - R_{HPA_SO_3H} - R_{HPA_diss} \quad (68)$$

$$\bullet \frac{dC_{Water}}{dt} = R_{HPA_noncat} + R_{HPA_RuC} + R_{HPA_SO_3H} + R_{HPA_diss} \quad (69)$$

$$\bullet \frac{dC_{GVL}}{dt} = R_{BHP_noncat} + R_{BHP_RuC} + R_{BHP_SO_3H} + R_{BHP_diss} + R_{HPA_noncat} + R_{HPA_RuC} + R_{HPA_SO_3H} + R_{HPA_diss} \quad (70)$$

Equation (64) expresses the mass balance for the dissolved hydrogen gas in the liquid bulk, $[H_2]_{liq}$. The term $[H_2]_{liq}^*$ corresponds to the concentration of hydrogen in the liquid-gas interphase, obtained by Henry's constant in GVL (Y. Wang et al., 2019).

$$He(T) = \frac{[H_2]_{liq}^*}{P_{H_2,Reactor}} \quad (71)$$

In equation (64), the term $k_L \cdot a$ corresponds to the gas-to-liquid mass transfer coefficient for hydrogen. The values of $k_L \cdot a$ were expressed as a function of parameters such as density, temperature, and viscosity. (Y. Wang et al., 2019)

4.6. Modeling

To estimate the multi-response parameters from rate equations in Table 4-2 and equations (55) along with the mass balances in equations (63) and (70), the method of nonlinear squares is commonly used (Kopyscinski et al., 2012; Stewart et al., 1992). However, the Bayesian framework approach has been considered a better option for this task (Kopyscinski et al., 2012; Stewart et al., 1992). In the Bayesian approach, the determinant criterion is used (Van Boekel, 1996). The commercial software, Athena Visual Studio, was used for parameter estimation and simulation via Bayesian statistics in this study. (Caracotsios & Stewart, 1985; *AthenaVisual, Inc.*, n.d.).

The concentrations of the reagents (BL and LA) and the intermediates (BHP and HPA) were used as observables in the parameter estimation. The differential equations obtained in material balances (63) and (70) were solved with DDAPLUS, a solver integrated into Athena Visual Studio. DDAPLUS is a modified Newton algorithm, where the first-order derivatives are approximated by a fixed leading coefficient backward difference method (Caracotsios & Stewart, 1985). Here the constants in the differential equations are fixed for each iteration, and the values obtained in the estimated equations are compared with the previous values.

Since the leading coefficients are fixed for each iteration, a sub-routine is needed to recalculate these parameters and improve the accuracy of the estimation for these values; this was performed by minimizing the objective function (72). Athena Visual Studio possesses a subroutine package called GREGPLUS; this subroutine is used for this minimization process and also allows us to calculate the credible intervals for the parameters and obtain the normalized parameter covariance matrix.

In order to minimize the objective function (72), one starts with initial values added to the subroutine package; the package will then use successive quadratic programming to minimize the function (Caracotsios & Stewart, 1985; Stewart et al., 1992).

$$S(\partial) = (a + b + 1) \cdot \ln|v(\partial)| \quad (72)$$

In equation (72), a is considered as the number of events in the response, b is considered as the number of responses observed, and $|v(\partial)|$ is the determinant of the covariance matrix of the responses. Each element of this matrix is defined by the sum of covariances between the experimental and estimated simulation for each observable:

$$v_{ij}(\partial) = \sum_{u=1}^n [Y_{iu} - f_{iu}(\partial)] \cdot [Y_{ju} - f_{ju}(\partial)] \quad (73)$$

In this equation, “ Y ” corresponds to the experimental concentration values, and “ $f(\partial)$ ” corresponds to the estimated values for each corresponding response (i, j) in each event “ u ”.

The credible intervals for each parameter were obtained using the quadratic expansion equation (72). The subroutine package, GREGPLUS, allowed us to calculate the precision of the parameters using the 95% marginal highest posterior density (HPD).

The modified Arrhenius equation was used to reduce the correlation between the activation energy and the pre-exponential factor in the kinetic constants.

$$k(T_R) = k(T_{ref}) \cdot \exp\left(-\frac{E_a}{R} \left(\frac{1}{T_R} - \frac{1}{T_{ref}}\right)\right) \quad (74)$$

In the Arrhenius equation (74), T_{ref} is the temperature selected as a reference for a given temperature span; R is the ideal gas constant.

Within the initial iteration in the modeling of the different kinetic models, it was observed that some constants tended approach the value of zero. The modeling was conducted after setting the following constants values to zero.

- The adsorption constants for BHP and HPA:
 - In the hydrogenation steps over Ru/C,
 - Over the acid sites on Ru/C,
 - Over Amberlite IR-120 for the cyclization steps.

- The activation energy for the cyclization of BHP and HPA:
 - Over Amberlite IR-120
 - Over the acid sites in Ru/C.
- The equilibrium constant K_{C2} , present in LA hydrogenation, given that it was low for the model NCLH2.2.

To compare the different models, Table 4-3 shows the regression parameters calculated for each kinetic model; these values, help in determining the best fitting models:

- Sum of Squared Residuals (SSR) $(Y_{ju} - f_{ju}(\theta))^2$
- Minimized objective function defined by Equation (72): $S(\theta)$
- Number of estimated parameters.
- Akaike information criterion (AIC)

The AIC considers the number of fixed parameters, giving a more extensive scope into selecting the best fitting model. This criterion correlates the fit of the model to the number of independent events and the complexity of each model by the amount of fixed estimated parameters (McDonald et al., 2018). According to this criterion, the model with a lower AIC value is considered more reliable.

$$AIC = \text{Number of independent event} \cdot \ln \left(\frac{[Y_{ju} - f_{ju}(\theta)]^2}{\text{number of independent event}} \right) + 2 \cdot \text{Number of estimated parameters} \quad (75)$$

1468 independent events were considered in the estimation of the kinetic models.

Table 4-3 - Regression parameters for each model

	SSR	Objective function	Number of estimated parameters	AIC
LH1	11693900	24125	19	13224.9
LH2	11665200	24127	19	13221.3
NCLH1.1	11697000	24154	19	13225.3

NCLH1.2	10757800	23987	19	13102.4
ER1	11685300	24153	19	13223.8
NCLH2.1	11773600	24142	17	13230.9
NCLH2.2	10443600	23940	18	13056.9

From Table 4-3, one would note that the models with lower SSR values, minimized values for the objective functions, and AIC number were the NCLH1.2 and NCLH2.2 models. From this observation, one would estimate that these models would better explain the experimental data. The values of the estimated parameters, their fit, and the normalized covariance matrix for each model are shown below:

4.6.1. Modeling results: Non-competitive Langmuir Hinshelwood 1.2

The estimated values and the associated credible intervals (HPD%) for this model are shown in Table 4-4. The credible intervals for most of the estimated parameters are considered small or medium, which implies that the selected changes in the operating conditions were significant to assess these parameters. However, for two parameters, K_{H_2} and $k_{HPA_{noncat}}(T_{Ref})$, their credible intervals were relatively higher compared to the other parameters. This difference is linked to the uncertainty of measurement due to the low effect of Hydrogen pressure in the kinetics (K_{H_2}) and to the difficulty in tracking HPA in the experiments given its reactivity ($k_{HPA_{noncat}}(T_{Ref})$).

Table 4-4 also shows that the rate constants for the reaction steps for BL, hydrogenation of BL, and cyclization of BHP, are lower than that for LA, hydrogenation of LA, and cyclization of HPA.

Table 4-4 - Estimated Values at $T_{ref} = 392.72$ K and statistical Data for NCLH1.2

Parameters	Units	Estimates	HPD%
Par1 $k_{BL_hyd}(T_{Ref})$	$m^3 \cdot mol^{-1} \cdot s^{-1} \cdot kg_dry\ basis$ RuC^{-1}	3.11E-06	14.57
Par2 Ea_{BL_hyd}	$J \cdot mol^{-1}$	3.62E+04	7.43
Par3 K_{H2}	$m^3 \cdot mol^{-1}$	7.36E-04	>100%
Par4 K_{BL}^{\wedge}	$m^3 \cdot mol^{-1}$	9.14E-04	29.02
Par5 K_{BHP}^{\wedge}	$m^3 \cdot mol^{-1}$	Fixed to zero	-
Par6 $k'_{BHP_cat_Amb}(T_{Ref})$	$s^{-1} \cdot kg_dry\ basis\ Amb^{-1}$	4.17E-05	49.21
Par7 $Ea'_{BHP_cat_Amb}$	$J \cdot mol^{-1}$	Fixed to zero	-
Par8 $k_{BHP_noncat}(T_{Ref})$	s^{-1}	5.78E-05	30.35
Par9 Ea_{BHP_noncat}	$J \cdot mol^{-1}$	8.67E+04	32.38
Par10 $k_{LA_hyd}(T_{Ref})$	$m^3 \cdot mol^{-1} \cdot s^{-1} \cdot kg_dry\ basis$ RuC^{-1}	8.08E-06	12.03
Par11 Ea_{LA_hyd}	$J \cdot mol^{-1}$	4.65E+04	6.47
Par12 K_{LA}^{\wedge}	$m^3 \cdot mol^{-1}$	1.75E-03	15.80
Par13 K_{HPA}^{\wedge}	$m^3 \cdot mol^{-1}$	Fixed to zero	-
Par14 $k'_{HPA_cat_Amb}(T_{Ref})$	$s^{-1} \cdot kg_dry\ basis\ Amb^{-1}$	4.84E-04	49.37
Par15 $Ea'_{HPA_cat_Amb}$	$J \cdot mol^{-1}$	Fixed to zero	-
Par16 $k_{HPA_noncat}(T_{Ref})$	s^{-1}	1.12E-06	>100%
Par17 Ea_{HPA_noncat}	$J \cdot mol^{-1}$	4.22E+05	23.87
Par18 $K_{BHP-SO3H}$	$m^3 \cdot mol^{-1}$	Fixed to zero	-
Par19 $K_{HPA-SO3H}$	$m^3 \cdot mol^{-1}$	Fixed to zero	-
Par20 $k_{BHP_RuC}(T_{Ref})$	$s^{-1} \cdot kg_dry\ basis\ RuC^{-1}$	2.43E-05	16.96
Par21 Ea_{BHP_RuC}	$J \cdot mol^{-1}$	Fixed to zero	-
Par22 $k_{HPA_RuC}(T_{Ref})$	$s^{-1} \cdot kg_dry\ basis\ RuC^{-1}$	5.80E-05	7.69
Par23 Ea_{HPA_RuC}	$J \cdot mol^{-1}$	Fixed to zero	-
Par24 $K_{\blacksquare BHP}$	$m^3 \cdot mol^{-1}$	Fixed to zero	-
Par25 $K_{\blacksquare HPA}$	$m^3 \cdot mol^{-1}$	Fixed to zero	-
Par26 $k_{BHP_diss}(T_{Ref})$	$m^3 \cdot mol^{-1} \cdot s^{-1}$	1.70E-06	16.83
Par27 Ea_{BHP_diss}	$J \cdot mol^{-1}$	1.06E+05	13.31
Par28 $k_{HPA_diss}(T_{Ref})$	$m^3 \cdot mol^{-1} \cdot s^{-1}$	4.73E-06	6.99
Par29 Ea_{HPA_diss}	$J \cdot mol^{-1}$	6.78E+04	7.96

The correlations between the parameters are shown in Table 4-5. It is observed that $k_{BL_hyd}(T_{Ref})$ and K_{BL}^{\wedge} have a noticeable correlation linked to the estimation of the adsorption constant. Another correlation is between $k_{BHP_noncat}(T_{Ref})$ and Ea_{BHP_noncat} , which would be linked to the slower speed observed in the non-catalytic cyclization pathway.

Figure 4-7 shows the parity plots for BL, LA, BHP, and HPA in the NCLH1.2 model. The figure shows that this model gives a good prediction of the reactant concentrations (BL and LA), while it was less reliable for the intermediates (BHP and HPA).

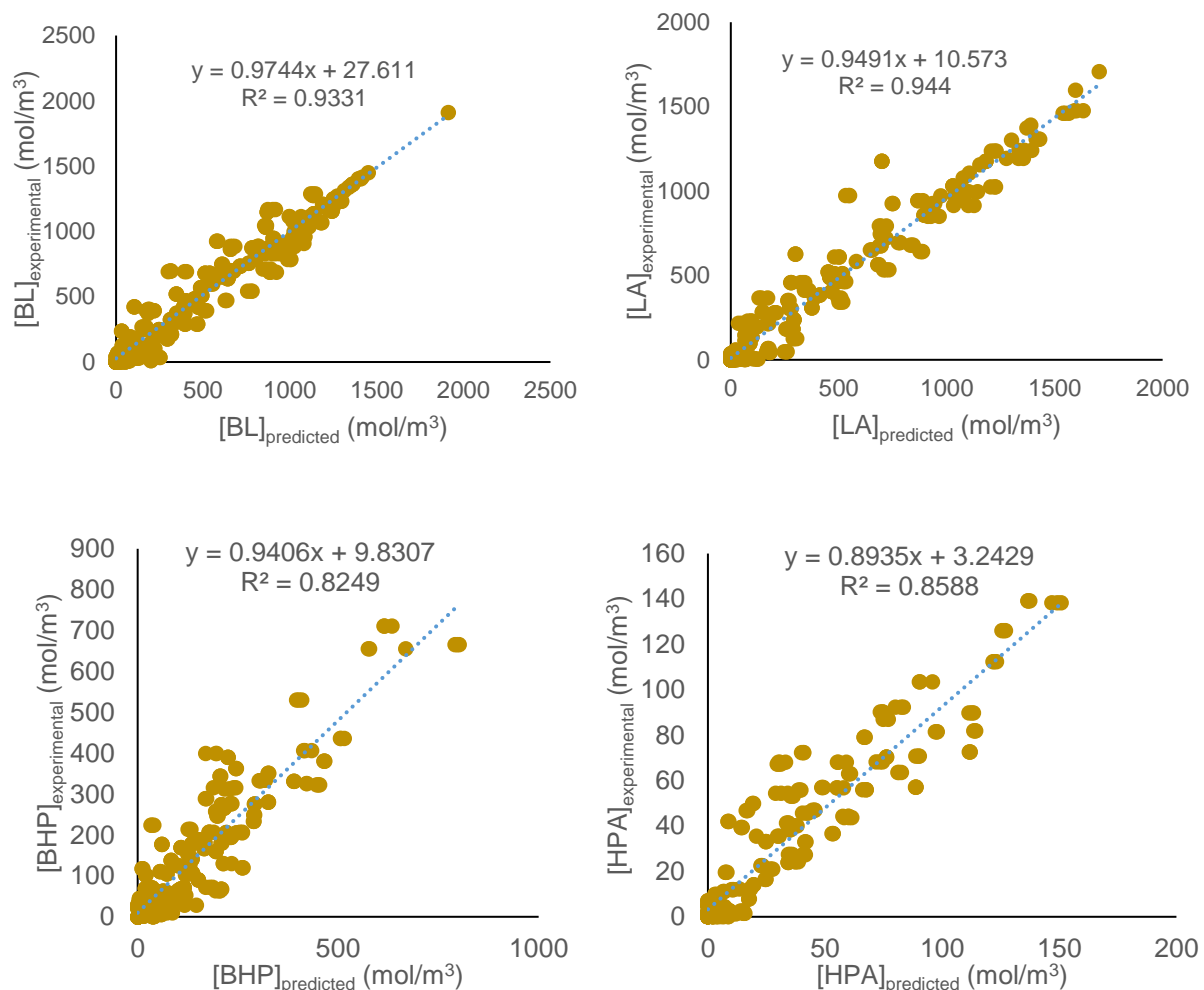


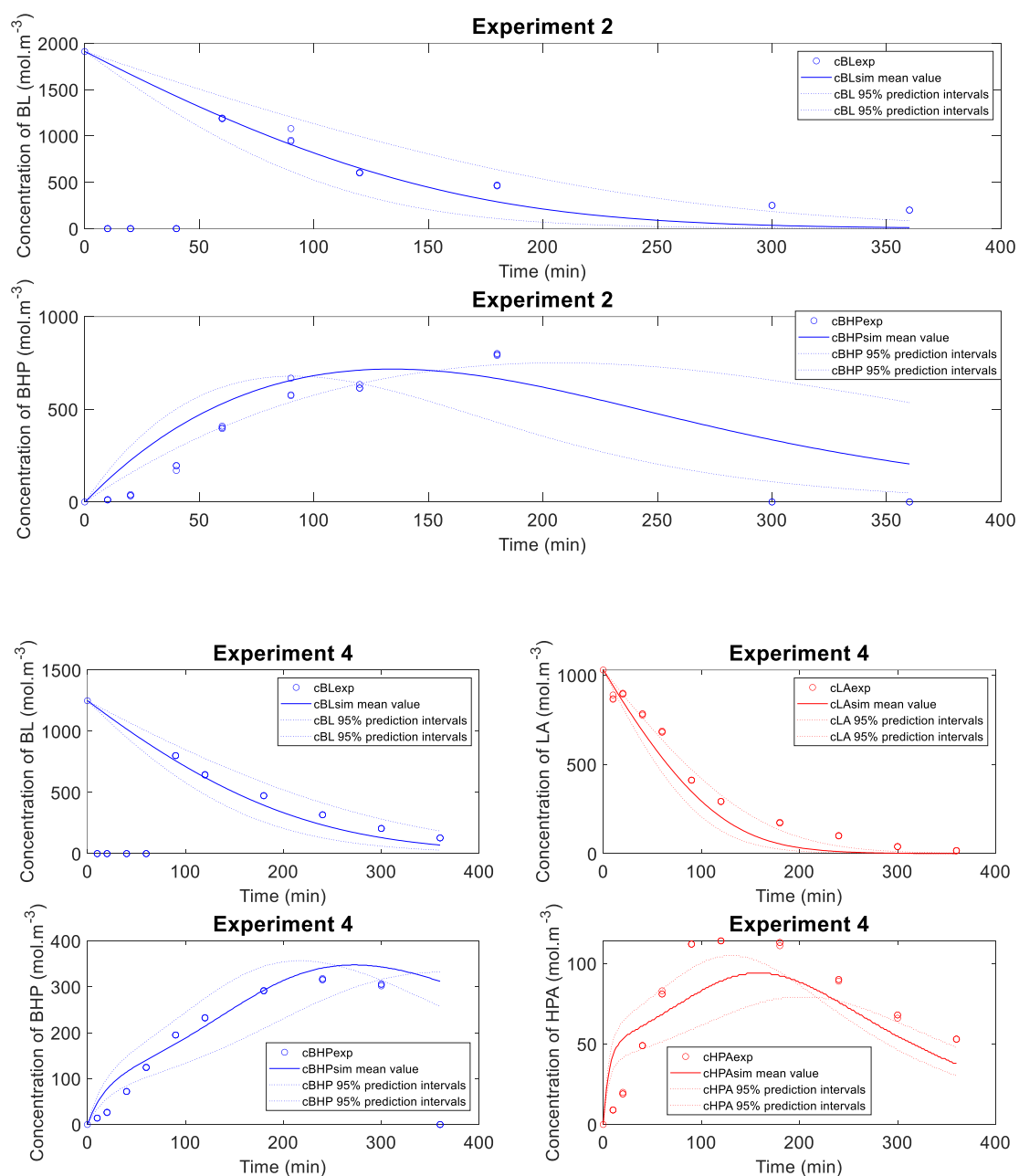
Figure 4-7 - Parity plots for the NCLH1.2 model

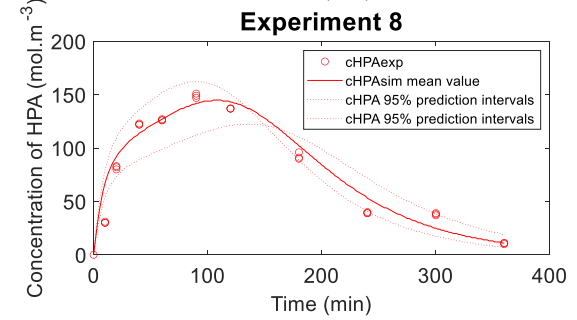
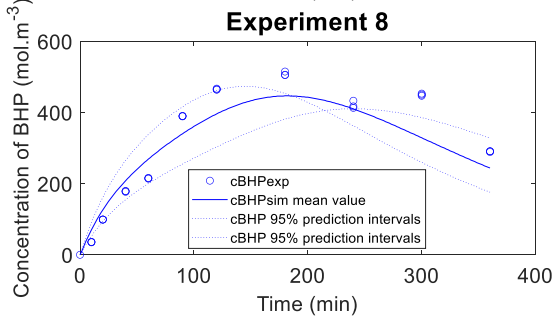
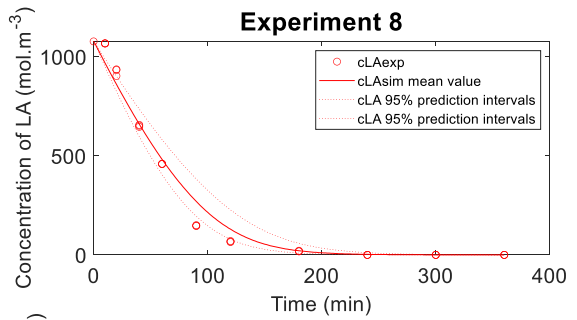
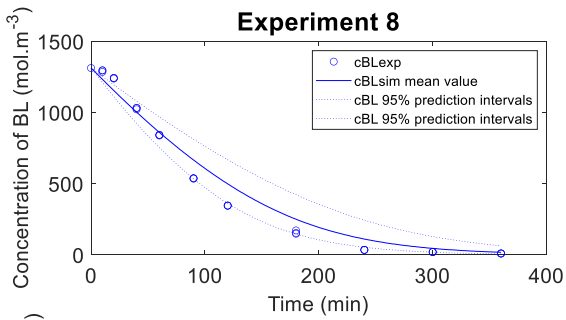
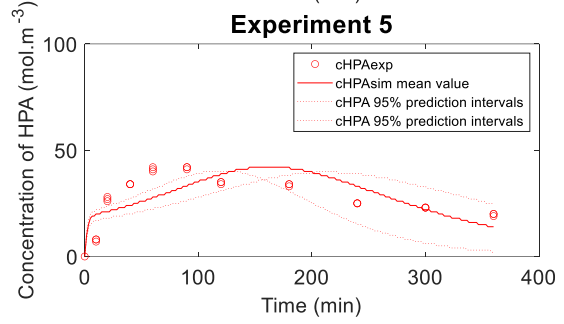
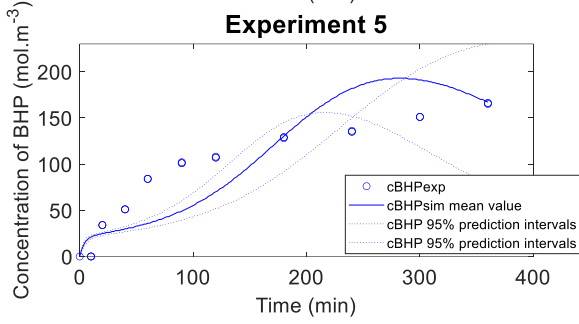
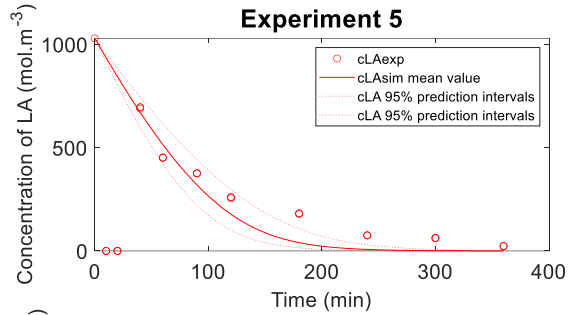
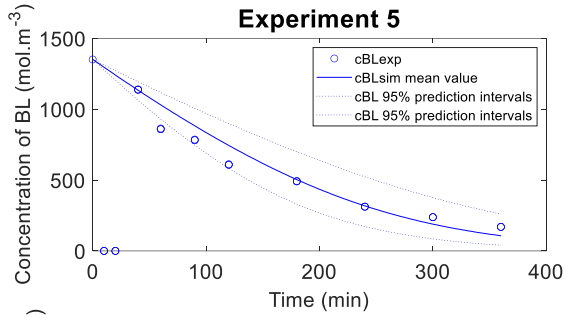
Table 4-5 - Normalized parameter covariance matrix for Model NCLH1.2.

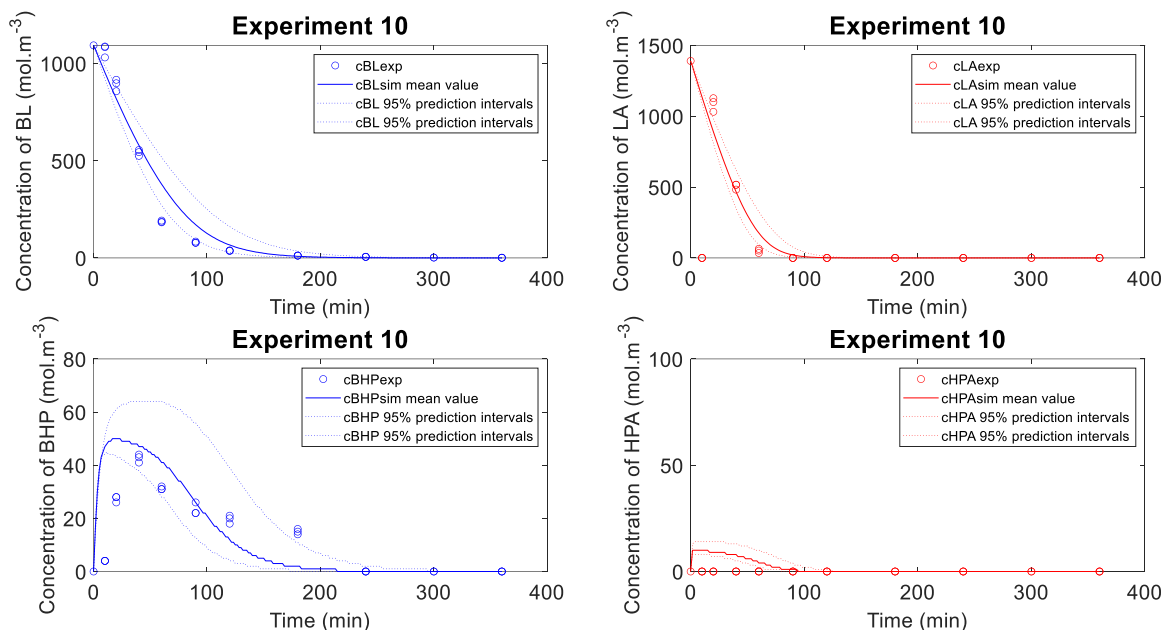
	Par1	Par2	Par3	Par4	Par6	Par8	Par9	Par10	Par11	Par12	Par14	Par16	Par17	Par20	Par22	Par26	Par27	Par28	Par29
Par1	1.000																		
Par2	0.170	1.000																	
Par3	0.453	0.069	1.000																
Par4	0.834	0.160	-0.072	1.000															
Par6	0.029	0.001	0.021	0.017	1.000														
Par8	-0.005	0.112	-0.070	0.035	0.005	1.000													
Par9	-0.028	-0.175	0.049	-0.066	-0.005	-0.932	1.000												
Par10	0.237	0.061	0.644	-0.127	0.002	-0.013	0.017	1.000											
Par11	0.013	0.095	0.039	-0.021	-0.006	-0.033	0.070	0.060	1.000										
Par12	-0.002	0.025	0.114	-0.081	-0.009	0.022	-0.011	0.783	-0.127	1.000									
Par14	0.006	0.001	0.016	-0.003	0.000	0.000	0.000	0.012	0.005	-0.006	1.000								
Par16	-0.009	-0.013	-0.033	0.012	0.002	0.012	-0.024	-0.019	-0.311	0.067	-0.002	1.000							
Par17	0.021	0.009	0.051	-0.008	0.000	-0.012	0.018	0.015	0.210	-0.060	0.002	-0.948	1.000						
Par20	0.061	0.074	0.052	0.066	0.002	-0.728	0.593	0.067	-0.014	0.059	0.000	0.006	-0.003	1.000					
Par22	0.096	0.029	0.187	0.002	0.005	-0.043	0.046	0.113	0.234	0.099	-0.005	-0.314	0.256	0.013	1.000				
Par26	0.102	-0.083	-0.123	0.140	-0.044	-0.085	0.084	0.170	0.261	0.166	0.006	-0.085	0.046	-0.123	-0.065	1.000			
Par27	0.112	0.327	0.088	0.096	-0.011	0.129	-0.245	0.217	0.392	0.130	0.005	-0.118	0.077	0.133	0.080	0.328	1.000		
Par28	-0.188	-0.006	-0.261	-0.082	-0.019	0.059	-0.031	0.305	0.189	0.377	0.005	-0.165	0.078	0.001	-0.368	0.381	0.187	1.000	
Par29	0.009	0.053	0.046	-0.027	-0.005	-0.030	0.061	0.140	0.764	0.042	0.000	-0.442	0.295	-0.004	0.398	0.207	0.310	0.292	1.000

Figure 4-8 shows the fits of the model to experimental data, along with the predicted intervals and the mean values of these estimated observables. One can observe that the experimental data lies within the margins of the predicted values of the model, implying a good fit. However, due to the catalytic effect of Amberlite IR-120, the concentrations of the intermediates were quite low.

Figure 4-8 - Fit of Model NCLH1.2 to the experimental concentrations with prediction intervals.







4.6.2. Modeling results: Non-competitive Langmuir Hinshelwood 2.2

Table 4-6 shows the values for the estimated parameters and their credible intervals. In the case of $k_{HPA_noncat}(T_{Ref})$, the credible interval was higher than the other parameters, given the high reactivity of HPA. The 95% HPD credible intervals for most parameters were considered low or average. The estimation of K_H and K_{BL} was not successful, hence, their values were set to zero. One can observe that BL's hydrogenation rate constant is lower than that of LA. Also, the cyclization rate constants for BHP reaction routes (Ru/C, Amberlite IR-120, and LA dissociation) are lower compared to the rate constants for HPA.

Table 4-6 - Estimated Values at $T_{ref} = 392.72\text{ K}$ and Statistical Data for NCLH2.2

	Parameters	Units	Estimates	HPD%
Par1	$k_{BL,hyd}(T_{Ref})$	$\text{m}^3.\text{mol}^{-1}.\text{s}^{-1}.\text{kg}_{dry}$ basis_{RuC}^{-1}	3.02E-06	11.42
Par2	$Ea_{BL,hyd}$	$\text{J}.\text{mol}^{-1}$	3.69E+04	7.17
Par3	K_H	$\text{m}^3.\text{mol}^{-1}$	Fixed to zero	-
Par4	K_{BL}^{\wedge}	$\text{m}^3.\text{mol}^{-1}$	Fixed to zero	-
Par5	K_{BHP}^{\wedge}	$\text{m}^3.\text{mol}^{-1}$	Fixed to zero	-
Par6	$k'_{BHP_cat_Amb}(T_{Ref})$	$\text{s}^{-1}.\text{kg}_{dry}\text{ basis}_{Amb}^{-1}$	4.36E-05	48.29
Par7	$Ea'_{BHP_cat_Amb}$	$\text{J}.\text{mol}^{-1}$	Fixed to zero	-
Par8	$k_{BHP_noncat}(T_{Ref})$	s^{-1}	5.93E-05	30.40
Par9	Ea_{BHP_noncat}	$\text{J}.\text{mol}^{-1}$	7.78E+04	35.92
Par10	$k_{LA,hyd}(T_{Ref})$	$\text{m}^3.\text{mol}^{-1}.\text{s}^{-1}.\text{kg}_{dry}$ basis_{RuC}^{-1}	7.75E-06	9.17
Par11	$Ea_{LA,hyd}$	$\text{J}.\text{mol}^{-1}$	4.61E+04	6.51
Par12	K_{LA}°	$\text{m}^3.\text{mol}^{-1}$	1.69E-03	15.86
Par13	K_{HPA}°	$\text{m}^3.\text{mol}^{-1}$	Fixed to zero	-
Par14	$k'_{HPA_cat_Amb}(T_{Ref})$	$\text{s}^{-1}.\text{kg}_{dry}\text{ basis}_{Amb}^{-1}$	4.79E-04	49.34
Par15	$Ea'_{HPA_cat_Amb}$	$\text{J}.\text{mol}^{-1}$	Fixed to zero	-
Par16	$k_{HPA_noncat}(T_{Ref})$	s^{-1}	1.25E-06	>100%
Par17	Ea_{HPA_noncat}	$\text{J}.\text{mol}^{-1}$	4.15E+05	24.08
Par18	$K_{BHP-SO3H}$	$\text{m}^3.\text{mol}^{-1}$	Fixed to zero	-
Par19	$K_{HPA-SO3H}$	$\text{m}^3.\text{mol}^{-1}$	Fixed to zero	-
Par20	$k_{BHP_RuC}(T_{Ref})$	$\text{s}^{-1}.\text{kg}_{dry}\text{ basis}_{RuC}^{-1}$	2.41E-05	17.61
Par21	Ea_{BHP_RuC}	$\text{J}.\text{mol}^{-1}$	Fixed to zero	-
Par22	$k_{HPA_RuC}(T_{Ref})$	$\text{s}^{-1}.\text{kg}_{dry}\text{ basis}_{RuC}^{-1}$	5.74E-05	7.61
Par23	Ea_{HPA_RuC}	$\text{J}.\text{mol}^{-1}$	Fixed to zero	-
Par24	$K_{\blacksquare BHP}$	$\text{m}^3.\text{mol}^{-1}$	Fixed to zero	-
Par25	$K_{\blacksquare HPA}$	$\text{m}^3.\text{mol}^{-1}$	Fixed to zero	-
Par26	Kc	$\text{m}^{9/2}.\text{mol}^{-3/2}$	1.59E-04	25.39
Par27	Kc2	$\text{m}^{9/2}.\text{mol}^{-3/2}$	Fixed to zero	-
Par28	$k_{BHP_diss}(T_{Ref})$	$\text{m}^3.\text{mol}^{-1}.\text{s}^{-1}$	1.69E-06	16.19
Par29	Ea_{BHP_diss}	$\text{J}.\text{mol}^{-1}$	1.09E+05	12.83
Par30	$k_{HPA_diss}(T_{Ref})$	$\text{m}^3.\text{mol}^{-1}.\text{s}^{-1}$	4.73E-06	6.71
Par31	Ea_{HPA_diss}	$\text{J}.\text{mol}^{-1}$	6.70E+04	8.01

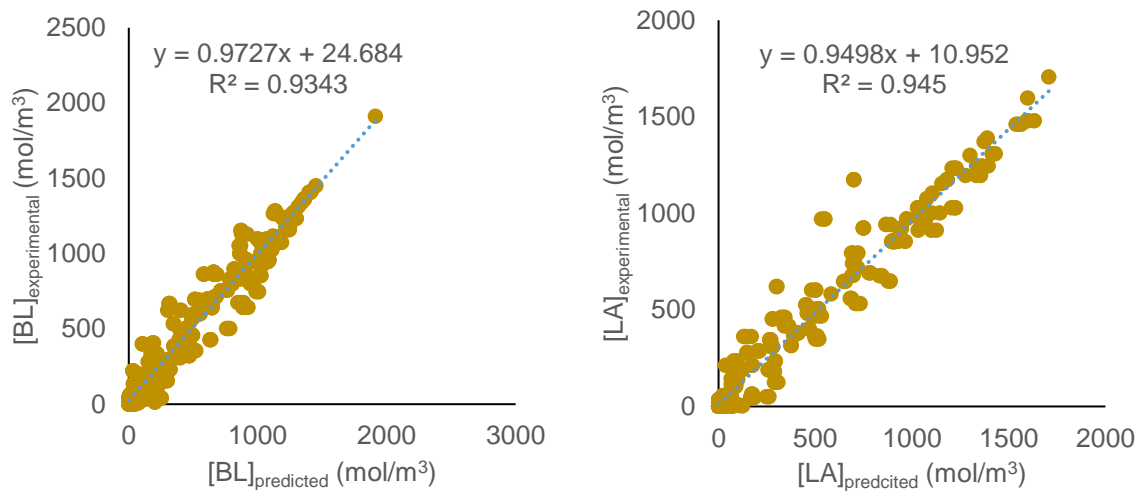
Table 4-7 - Normalized parameter covariance matrix for Model NCLH2.2

	Par1	Par2	Par6	Par8	Par9	Par10	Par11	Par12	Par14	Par16	Par17	Par20	Par22	Par26	Par28	Par29	Par30	Par31
Par1	1.000																	
Par2	0.190	1.000																
Par6	0.026	0.002	1.000															
Par8	0.113	0.165	0.011	1.000														
Par9	-0.163	-0.234	-0.011	-0.931	1.000													
Par10	-0.074	0.025	-0.017	0.035	-0.007	1.000												
Par11	-0.012	0.081	-0.008	-0.044	0.083	0.040	1.000											
Par12	-0.062	0.021	-0.013	0.025	-0.009	0.933	-0.139	1.000										
Par14	-0.002	0.000	0.000	0.001	-0.001	0.002	0.005	-0.008	1.000									
Par16	0.009	-0.007	0.003	0.014	-0.027	0.006	-0.300	0.073	-0.001	1.000								
Par17	-0.005	0.003	-0.001	-0.011	0.019	-0.026	0.196	-0.066	0.001	-0.946	1.000							
Par20	-0.020	0.019	-0.001	-0.768	0.635	0.044	-0.001	0.051	-0.001	0.002	-0.002	1.000						
Par22	-0.002	0.010	0.001	-0.035	0.042	-0.009	0.229	0.079	-0.008	-0.308	0.242	0.010	1.000					
Par26	0.970	0.209	0.023	0.117	-0.174	-0.102	-0.027	-0.077	-0.002	0.013	-0.007	0.006	0.000	1.000				
Par28	0.142	-0.110	-0.045	-0.106	0.109	0.342	0.273	0.193	0.008	-0.089	0.049	-0.106	-0.043	0.088	1.000			
Par29	0.137	0.356	-0.007	0.211	-0.329	0.207	0.375	0.121	0.003	-0.106	0.064	0.058	0.061	0.167	0.265	1.000		
Par30	-0.064	0.017	-0.016	0.036	-0.009	0.639	0.202	0.423	0.009	-0.176	0.087	0.015	-0.335	-0.090	0.376	0.214	1.000	
Par31	-0.024	0.039	-0.008	-0.040	0.074	0.139	0.762	0.030	-0.001	-0.431	0.277	0.007	0.394	-0.037	0.219	0.294	0.315	1.000

Table 4-7 displays the covariance matrix for the NCLH2.2 model, highlighting the correlations between the estimated parameters. From the table, one can notice that some parameters present a significant correlation: $k_{BL_{hyd}}(T_{Ref})$ with K_C ; $k_{LA_{hyd}}(T_{Ref})$ with K_{LA° ; $k_{BHP_{noncat}}(T_{Ref})$ with $Ea_{BHP_{noncat}}$; and $k_{HPA_{noncat}}(T_{Ref})$ with $Ea_{HPA_{noncat}}$.

As the previous model, the correlations between the non-catalytic cyclization constants, $k_{BHP_{noncat}}(T_{Ref})$ and $k_{HPA_{noncat}}(T_{Ref})$, with their activation energies is linked to slow speed compared to the faster catalytic pathways. The difficulties to estimate the adsorption constants, K_C and K_{LA° , would indicate the high correlation with the hydrogenation constants.

Figure 4-9 shows the parity plots for BL, LA, BHP, and HPA. As noted in model NCLH1.2, the prediction of the observables for the reactants is better than those of the intermediates. A relatively high dispersion is still observed in the estimation of the intermediates. The parity plots of this model compared to the NCLH1.2 model shows a better predictability on the concentrations for BL, LA, BHP, and HPA.



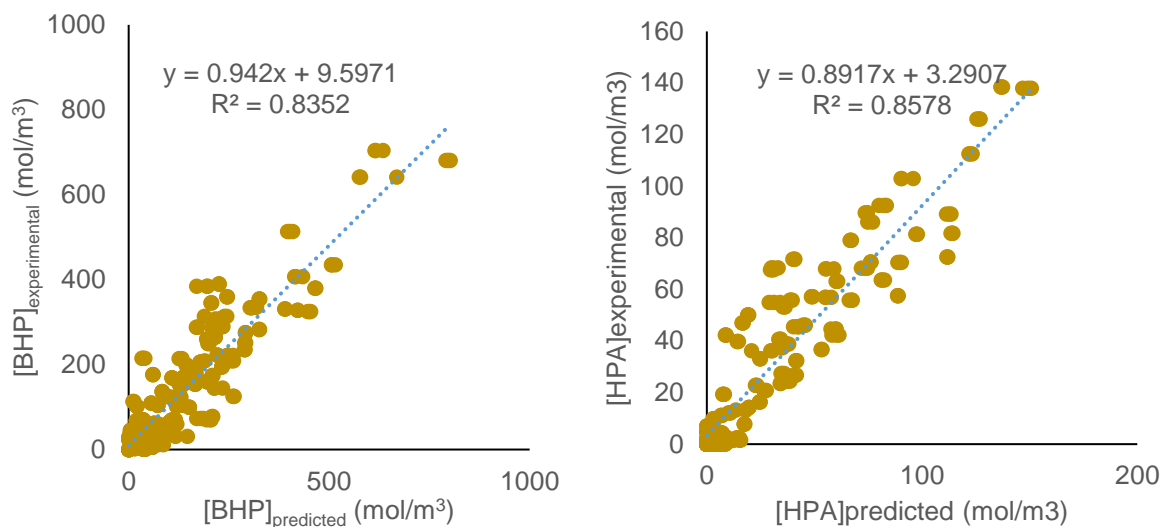
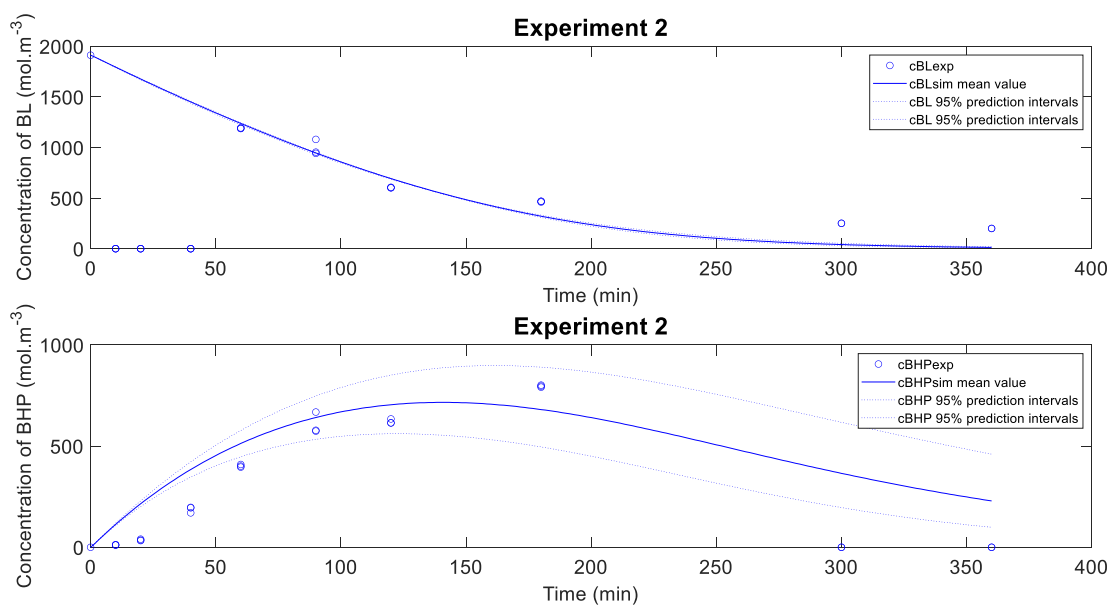


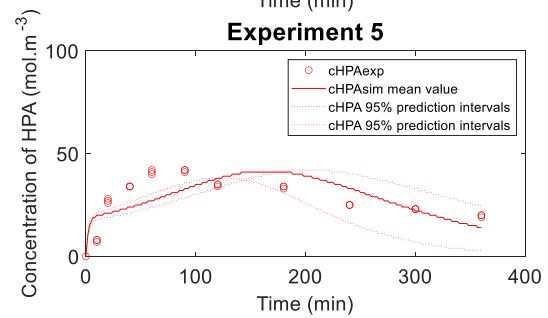
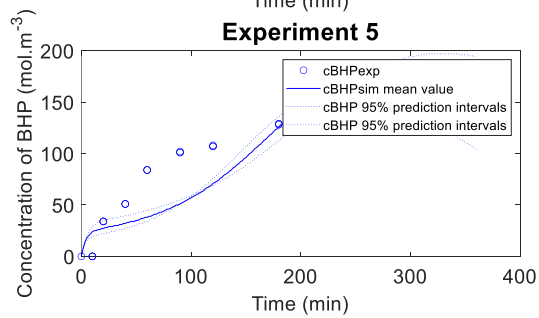
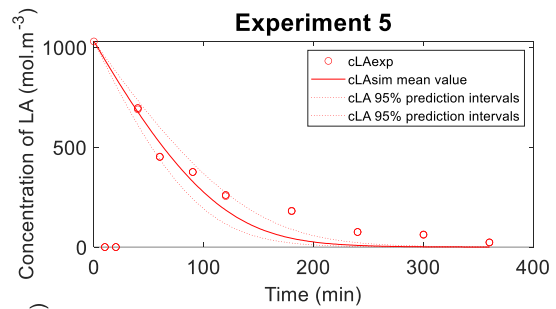
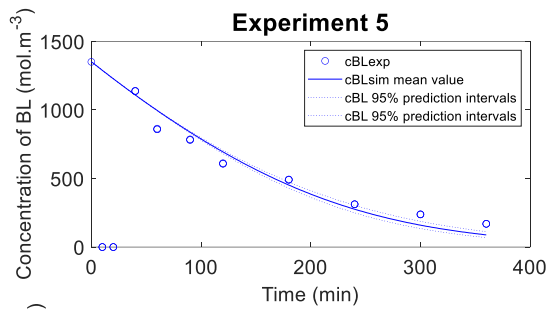
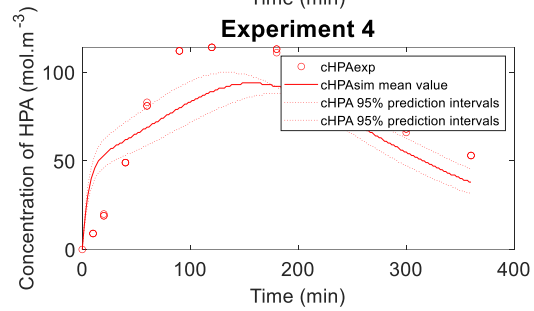
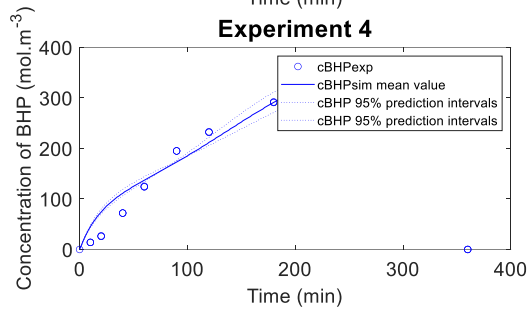
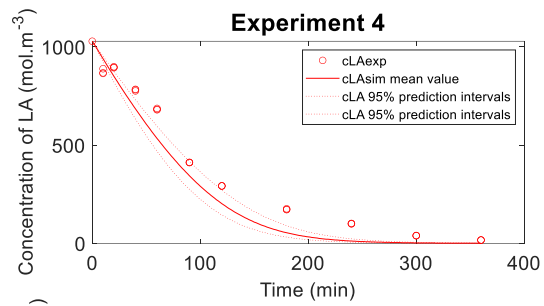
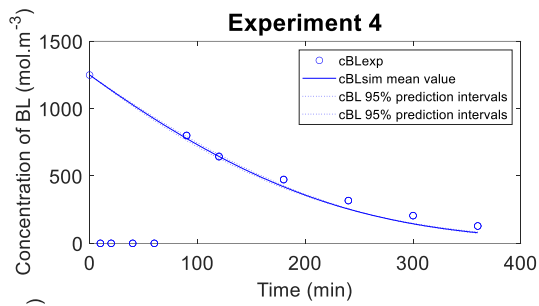
Figure 4-9 - Parity plots for concentrations with the NCHL2.2 modeling results.

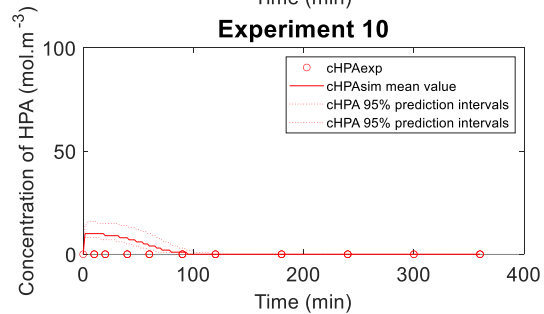
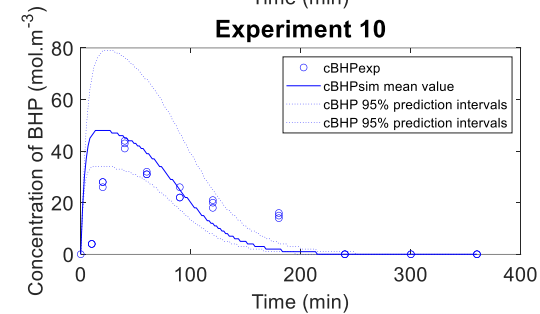
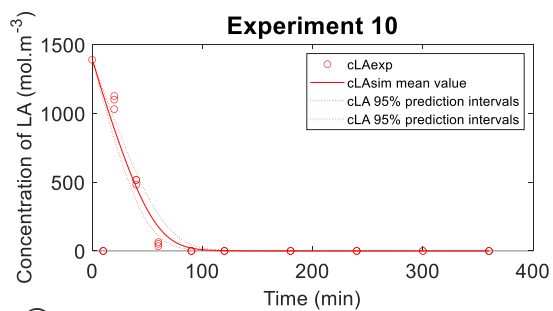
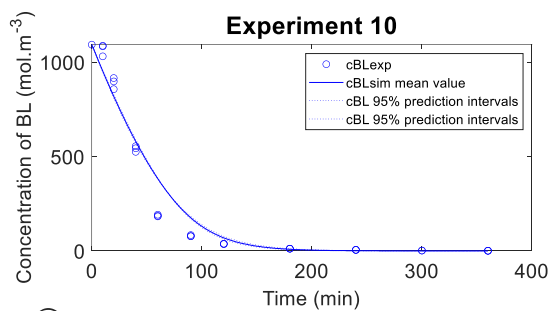
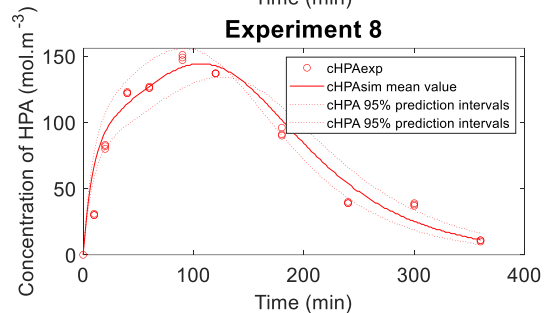
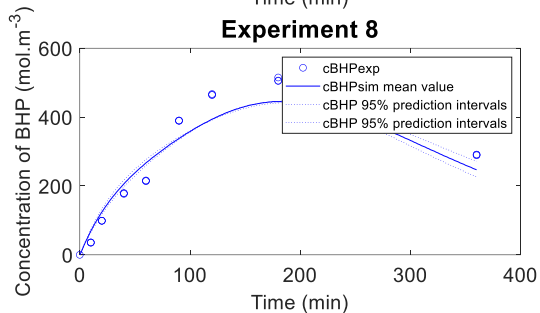
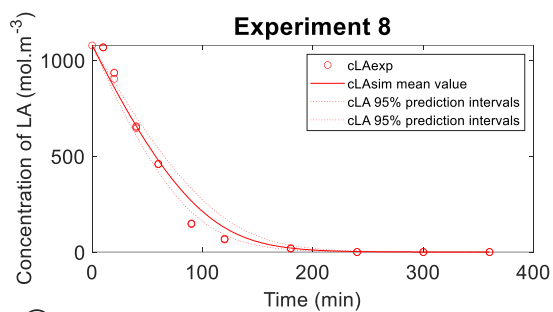
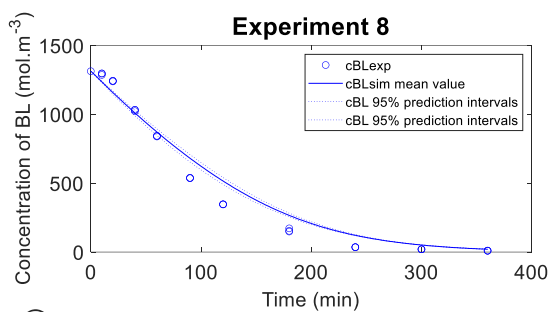
Figure 4-10 shows the model's fit to the experimental data and the 95% confidence interval. Comparing the fit of this model to the NCLH1.2 model, the concentrations estimations are similar but the estimation of the concentrations for the intermediates is slightly better for this model. This model estimates narrower prediction intervals compared to the previous model.

Figure 4-10 - Fit of Model NCLH2.2 with prediction intervals to the experimental concentrations.



Production of γ -valerolactone, a green platform molecule





Comparing both models, the results are similar even if the NCLH2.2 model might have a slightly better fitting to the experimental data. A method to estimate the reliability of the models is needed, as the results obtained might not be enough for discern the better model.

4.7. Cross-validation: K-fold method

An approach to evaluate which model would be the most reliable to describe the experimental data is cross-validation (Slotboom et al., 2020). Here, the experiments were randomly arranged in 7 groups (folds) of 2 experiments each. In this method, six folds are used to perform a regression of each model, then the obtained model is used to predict the remaining fold. These folds are presented in Table 4-9

Table 4-8 - Distribution of the 14 experiments in the seven folds

FOLD	EXPERIMENTS
Fold 1	10
Fold 2	11
Fold 3	14
Fold 4	9
Fold 5	8
Fold 6	1
Fold 7	13
Fold 8	7
Fold 9	12
Fold 10	2
Fold 11	6
Fold 12	4
Fold 13	5
Fold 14	3

Table 4-9 - Different sets for regression and validation.

Set	Regression/Train	Validation/Test
Set 1	Folds 1-2-3-4-5-6	Fold 7
Set 2	Folds 7-1-2-3-4-5	Fold 6
Set 3	Folds 6-7-1-2-3-4	Fold 5
Set 4	Folds 5-6-7-1-2-3	Fold 4
Set 5	Folds 4-5-6-7-1-2	Fold 3
Set 6	Folds 3-4-5-6-7-1	Fold 2
Set 7	Folds 2-3-4-5-6-7	Fold 1

The kinetic constants in every set were estimated from the regression, and these values were compared with the model in the validation step. The fit of each model was obtained by the average of the sum of least squares $CV_{(K)}$:

$$CV_{(K)} = \frac{1}{7} \cdot \sum_{K=1}^7 (Y_{i,experimental} - Y_{i,simulated})_K^2 \quad (76)$$

As in the AIC, models with the lower $CV_{(K)}$ value have better fits to experimental data. The results are shown in Table 4-10, where the CV and standard deviation indicate that the more repeatable models are indeed the NCLH1.2 and NCLH2.2 models. The standard deviation results show that the models had a similar result in the validation steps.

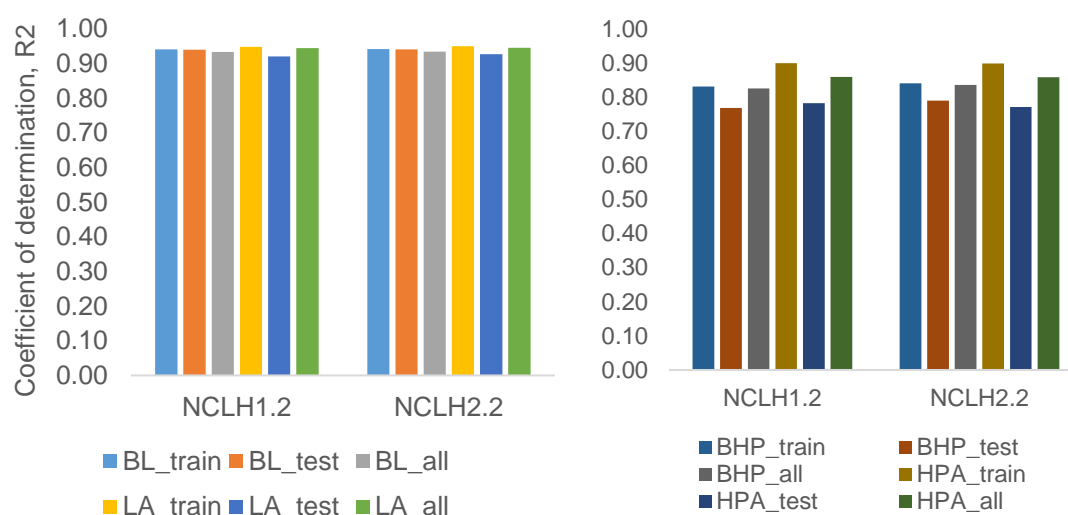
Table 4-10 - $CV_{(K)}$ and standard deviation for each model

	$CV_{(K)}$	$SD(CV_{(K)})/\%$
LH1	3 586 050	99.88
LH2	3 656 893	93.19
NCLH1.1	3 635 269	94.19
NCLH1.2	2 168 016	28.66
ER1	3 595 498	95.09
NCLH2.1	3 690 655	92.00
NCLH2.2	1 978 294	27.47

The estimated values of the parameters in each regression are displayed in the supplementary data in (Delgado et al., 2022), for the NCLH1.2 and NCLH2.2 models. The values obtained for each parameter from the regressions in the cross-validation were similar to those obtained without segmenting the data into sets shown in Table 4-4 and Table 4-6.

To validate the models, the coefficients of determination for each step of the cross-validation, namely the training, the set, and all data, are compared and shown in Figure 4-11. Since the results are similar, the models can be considered validated.

Figure 4-11 - Coefficient of determinations for training, test, and all for the different models.



4.8. Conclusions and perspectives

This chapter explored the production of GVL by the hydrogenation of BL in the presence of LA and a dual catalytic system consisting of Ru/C and Amberlite IR-120 catalysts.

As levulinic acid is generated as a side product during the production of alkyl levulinates from, via fructose alcoholysis, the effect of this compound in the hydrogenation of BL was also studied. An acidic catalyst, Amberlite IR-120, was also incorporated into the reaction mixture to improve the kinetics in the secondary step in the reaction scheme i.e., the cyclization reaction. It was observed that the kinetics in the cyclization reaction step was increased in the presence of levulinic acid, and Amberlite IR120.

Bayesian inference and K-fold cross-validation methods were used for the evaluation and assessment of the modeling results. Seven kinetic models were tested, and the results were evaluated via Bayesian statistics and cross validation. These models considered the effect of acid sites in both catalysts, the protons liberated in the dissociation of LA and the possibility of a non-catalyzed reaction pathway in the cyclization reaction. The seven models compared different mechanisms for the hydrogenation reaction step and the models with the best fit where the non-competitive Langmuir Hinshelwood catalytic models with different adsorptive sites for BL, LA, and hydrogen. Either model with and without dissociation of hydrogen (NCLH1.2 and NCLH2.2) produced good results which are in coherence with the previous results in Chapter 3 - .

The results show that the hydrogenation of alkyl levulinate with levulinic acid would be possible from the alcoholysis process. The adsorption mechanism should be better explored in further research.

Chapter 5 - Substituent effect on Reaction Enthalpies for the hydrogenation of alkyl levulinates into γ -valerolactone

Part of this chapter is adapted from the following article: J. Delgado et al., “Reaction enthalpies for the hydrogenation of alkyl levulinates and levulinic acid on Ru/C– influence of experimental conditions and alkyl chain length”, *Process Safety and Environmental Protection*, Vol 171, 2023, Pages 289-298, ISSN 0957-5820, <https://doi.org/10.1016/j.psep.2023.01.025>.

Further permissions related to the material excerpted should be directed to Elsevier. Copyright © 2023 Elsevier.

5.1. Introduction

Understanding the reaction enthalpies for chemical processes is essential for safety and energy optimization (Dakkoune et al., 2019; Stoessel, 2008). In terms of process safety, the enthalpy of a chemical reaction influences the severity of a thermal runaway. In addition, this thermodynamic feature is essential for generating effective process flow diagrams in order to identify the optimal operating conditions and enhance energy management.

Biomass valorization poses a challenge in the field of thermodynamics and process safety, as the physicochemical properties of a large number of biomass molecules are not yet known. As existing petrochemical thermodynamic models may not effectively explain biomass-based processes, new thermodynamic models must be generated. Hence, it is essential to obtain correct thermodynamic data and models for these processes. Knowledge of reaction enthalpies is essential for performing an accurate pinch analysis and assists in determining the optimal design in terms of energy usage.

Although several studies have been performed on the choice of catalysts (Dutta et al., 2019; Kuwahara et al., 2017; Liguori et al., 2015; Tang et al., 2014; K. Yan et al., 2013; Z. P. Yan et al., 2009; Y. Yang et al., 2014), kinetic modeling (Capecchi, Wang, Casson Moreno, et al., 2021; Capecchi, Wang, Delgado, et al., 2021; Delgado et al., 2022; Mamun et al., 2017; Piskun et al., 2016; Y. Wang et al., 2019), and some on the physicochemical properties (Ariba et al., 2020; Lomba et al., 2011) or thermal risk assessment. to the best of our knowledge, there are no studies on the evolution of the reaction enthalpies for different substituents in different solvents and temperatures. Such information is crucial to find the optimum process design as well as the best starting materials.

In this Chapter, we focus on the estimation of reaction enthalpies of the production of GVL from the hydrogenation of alkyl levulinates and/or levulinic acid. The influence of different factors on reaction enthalpies, notably the substrate concentration, temperature, and solvent effect, are explored for butyl levulinate as a reference molecule, given that this molecule has higher vapor pressures than other shorter substituent levulinates (Ariba et al., 2020). In the following step, the methodology and calculation of reaction enthalpies for various alkyl levulinates, namely methyl levulinate (ML), ethyl levulinate (EL), n-propyl levulinate (PrL), n-butyl levulinate (BL), and n-pentyl levulinate (PeL) were explored.

Reaction enthalpies were evaluated with the aid of calorimeters, reactors able to track small thermal changes in reaction media. The energy released or absorbed by the reactive media is correlated to the difference of internal energy between the reagents and products, and their physical properties such as heat capacity. Heat of reaction can be obtained by performing an energy balance of the reaction system knowing the thermal properties of the reactive media, the amount of heat transferred through the vessel and the conversion of the reagents. The temperature signal read by the calorimeter allows to determine the heat flow generated by the reaction, which is then converted to the amount of energy transferred per mass or reactive media. This principle is the basis for this Chapter. (Y. Wang et al., 2018)

5.2. Calorimetry

A difference between the enthalpies or energies of the reagents and products is observed whenever a reaction occurs. As the reaction occurs, heat is absorbed from the environment or released. Reaction Calorimeters are thermally well insulated reactors. In calorimetry, the heat transfer is measured between the reactive media and a heating/cooling fluid in an outer jacket of the reactor or into sensors.

5.2.1. Calorimetry measurements

In order to estimate the reaction enthalpies of both reaction steps, two different calorimeters were used. The Tian-Calvet C80 micro-calorimeter was used for the second reaction step, i.e., cyclization; and the Mettler Toledo RC1mx calorimeter was used for the first reaction step, i.e., hydrogenation.

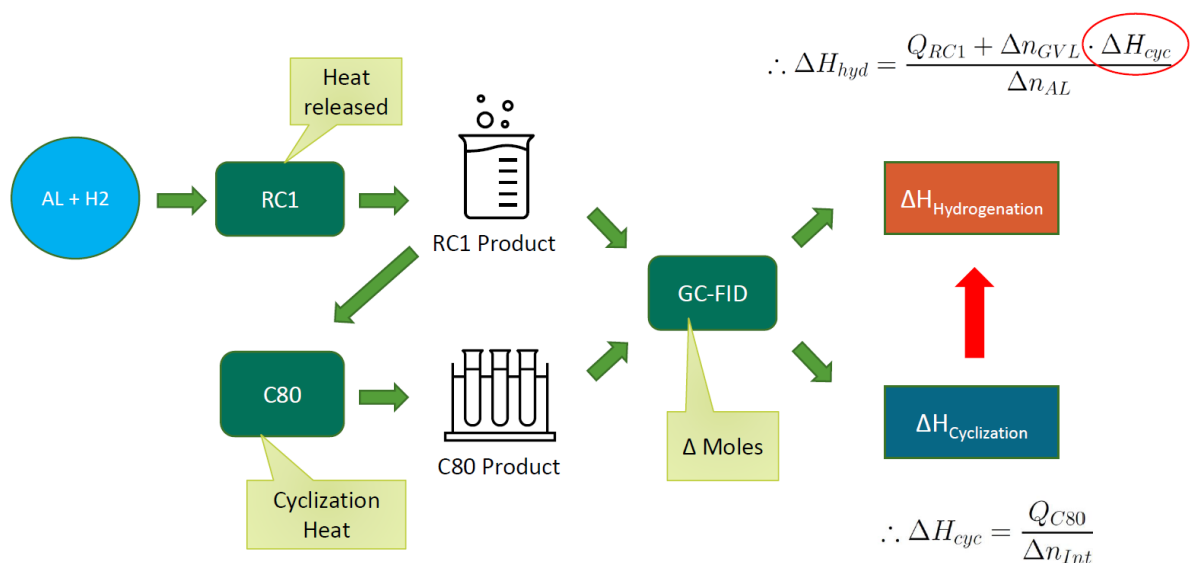


Figure 5-1 - Procedure to estimate hydrogenation and cyclization enthalpies for alkyl levulinates and levulinic acid.

From Figure 5-1, the procedure is as follows, an initial hydrogenation reaction is performed in the RC1, from which the 4-hydroxyalkyl valerate concentrated product is used as a reagent for the C80 calorimeter. Energy exchange is measured by the calorimeters. The concentrations of both products, cyclization, and hydrogenation, is measured before and after the reactions are performed, in order to estimate the difference of moles for the alkyl levulinate and the 4-

hydroxyalkyl levulinates. With the difference of moles and the heat measurement from the C80 reactor, the cyclization enthalpy is measured and subsequently used for the estimation of the hydrogenation enthalpy. This method is required since the RC1 measures the total energy released by the hydrogenation and the cyclization.

Cyclization enthalpy – C80 Calorimeter

In the C80 microcalorimeter, the cells have two different compartments, an inner and annular compartment. In an experiment, the inner compartment of both cells was filled with the sample to analyze. In the annular compartment of the measurement cell, a reactive solution (0.01 mol/L of H₂SO₄ in GVL solvent) was placed while pure GVL solution was placed in the annular compartment of the reference cell Figure 2-3. H₂SO₄ is used to accelerate the cyclization reaction rate. The cells were then introduced into the calorimeter and the operating conditions were set. Once temperature and heat flow between the cells were stable enough, the calorimeter was set to turn 180° periodically, allowing the mixing of the compartments in each cell and start the reaction. All experiments in C80 calorimeter were performed under isothermal conditions.

Hydrogenation enthalpy - RC1 Calorimeter

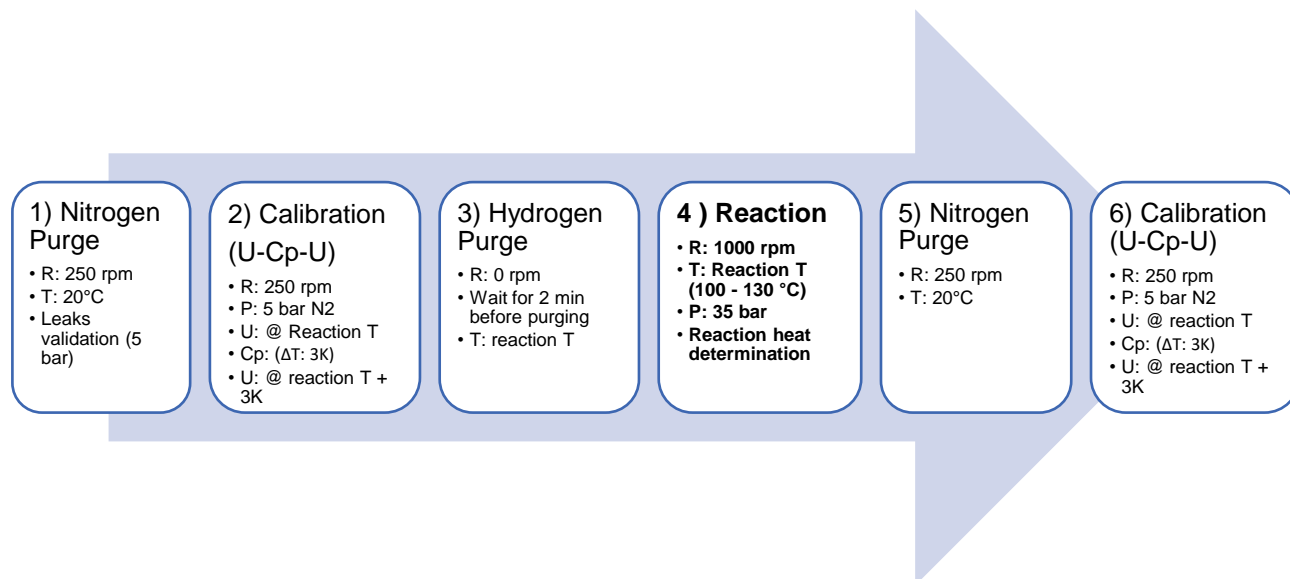


Figure 5-2 – Experimental procedure in RC1 experiments.

Figure 5-2 shows the different steps for experiments carried out in RC1. In an experiment, the reactive media and catalyst were incorporated into the vessel, which was then closed. Later on, stirring was set to 250 rpm.

In step 1, N₂ was used to purge the air from the head of the reactor and filled with 5 bars of N₂. The reaction mixture was then heated to the reaction temperature and an initial calibration (step 2) was performed to estimate the Cp of the reaction mixture and the heat transfer coefficient between reaction mixture and heat-carrier in the reactor's jacket.

The stirrer was then stopped, and the mixture was let to rest for at least two minutes so that the catalyst settled on the bottom of the vessel. This step is crucial because it reduces the possible interaction of H₂ with the catalyst, delaying the start of the reaction in the next step where the head of the reactor is purged with H₂ several times (step 3). When the reactor pressure reached the desired value, stirring was increased to 1000 rpm to initiate the hydrogenation reaction (step

4) and measure the heat transfer in the system. The reactor stirring is limited to 1200 rpm in the RC1 to reduce mechanical risks of the equipment.

Once the reaction heat flow stopped completely, the reactor was cooled down to 20°C. The pressure was removed from the reactor, and a N₂ purge was performed (step 5). The pressure was set to 5 bars of N₂ and the reaction mixture was heated up to the reaction temperature used in step 4. After these conditions were met, a second calibration (step 6) was performed to estimate the Cp and heat transfer coefficient of the product mixture. The product was then cooled down and the pressure was let out from the reactor.

5.2.2. Synthesis of n-propyl levulinate and n-pentyl levulinate by transesterification:

n-propyl levulinate and n-pentyl levulinate were synthesized for research purposes via transesterification as it was not as readily available as other levulinates from the suppliers. According to (Melchiorre et al., 2020), high yields of longer chain levulinates can be obtained from the trans-esterification of ML in the presence of an acid catalyst. A scheme for n-PrL production from transesterification is shown in *Figure 5-3*. The synthesis was performed in a 300mL glass batch reactor coupled to a temperature-regulated water bath, a stirrer, and a water condenser. Figure 2-5

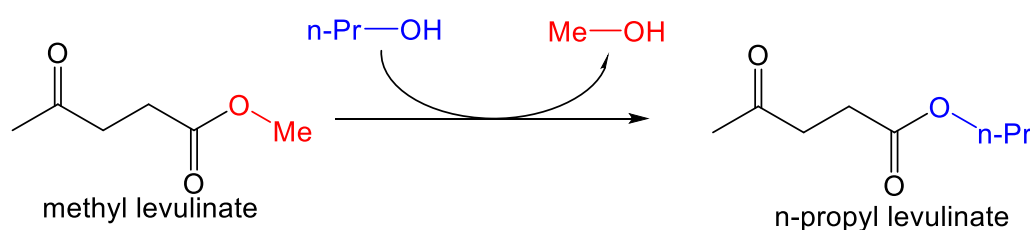


Figure 5-3 – Transesterification of methyl levulinate (ML) into propyl levulinate (n-PrL).

The solid acidic catalyst (Figure 5-4), used in the experiments was a sulphonated resin, Amberlite IR 120 Hydrogen form. This catalyst has been reported to be a high performance and relatively low-cost catalyst (Russo et al., 2020).

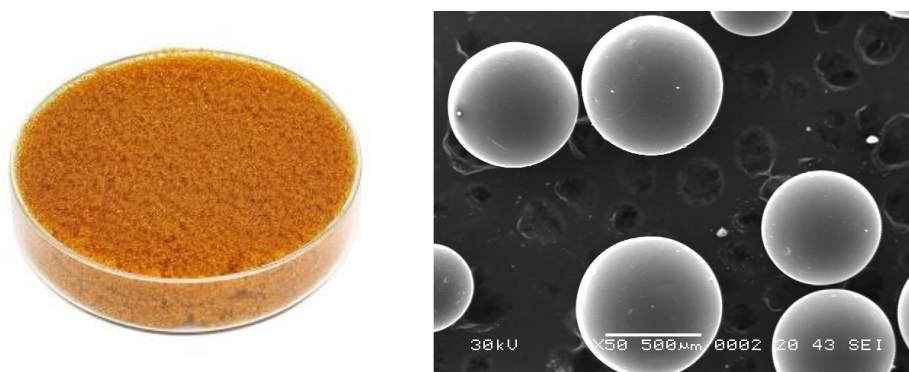


Figure 5-4 - Amberlite IRI20 H form, normal picture of catalyst (left) and SEM image at 500 μ m (right, with permission from (Gawad, 2019))

For the reaction in *Figure 5-3*, pure methyl levulinate solution and Amberlite were added to the reactor and heated to 80°C. Separately, a 3:1 ratio of corresponding alcohol was heated to 80°C and added to the reactor. The experiment lasted for 5 hours after which the product mixture and catalyst were removed and separated. To remove the remaining alcohol from the levulinates mixture, a rotavapor was used (the alcohols were evaporated and separated at 70°C and 100mbar pressure). This operation was repeated until a 1:4 mixture of methyl levulinate: propyl levulinate was obtained. The same method was used for the production of n-pentyl levulinate from the use of ethyl levulinate as reagent.

5.3. Experimental results

The reaction enthalpies were determined in different conditions to observe the influence of different parameters on it. For the hydrogenation of BL, the following parameters were varied: temperature, initial concentration, and solvent. The main goal of the experiments was to study, the effect of the different substituents on the reaction enthalpies at fixed conditions. The reaction mixture consisted of levulinates (ML,EL, PrL, BL, PeL) and levulinic acid (LA).

The hydrogenation enthalpy was measured using the heat signal from the RC1 calorimeter, however, once the hydrogenation reaction took place and intermediates were formed, the cyclization reaction was also started. At this point, the signal in the RC1 included the heat of both reactions and they cannot be directly distinguished from each other. In order to isolate and

measure the reaction enthalpy of the cyclization step, the C80 microcalorimeter was used. The cyclization enthalpy was measured before obtaining the values for the hydrogenation enthalpy.

5.3.1. Cyclization reactions

After performing the hydrogenation of solvent free ML, EL and BL in the RC1, the solutions were stored in a refrigerator. These solutions were highly concentrated in the intermediates MHP, EHP and BHP, which enabled the evaluation of the reaction enthalpy of the cyclization in the calorimetry experiments in the C80 micro-calorimeter. Unfortunately, this approach was not possible for HPA, which is the intermediate of LA hydrogenation, given that HPA was not stable enough.

The reaction enthalpy of cyclization, when using the Tian-Calvet calorimeter C80, can be calculated as:

$$\Delta H_{R,2} = \frac{Q_{measured\ by\ C80}}{n_{Intermediate,0} - n_{Intermediate,final}} \quad (77)$$

where, $Q_{measured\ by\ C80}$ is the energy released or absorbed by the chemical system and determined by the micro-calorimeter C80, and the intermediate concentrations (MHP, EHP, BHP) were analyzed by GC.

Table 5-1. Operating conditions and experimental results for the cyclization experiments in C80 calorimeter in isothermal conditions.

Substrate	Initial substrate concentration (mol/L)	Final substrate concentration (mol/L)	Q_{C80} (J)	T (°C)	$\Delta H_{R,2}$ (kJ/mol)	STD (kJ/mol)
MHP	1.945	0.291	-31.07	60	9.39	0.003
EHP	1.142	0.140	-13.53	60	6.51	0.52
BHP	1.407	0.248	-14.77	60	6.40	0.69

Table 5-1 shows the reaction enthalpy of cyclization for MHP, EHP and BHP as well as their experimental standard deviations. The standard deviation values are low, showing the good repeatability of the experiments. Cyclization is an endothermic reaction, and the values are similar to the ones obtained for EHP and BHP. The cyclization enthalpy for MHP is higher than for EHP showing that the cyclization of MHP is faster and it absorbs more heat than the other levulinates.

As presented in Figure 5-5, the normalized heat-flow rate (78) vs time was used to compare experiments.

$$Q_w = \frac{\text{heat - flow rate due to chemical reaction [mW]}}{\text{Initial concentration of hydroxyalkyl levulinates [mol/L]}} \quad (78)$$

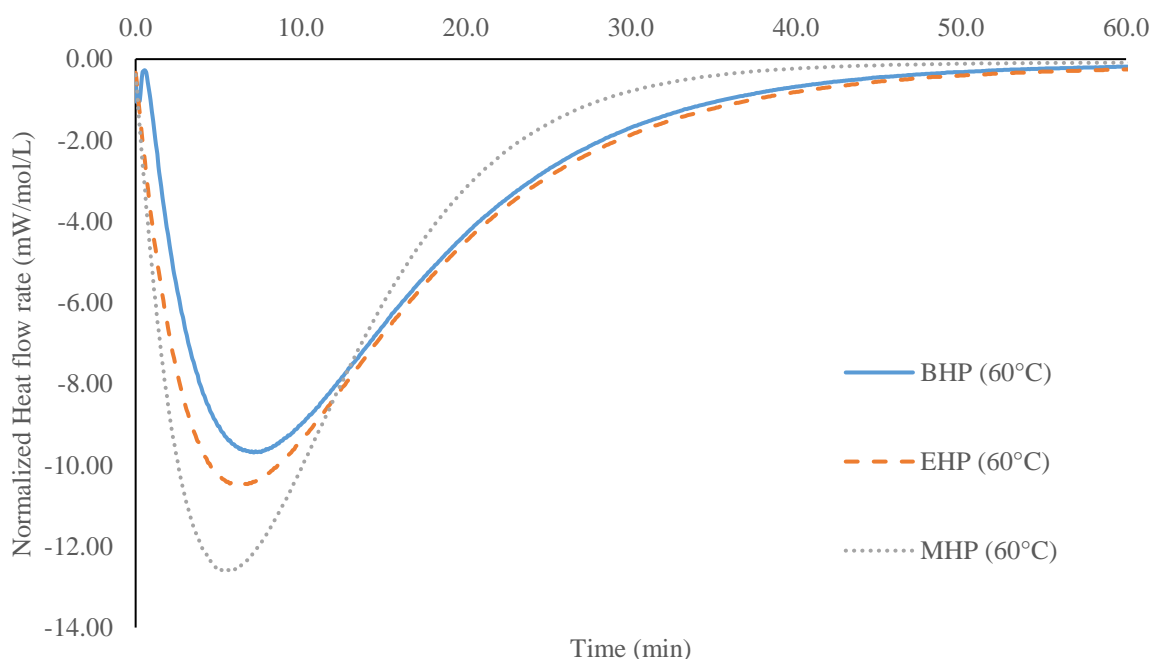


Figure 5-5 - Heat-flow rate normalized by the initial intermediate concentration for the cyclization of MHP, BHP and EHP and with 0.01 mol/L of H_2SO_4 in GVL solvent at 60°C versus time.

5.3.2. Hydrogenation reactions

Calorimetric study for BL

The effect of reaction temperature, substrate concentration and solvents on the enthalpy of hydrogenation ($\Delta H_{R,1}$) of BL were investigated. All experiments were carried out in isothermal conditions without withdrawing any samples during the reaction.

The enthalpy of hydrogenation was expressed as (Y. Wang et al., 2020):

$$\Delta H_{R,1} = \frac{Q_{RC1} + (n_{GVL_{final}} - n_{GVL_0}) * \Delta H_{R,2}}{n_{Substrate_{final}} - n_{Substrate_0}} \quad (79)$$

where, Q_{RC1} is the total energy released or absorbed during the reaction and evaluated by RC1 Mx, n_{GVL} is the number of moles of GVL in the reaction mixture, $n_{substrate}$ is the number of moles of levulinate in the reaction mixture, and $\Delta H_{R,2}$ is the enthalpy of cyclization. The values of $\Delta H_{R,2}$ shown in Table 5-1 were found to be less sensitive to solvent or temperature. Also, the values for the cyclization reaction enthalpy were found to be around four times lower than the hydrogenation step.

Hydrogenation in the absence of Ru/C catalyst

The hydrogenation in the absence of Ru/C catalyst i.e., a blank experiment, was performed in RC1. Figure 5-6 shows the evolution of the heat-flow rate in the absence of the catalyst. In the first stage, the heat-flow rate decreases due to the temperature difference between the gaseous and liquid phase, then a slight exothermic phenomenon, due to the heat of solubilization of H₂ can be seen. One can notice that the heat-flow rate is negligible compared to experiments performed in the presence of the Ru/C catalyst, Figure 5-7. As such, the heat of mixing and heat of solubilization could be neglected. The concentration of BL did not change, and no other products were observed in the analytical results.

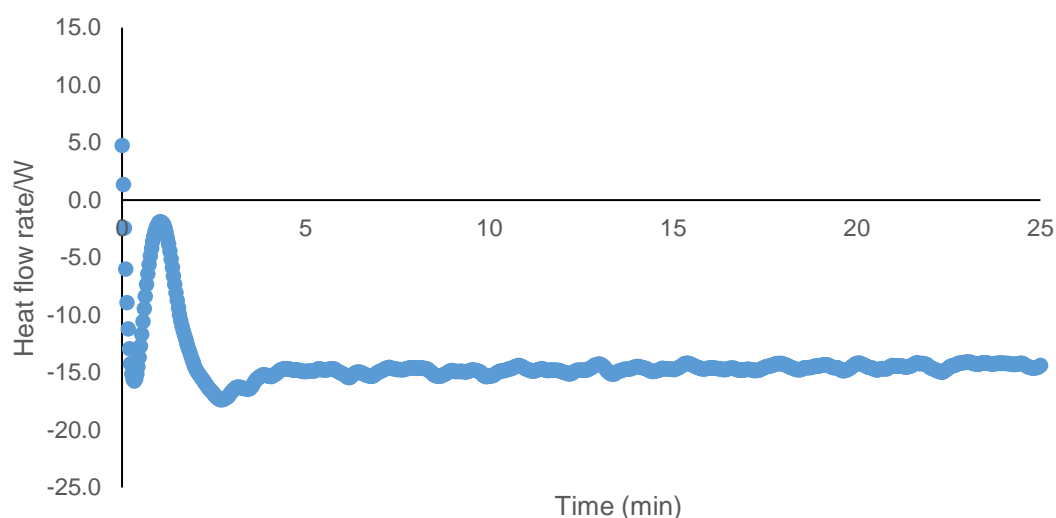


Figure 5-6 - Evolution of heat-flow rate for BL hydrogenation at 130°C, 35 bars of hydrogen and with an initial BL concentration of 2.03 mol/L in GVL solvent.

Effect of Temperature

The effect of temperature on the enthalpy of hydrogenation was evaluated for the hydrogenation of BL in GVL solvent. Table 5-2 summarizes the values obtained from GC analysis and RC1 calorimeter. Contrary to cyclization, hydrogenation is exothermic.

One can notice that reaction enthalpy evaluated at 100°C and 130°C are similar with a range of 2.57kJ/mol in all experiments. Thus, the temperature does not significantly affect the hydrogenation enthalpy for this system in the studied temperature range. Generally, for great increases of temperature, enthalpy may change since it has a direct dependence to temperature from Kirchhoff's Law, correlating enthalpy with temperature and heat capacity. Also, one could assume that the heat capacity does not strongly depend on temperature between 100°C and 130°C as it was found that the heat capacity had a mean value of 2.313 J/g*K with a 0.04437 J/g*K standard deviation taking in account the values measured in the calibration steps.

Figure 5-7 shows the evolution of the heat-flow due to chemical reaction released during the hydrogenation of BL. The results are presented in Figure 5-7, which shows that the kinetics is faster at a higher temperature.

Table 5-2. GC and RCI results for experiments in isothermal conditions at different temperatures for the hydrogenation of BL in GVL solvent at 35 bars of hydrogen.

Temperature (°C)	Total mass (g)	Cat. mass* (g)	[BL] initial (mol/L)	[BL] final (mol/L)	[GVL] initial (mol/L)	[GVL] final (mol/L)	$\Delta H_{R,1}$ (kJ/mol)	STD $\Delta H_{R,1}$ (kJ/mol)
130	551.0	6.3	2.050	0.010	6.661	8.607	-35.58	0.86
100	551.0	6.3	2.043	0.013	7.049	8.142	-35.27	1.29

*Including 50% of water

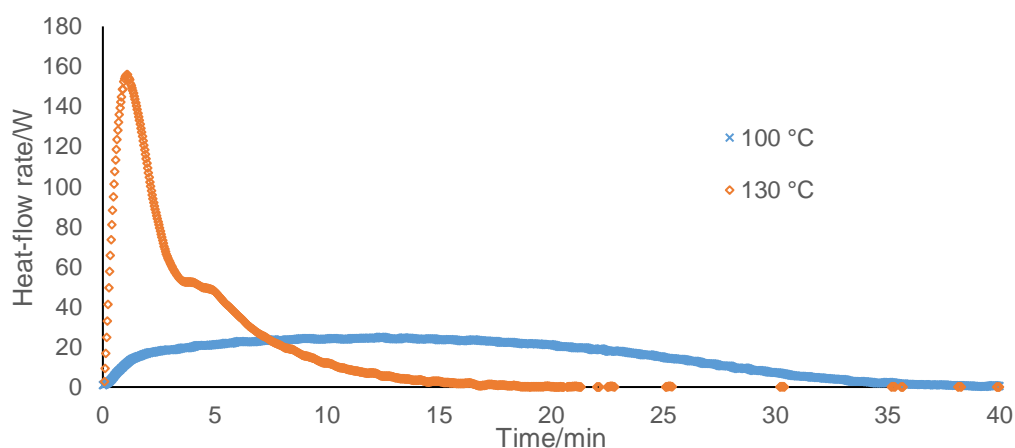


Figure 5-7 - Heat-flow rate evolution for the hydrogenation of BL in GVL solvent at different temperatures.

Effect of initial concentration

The initial concentration of BL could not affect the enthalpy of hydrogenation. Table 5-3 shows that the reaction enthalpy slightly decreases when BL concentration increases. Nevertheless, this slight change can be neglected and is within measurement uncertainty. Surprisingly, the initial concentration of BL does not affect the maximum heat-flow rate value, Figure 5-8. However, increasing the initial BL concentration slows the heat-flow rate decrease, which

might be due to overall increased heat release, and more time would be required to convert BL as more reagent per catalyst mass is present.

Table 5-3. GC and RC1 results for experiments in isothermal conditions at different initial BL concentrations for the hydrogenation of BL in GVL solvent at 35 bars of hydrogen.

Temperature (°C)	Total mass (g)	Cat. Mass * (g)	[BL] initial (mol/L)	[BL] final (mol/L)	[GVL] initial (mol/L)	[GVL] final (mol/L)	$\Delta H_{R,1}$ (kJ/mol)	Standard deviation for $\Delta H_{R,1}$ (kJ/mol)
130	552.0	6.3	1.06	0.001	8.81	9.30	-36.12	._**
130	551.0	6.3	2.05	0.001	6.66	8.61	-35.58	0.86
130	551.0	6.3	5.69	0.001	0	2.14	-34.18	._**

*Including 50% of water

**performed once

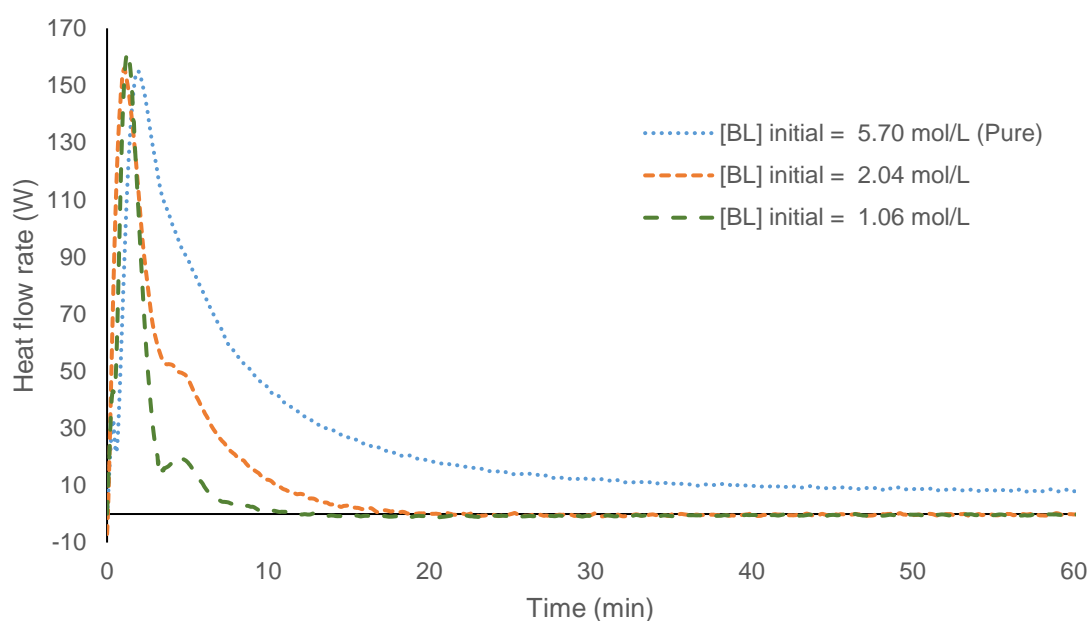


Figure 5-8. BL concentration effect on heat-flow rate at isothermal and isobaric conditions: at 130°C and hydrogen pressure of 35 bars.

Effect of solvents

The effect of the solvent on the reaction enthalpy of the hydrogenation of BL was studied. The results in Table 5-4 shows that hydrogenation of BL is slightly more exothermic in butanol compared to GVL, but this aspect can be neglected as the difference between the reactions enthalpies is quite low. The reaction enthalpy in butanol or GVL solvent is slightly higher compared to the hydrogenation enthalpy of BL in BL solvent (Table 5-4). However, Figure 5-9 shows that the heat-flow rate due to chemical reaction is slower in butanol solvent. Due to the low value of the enthalpy of cyclization, the heat-flow rate is mainly governed by the hydrogenation. Thus, the kinetics of hydrogenation can be concluded to be slower in butanol solvent, which complies with the results reported by Capecci et al in 2021 (Capecci, Wang, Casson Moreno, et al., 2021).

Table 5-4. GC and RC1 results for experiments in isothermal and isobaric conditions for the hydrogenation of BL in GVL solvent and in butanol solvent at 100°C and 35 bar of hydrogen.

Solvent	T (°C)	Total mass (g)	Cat. Mass* (g)	[BL] initial (mol/L)	[BL] final (mol/L)	[GVL] initial (mol/L)	[GVL] final (mol/L)	$\Delta H_{R,1}$ (kJ/mol)	Standard deviation for $\Delta H_{R,1}$ (kJ/mol)
GVL	100	551.0	6.3	2.043	0.013	7.049	8.142	-35.27	1.29
BuOH	100	532.0	6.3	2.180	0.004	0.013	1.656	-37.96	0.40

*Including 50% of water

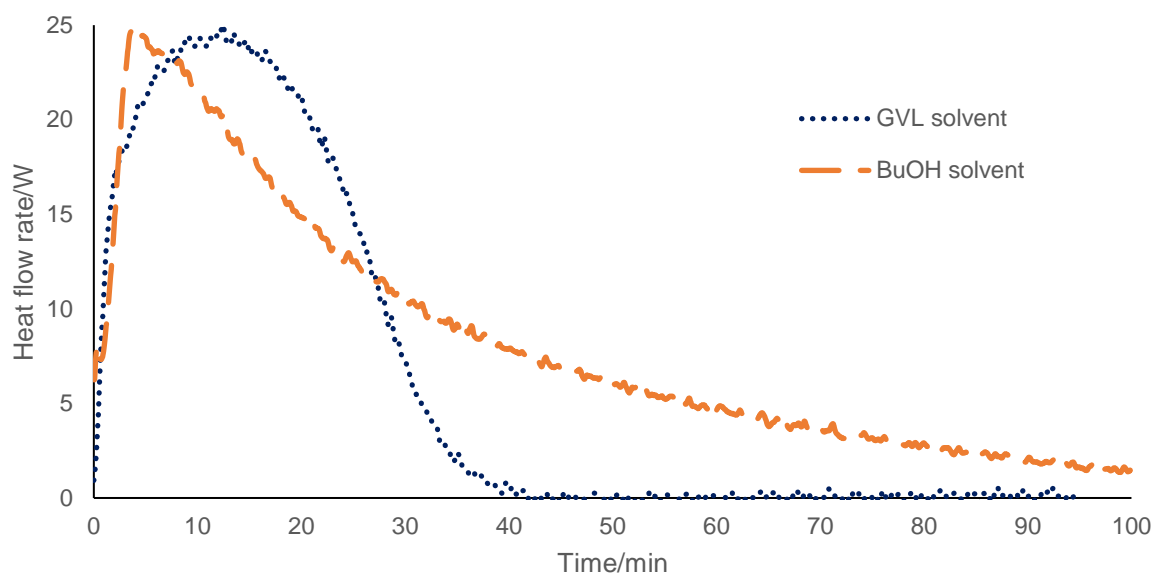


Figure 5-9. Solvent effect on the heat-flow rate of BL hydrogenation at isothermal and isobaric conditions: 100 °C and 35 bar of hydrogen.

Effect of substituent

From the previous results, it can be concluded that the dependence of the enthalpy of BL hydrogenation on reaction temperature, substrate concentration and solvent conditions is very weak or negligible. This information is vital in comparing the hydrogenation enthalpy of ML, BL, EL or LA. Even if the initial substrate concentrations are similar, the reaction-environment can be different due to the different molar masses changing the solvent-reagent ratio, as the mass ratios of reagent to solvent varies to attain the comparable molar concentration and total reaction media mass.

The results in Table 5-5 show the hydrogenation enthalpies for ML, EL and BL in GVL and alkyl levulinate solvent. One can notice that the hydrogenation enthalpy for ML and BL are similar, i.e., within the range -36.84 to -34.18 kJ/mol. The hydrogenation of EL is less exothermic, i.e., -25.17 kJ/mol. It should be noted that in the hydrogenation of pure EL, a conversion of 60% was obtained at 3h, compared to other levulinates where total conversion was achieved at the same time. This behavior was not expected as different kinetics were

observed in the work of Wang et al. (Y. Wang et al., 2019). By neglecting the enthalpy of HPA cyclization, a minimum value for the LA hydrogenation enthalpy was found to be -49.73 kJ/mol, which was higher compared to the levulinates. Table 5-5 shows that there is no linear correlation between the alkyl chain length and the reaction enthalpy values.

Table 5-5. GC and RC1 results for experiments in isothermal conditions for the hydrogenation of substrates at 130°C and 35 bar of hydrogen.

Sub st.	Solve nt	Total mass (g)	^a Cat. Mass (g)	T (°C)	[Subst.] Initial (mol/L)	[Subst.] Final (mol/L)	[GVL] initial (mol/L)	[GVL] final (mol/L)	$\Delta H_{R,1}$ (kJ/mol)	STD $\Delta H_{R,1}$ (kJ/mol)
LA	GVL	0.550	0.006	130	806	0	9296	10504	-49.73*	1.81
ML	GVL	0.610	0.006	130	2238	24	7964	8948	-36.84	0.83
EL	GVL	0.550	0.006	130	2164	9	7762	9128	-26.17	0.04
BL	GVL	0.551	0.006	130	2050	10	6661	8607	-35.58	0.86
ML	ML	0.550	0.006	130	7894	11	0	2387	-35.64	1.46
EL	EL	0.550	0.006	130	6589	3450	13	1337	-25.17	0.68
BL	BL	0.551	0.006	130	5693	10	0	2140	-34.18	-

^a Including 50% of water

^b Not the true reaction enthalpy because second reaction was not estimated

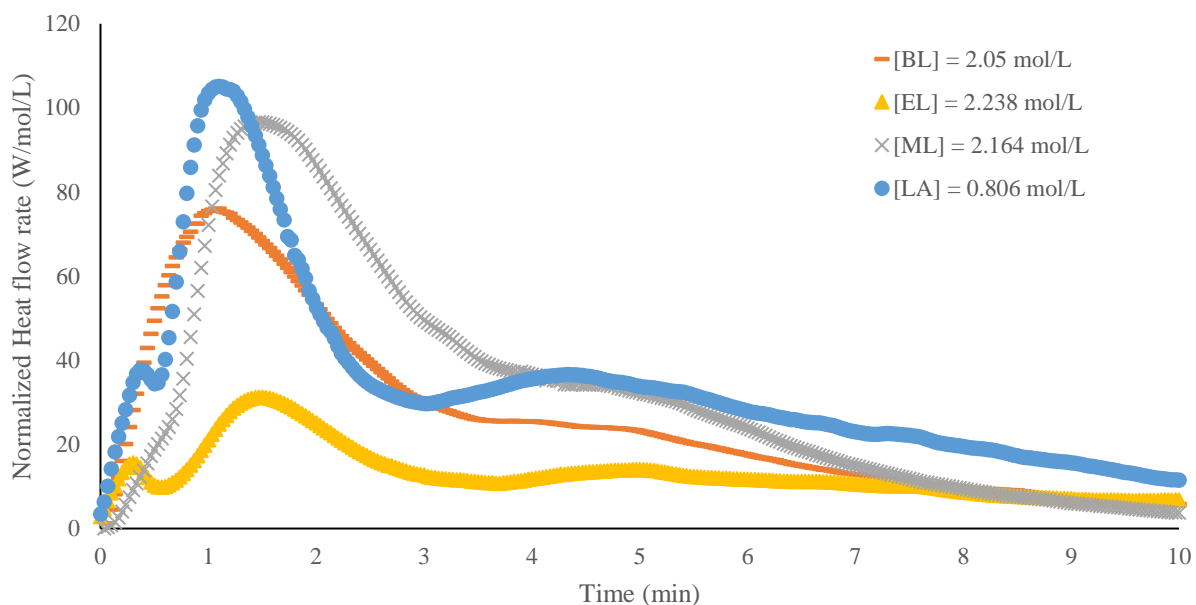


Figure 5-10. Effect of substituent on the normalized heat-flow rate of hydrogenation at 130°C and 35 bars of hydrogen for substrates in GVL.

Figure 5-11 show that the heat-flow release normalized by the initial concentration of substrate during the hydrogenation is more significant for ML and BL than for EL. Due to corrosion issues, the hydrogenation of LA was performed at a lower concentration. One can observe that the normalized heat-flow rate with LA is the highest. The normalized heat-flow rate for EL hydrogenation is lower than BL. According to Wang et al. (Y. Wang et al., 2019), the kinetics of EL hydrogenation should be faster than for BL. However, the hydrogenation of EL experiments showed a different result. EL hydrogenation experiments were repeated twice, and the same trend was observed, where low conversion was observed. EL hydrogenation is less exothermic than BL explaining the lowest normalized heat-flow rate for EL.

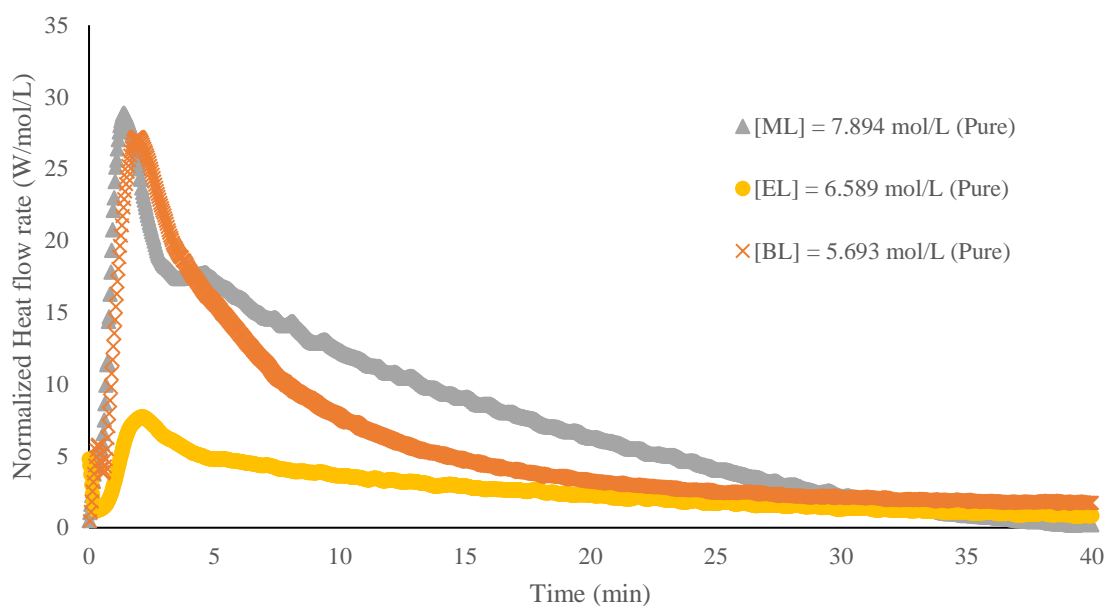


Figure 5-11. Effect of substituent on the normalized heat-flow rate of hydrogenation at 130°C and 35 bars of hydrogen for pure substrates.

Reaction enthalpies in mixtures

To evaluate the possible synergistic effect on the energy release for the hydrogenation of a levulinates mixture, experiments containing EL/BL in GVL as solvent were performed. The mixing enthalpies and interactions between the reagents would influence the enthalpy of reaction. From the hydrogenation enthalpies obtained previously, one could estimate the heat released from a reactive mixture consisting of 2 levulinates using equation (80):

$$\begin{aligned}
 Q_{RC1} = & \left(n_{BL_{final}} - n_{BL_0} \right) * \Delta H_{R,1} (BL) + \left(n_{BuOH_{final}} - n_{BuOH_0} \right) * \Delta H_{R,2} (BL) \\
 & + \left(n_{EL_{final}} - n_{EL_0} \right) * \Delta H_{R,1} (EL) + \left(n_{EtOH_{final}} - n_{EtOH_0} \right) \\
 & * \Delta H_{R,2} (EL)
 \end{aligned} \quad (80)$$

As seen in Table 5-6, no synergistic effect was observed for this reaction mixture. These additional properties were applied to estimate the reaction enthalpies of PrL and PeL system.

Table 5-6. GC and RC1 results for experiments in isothermal conditions for the hydrogenation of EL-BL mixture in GVL solvent at 130°C and 35 bar of hydrogen.

Total mass (g)	Cat. Mass* (g)	[BL] Initial (mol/L)	[BL] Final (mol/L)	[EL] Initial (mol/L)	[EL] Final (mol/L)	[GVL] Initial (mol/L)	[GVL] Final (mol/L)	Heat Released (kJ)	
								observed	estimated
551	6.30	1.768	0.474	1.999	0.491	3.381	4.669	-46.48	-44.39
550	6.30	1.817	0.051	2.172	0.054	3.620	5.109	-63.16	-62.30

* Including 50% of water

5.3.3. Hydrogenation and cyclization of propyl and pentyl levulinate

Hydrogenation of synthesized n-PrL-ML and n-PeL-EL mixtures were carried out in RC1 calorimeter. As an example, for a n-PrL-ML mixture, the total energy due to chemical reaction can be calculated, as shown in Equation (81):

$$\begin{aligned}
 Q_{RC1} = & \left(n_{ML_{final}} - n_{ML_0} \right) * \Delta H_{R,1 \text{ from } ML} + \left(n_{PrL_{final}} - n_{PrL_0} \right) \\
 & * \Delta H_{R,1 \text{ from } PrL} - \left(n_{PrOH_{final}} - n_{PrOH_0} \right) * \Delta H_{R,2 \text{ from } PrHP} \\
 & - \left(n_{MeOH_{final}} - n_{MeOH_0} \right) * \Delta H_{R,2 \text{ from } MHP}
 \end{aligned} \quad (81)$$

Due to the low boiling point of methanol, it is challenging to measure accurately its concentration from the liquid phase. Hence, the difference $(n_{MeOH_{final}} - n_{MeOH_0})$ was expressed as the following material balance where M corresponds to the molar mass of each compound:

$$\begin{aligned}
 & \left(n_{MeOH_{final}} - n_{MeOH_0} \right) \\
 & = \left(\frac{(n_{GVL_{final}} - n_{GVL_0})}{M_{GVL}} - \frac{(n_{PrOH_{final}} - n_{PrOH_0})}{M_{n-PrOH}} \right) M_{MeOH}
 \end{aligned} \quad (82)$$

At the end of the RC1 experiment, the reaction mixture was concentrated in intermediates, namely MHP and PrHP. This reaction mixture was used in the C80 micro-calorimeter to assess the reaction enthalpy of the intermediate's cyclization. The total energy due to cyclization in C80 can be expressed as:

$$Q_{C80} = \left(n_{PrHP\ final} - n_{PrHP_0} \right) * \Delta H_{R,2\ from\ PrHP} + \left(n_{MHP\ final} - n_{MHP_0} \right) * \Delta H_{R,2\ from\ MHP} \quad (83)$$

In Equations (82) and (83), the reaction enthalpies calculated previously ($\Delta H_{R,2\ from\ MHP}$ and $\Delta H_{R,1\ from\ ML}$) were used to determine the ones for the hydrogenation of n-PrL.

Table 5-7 - Operating conditions for the cyclization experiment in C80 in isothermal conditions at 60 °C and 0.01 mol/L of H₂SO₄ in GVL solvent.

Subst	[MHP] ₀ (mol/m ³)	[MHP] _{final} (mol/m ³)	[PrHP] ₀ (mol/m ³)	[PrHP] _{final} (mol/m ³)	Q_C80 (J)	$\Delta H_{R,2\ from\ PrHP}^m$ (kJ/mol)	Standard deviation for $\Delta H_{R,2\ from\ PrHP}^m$ (kJ/mol)
MHP & PrHP	23	63	107	31	-6.645	15.96	2.91

Table 5-8 - GC and RC1 results for experiments at isothermal conditions for the hydrogenation of substrates at 130°C, 35 bar of hydrogen, reaction mass of 550 g and 6.3 g of Ru/C

[ML] Initial (mol/L)	[ML] final (mol/L)	[PrL] Initial (mol/L)	[PrL] final (mol/L)	[GVL] 0 (mol/L)	[GVL] final (mol/L)	[PrOH] Initial (mol/L)	[PrOH] final (mol/L)	$\Delta H_{R,1}$ Enthalpy for n-PrL (kJ/mol)	STD $\Delta H_{R,1}$ Enthalpy for n-PrL (kJ/mol)
0.604	0.160	1.766	0.611	5.875	6.686	0.338	0.672	-36.60	6.80

Production of γ -valerolactone, a green platform molecule

Table 5-7 and Table 5-8 show the reaction enthalpy values calculated from RC1 and C80 for the hydrogenation of n-PrL reaction mixtures. The reaction enthalpy of n-PrL hydrogenation is of the same order of magnitude as for ML and BL. However, the cyclization enthalpy for PrHP is more endothermic than for the other levulinates.

A reaction mixture constituted of EL and PeL, obtained from the transesterification of EL by pentanol, was used to estimate the hydrogenation and cyclization enthalpies of pentyl levulinate (PeL). The method for the estimation of the hydrogenation and cyclization enthalpies were the same as the method described previously. As seen in Table 5-9 and Table 5-10, the hydrogenation enthalpy for n-PeL follows the trend as the other levulinates, but the cyclization enthalpy is similar to that of n-PrHP.

Table 5-9 - Operating conditions for the cyclization experiment in C80 in isothermal conditions at 60 °C and 10 mol/m³ of H₂SO₄ in GVL solvent.

Substituent.	[EtOH] ₀ (mol/m ³)	[EtOH] _{final} (mol/ m ³)	[PeOH] ₀ (mol/ m ³)	[PeOH] _{final} (mol/ m ³)	Q_C80 (J)	$\Delta H_{R,2}$ Cyclization Enthalpy for PeHP (kJ/mol)	STD $\Delta H_{R,2}$ Cyclization Enthalpy for PeHP (kJ/mol)
EHP & PeHP	254	376	661	887	-7.587	13.33	-

Table 5-10 - GC and RC1 results for experiments at isothermal conditions for the hydrogenation of substrates at 130°C, 35 bar of hydrogen, reaction mass of 0.550 kg and 0.0063 kg of Ru/C (containing 50 wt% of water).

[EL] _{Init} ial (mol/ m ³)	[EL] _{fin} al (mol/ m ³)	[PeL] _{Init} ial (mol/ m ³)	[PeL] _{fi} nal (mol/ m ³)	[GVL] _{Init} ial (mol/ m ³)	[GVL] _{fi} nal (mol/ m ³)	[PeOH] _{Init} ial (mol/ m ³)	[PeOH] _{fi} nal (mol/ m ³)	$\Delta H_{R,1}$ Hydrogenat ion of PeL (kJ/mol)	STD $\Delta H_{R,1}$ Hydrogenation of PeL (kJ/mol)
909	259	224	665	4046	5122	31	911	-38.612	1.05

5.4. Conclusions

In this Chapter, the study of the reaction enthalpies for the hydrogenation and subsequent cyclization of alkyl levulinates and levulinic acid for the production of γ -valerolactone was explored. Different alkyl levulinates and levulinic acid were used to observe the possible effect of the alkyl substituent on the reaction enthalpies. Parameters such as concentration, solvent effect and temperature were evaluated for the hydrogenation of BL in order to estimate their possible effect on the hydrogenation reaction enthalpy.

The following tables summarize the obtained results:

Table 5-11 - Mean values for hydrogenation reaction enthalpies for LA and AL between 100 and 130 °C at 35 bar of Hydrogen

Substituent	Hydrogenation enthalpy (kJ/mol)	STD Hydrogenation enthalpy (kJ/mol)
H	-49.73 *	1.31
Me	-36.84	1.19
Et	-26.17	0.36
n-Pr	-36.60	6.00
n-Bu	-35.58	1.01
n-Pe	-38.61	1.05

*Estimated without cyclization enthalpy

Table 5-12 - Mean values for cyclization reaction enthalpies for AL at 60°C

Substituent	Cyclization Enthalpy (kJ/mol)	STD Cyclization Enthalpy (kJ/mol)
Me	9.39	0.003
Et	6.52	0.49
n-Pr	15.96	0.30

Production of γ -valerolactone, a green platform molecule

n-Bu	6.40	0.69
n-Pe	13.33	-

From these results, one could estimate that the hydrogenation enthalpies of the different levulinates shows an approximated value around -35 kJ/mol. Where the most peculiar value obtained corresponds to EL, with the lowest hydrogenation enthalpy and a lower conversion. Levulinic acid would possess the highest value for the hydrogenation without considering the cyclization enthalpy. In the case of the cyclization enthalpies, a clear correlation was not observed. As the different values show, an explicit correlation linking the reaction enthalpies with their substituent was not found. The difference of these results implies that there might be other factors affecting these properties. Nevertheless, these values would be used for future reference to perform the pinch analysis and look for the better operating conditions of this reaction system.

General conclusions and perspectives

The production of γ -valerolactone (GVL) is very relevant given that this chemical compound can be versatility used as a platform molecule and it can be obtained from renewable biomass, posing as an interesting alternative for fossil based non-renewable sources. Among the possible ways to obtain GVL, the hydrogenation of levulinic acid or alkyl levulinates can be considered as one of the most viable pathways, as such, the study of these reaction's kinetics and estimation of thermodynamic properties, notably reaction enthalpies, were performed.

From the experimental results, the most probable reaction path for the explored catalytic systems in this work was a hydrogenation reaction step followed by a cyclization/lactonization reaction step producing GVL.

In the first step, the kinetics of the hydrogenation of butyl levulinate in GVL as solvent over Ru/C catalyst was explored using an autoclave under isothermal and isobaric conditions. Butyl levulinate was chosen as the main reagent due to its low vapor pressure and to avoid the risk of corrosion observed with levulinic acid.

Different kinetic models were proposed and evaluated to estimate the most probable reaction mechanism. Bayesian inference was used to estimate the best fitting model and the Akaike information criterion (AIC) to validate the results. The most probable reaction mechanism based on the modeling is a non-competitive Langmuir Hinshelwood adsorption of hydrogen without dissociation for the hydrogenation reaction step and the catalytic effect of the catalysts support in the cyclization reaction step.

A different kinetic study was also performed to evaluate the effect of levulinic acid as an impurity present in the reaction mixture in the production of alkyl levulinates. The reaction system comprised levulinic acid and butyl levulinate as reagents, GVL as a solvent, and a dual catalytic system: Ru/C and a sulphonic resin, Amberlite IR120. Amberlite IR120 was included

to increase the kinetics of the cyclization reaction step. It was observed that the presence of LA and the sulfonic resin improved the kinetics of the cyclization reaction step.

Bayesian inference was used to identify the better fitting model and the K-fold method, along with the AIC, were used to validate the model estimations. K-fold method allowed to compare the predictive power of the models. Seven kinetic models were evaluated where the two most probable ones were NCLH1.2 and NCLH2.2. These models considered a Langmuir-Hinshelwood non-competitive adsorption of BL, LA, and hydrogen on different sites, differing in the dissociation of hydrogen on the Ru/C catalyst for the hydrogenation step. The cyclization step considered the dissociation of levulinic acid and the presence of acid sites in the amberlite IR120 catalyst.

The reaction enthalpies for the hydrogenation of levulinic acid and some substituted n-alkyl levulinates using molecular hydrogen with a Ru/C catalyst were evaluated. These values are relevant to estimate the thermal risks related in the production of GVL and perform pinch analysis on process flow diagrams. Two types of calorimeters were used; a Tian-Calvet micro calorimeter (Setaram C80) was used in the estimation of cyclization enthalpies while an RC1mx calorimeter (Mettler Toledo) was used for the hydrogenation enthalpy measurement.

Enthalpy measurements were performed for levulinic acid, methyl levulinate, ethyl levulinate, n-propyl levulinate, n-butyl levulinate and n-pentyl levulinate. It was found that the reaction enthalpies for hydrogenation were exothermic and equal to -49.73 kJ/mol, -36.84 kJ/mol, -26.17 kJ/mol, -36.60 kJ/mol, -35.58 kJ/mol and -38.61 kJ/mol, respectively. The enthalpy of cyclization was found to be endothermic, and were equal to 9.39 kJ/mol, 6.51 kJ/mol, 15.96 kJ/mol, 6.40 kJ/mol and 13.33 kJ/mol for MHP, EHP, PrHP, BHP and PeHP respectively. No relationship for the alkyl chain length and the reaction enthalpies obtained was found.

The effect of solvent, temperature, and initial concentrations was observed for the hydrogenation of butyl levulinate. It was found that the hydrogenation reaction enthalpy was independent from these operating conditions. Reaction mixtures comprising two levulinates were evaluated to observe a possible synergistic effect on the hydrogenation enthalpies. No synergistic effect was found.

To conclude, the production of γ -valerolactone from the hydrogenation of butyl levulinate over Ru/C was thoroughly investigated from a kinetic and thermodynamic standpoint. The use of Ru/C and Amberlite IR-120 catalysts in tandem allows the increase in the kinetics of the two-reaction steps: hydrogenation and cyclization. A methodology was developed to measure the reaction enthalpy of these two steps.

Based on our work, one can develop a continuous process using both catalysts for the hydrogenation of butyl levulinate into γ -valerolactone. One can evaluate the robustness of the different developed kinetic models by testing different thermal modes such as isoperibolic and/or adiabatic ones.

Quantum mechanics such as DFT could contribute to unravel the reaction mechanism and verify the reliability of the estimated adsorption constants.

Notations

Nomenclature

D_j	molecular diffusion coefficient of j [$\text{m}^2 \cdot \text{s}^{-1}$]
Ea_i	activation energy of reaction i [$\text{J} \cdot \text{mol}^{-1}$]
H_e	Henry's coefficient [$\text{mol} \cdot \text{m}^{-3} \cdot \text{bar}^{-1}$]
ΔH_{sol}	dissolution enthalpy [$\text{J} \cdot \text{mol}^{-1}$]
k_i	Rate constant of reaction i
$k_L a$	volumetric mass transfer coefficient [s^{-1}]
$(k_L a)_{modified}$	modified volumetric mass transfer coefficient $\left[\left(\frac{\text{Pa} \cdot \text{s}}{\text{K}} \right)^{0.5} \cdot \left(\frac{\text{Pa} \cdot \text{s}}{\text{kg} \cdot \text{m}^{-3}} \right)^{0.25} \cdot \text{s}^{-1} \right]$
r_j	rate of formation or disappearance of compound j [$\text{mol} \cdot \text{m}^{-3} \cdot \text{s}^{-1}$]
P	pressure [bar]
R_i	reaction rate i [$\text{mol} \cdot \text{m}^{-3} \cdot \text{s}^{-1}$]
R	gas constant [$\text{J} \cdot \text{K}^{-1} \cdot \text{mol}^{-1}$]
R^2	coefficient of explanation [%]
T	temperature [K]
V_{molar}	molar volume [$\text{cm}^3 \cdot \text{mol}^{-1}$]
w_i	weight percent
y_i	experimental observable
\hat{y}_i	observable simulated by the model

\bar{y}	mean value of the experimental observables
C_p	Specific heat-capacity [J/(kg.K)]
$\Delta H_{R,i}^m$	Reaction enthalpy [J/mol]
V_{liq}	Volume of liquid [L]
m_{insert}	Insert mass [kg]
P	Pressure [bar]
Q_{C80}	Total energy released or absorbed and measured by C80 [J]
Q_{RC1}	Total energy released or absorbed and measured by RC1 [J]

Greek Letters

δ	sensitivity factor of a reaction series to steric effects
μ	liquid viscosity [Pa.s]
ρ	mass density [kg.m ⁻³]
ω	objective function
ω_{Cat}	catalyst loading [kg_dried basis.m ⁻³]

Abbreviations

AL alkyl levulinate

Production of γ -valerolactone, a green platform molecule

AHP	alkyl 4-hydroxypentanolate
BL	butyl levulinate
BHP	n-butyl 4-hydroxypentanoate
BuOH	n-butanol
EL	ethyl levulinate
EHP	ethyl 4-hydroxypentanoate
EtOH	ethanol
GVL	γ -valerolactone
HPA	4-hydroxypentanoic acid
LA	levulinic acid
ML	methyl levulinate
MHP	methyl 4-hydroxypentanoate
MeOH	methanol
PeL	pentyl levulinate
PeHP	pentyl 4-hydroxypentanoate

PeOH	n-pentanol
PrL	propyl levulinate
PrHP	propyl 4-hydroxypentanoate
PrOH	n-propanol
ROH	R alkyl substituent alcohol (methanol, ethanol...)
STD	standard deviation

References

- Abdelrahman, O. A., Heyden, A., & Bond, J. Q. (2014). Analysis of Kinetics and Reaction Pathways in the Aqueous-Phase Hydrogenation of Levulinic Acid To Form γ -Valerolactone over Ru/C. *ACS Catalysis*, 4(4), 1171–1181. <https://doi.org/10.1021/cs401177p>
- Alonso, D. M., Wettstein, S. G., & Dumesic, J. A. (2013). Gamma-valerolactone, a sustainable platform molecule derived from lignocellulosic biomass. *Green Chemistry*, 15(3), 584. <https://doi.org/10.1039/c3gc37065h>
- Arevalo-Gallegos, A., Ahmad, Z., Asgher, M., Parra-Saldivar, R., & Iqbal, H. M. N. (2017). Lignocellulose: A sustainable material to produce value-added products with a zero waste approach—A review. *International Journal of Biological Macromolecules*, 99, 308–318. <https://doi.org/10.1016/j.ijbiomac.2017.02.097>
- Ariba, H., Wang, Y., Devouge-Boyer, C., Stateva, R. P., & Leveneur, S. (2020). Physicochemical Properties for the Reaction Systems: Levulinic Acid, Its Esters, and γ -Valerolactone. *Journal of Chemical & Engineering Data*, 65(6), 3008–3020. <https://doi.org/10.1021/acs.jced.9b00965>
- Assary, R. S., Curtiss, L. A., & Dumesic, J. A. (2013). Exploring Meerwein–Ponndorf–Verley Reduction Chemistry for Biomass Catalysis Using a First-Principles Approach. *ACS Catalysis*, 3(12), 2694–2704. <https://doi.org/10.1021/cs400479m>
- AthenaVisual, Inc.* (n.d.). Retrieved October 10, 2022, from <https://athenavisual.com/>
- Bababrik, R. M., Wang, B., & Resasco, D. E. (2017). Reaction Mechanism for the Conversion of γ -Valerolactone (GVL) over a Ru Catalyst: A First-Principles Study. *Industrial & Engineering Chemistry Research*, 56(12), 3217–3222. <https://doi.org/10.1021/acs.iecr.7b00196>

- Bajwa, D. S., Pourhashem, G., Ullah, A. H., & Bajwa, S. G. (2019). A concise review of current lignin production, applications, products and their environmental impact. *Industrial Crops and Products*, *139*, 111526. <https://doi.org/10.1016/j.indcrop.2019.111526>
- Bar-On, Y. M., Phillips, R., & Milo, R. (2018). The biomass distribution on Earth. *Proceedings of the National Academy of Sciences*, *115*(25), 6506–6511. <https://doi.org/10.1073/pnas.1711842115>
- Berczky, Á., Lukács, K., Farkas, M., & Dóbbé, S. (2014). Effect of γ -Valerolactone Blending on Engine Performance, Combustion Characteristics and Exhaust Emissions in a Diesel Engine. *Natural Resources*, *05*(05), 177–191. <https://doi.org/10.4236/nr.2014.55017>
- Birgen, C., Dürre, P., Preisig, H. A., & Wentzel, A. (2019). Butanol production from lignocellulosic biomass: Revisiting fermentation performance indicators with exploratory data analysis. *Biotechnology for Biofuels*, *12*(1), 167. <https://doi.org/10.1186/s13068-019-1508-6>
- Bomtempo, J.-V., Chaves Alves, F., & de Almeida Oroski, F. (2017). Developing new platform chemicals: What is required for a new bio-based molecule to become a platform chemical in the bioeconomy? *Faraday Discuss.*, *202*, 213–225. <https://doi.org/10.1039/C7FD00052A>
- Bonrath, W., Castelijns, A. M. C. F., de Vries, J. G., Guit, R. P. M., Schütz, J., Sereinig, N., & Vaessen, H. W. L. M. (2016). Gas Phase Hydrogenation of Levulinic Acid to γ -Valerolactone. *Catalysis Letters*, *146*(1), 28–34. <https://doi.org/10.1007/s10562-015-1661-x>
- Bozell, J. J., & Petersen, G. R. (2010). Technology development for the production of biobased products from biorefinery carbohydrates—The US Department of Energy’s “Top 10” revisited. *Green Chemistry*, *12*(4), 539. <https://doi.org/10.1039/b922014c>
- Brenna, E., Distante, F., Gatti, F. G., & Gatti, G. (2017). Substituent and catalyst effects on GAC lactonization of γ -hydroxy esters. *Catalysis Science & Technology*, *7*(7), 1497–1507. <https://doi.org/10.1039/C6CY02177H>

- Bruice, P. Y. (2010). *Organic Chemistry: United States Edition—Bruice, Paula Yurkanis: 0321663136—AbeBooks*. <https://www.abebooks.fr/9780321663139/Organic-Chemistry-United-States-Edition-0321663136/plp>
- Brunner, E. (1985). Solubility of hydrogen in 10 organic solvents at 298.15, 323.15, and 373.15 K. *Journal of Chemical & Engineering Data*, 30(3), 269–273. <https://doi.org/10.1021/jc00041a010>
- Bruno, T. J., Wolk, A., & Naydich, A. (2010). Composition-Explicit Distillation Curves for Mixtures of Gasoline and Diesel Fuel with γ -Valerolactone. *Energy & Fuels*, 24(4), 2758–2767. <https://doi.org/10.1021/ef100133a>
- Capecchi, S., Wang, Y., Casson Moreno, V., Held, C., & Leveneur, S. (2021). Solvent effect on the kinetics of the hydrogenation of n-butyl levulinate to γ -valerolactone. *Chemical Engineering Science*, 231, 116315. <https://doi.org/10.1016/j.ces.2020.116315>
- Capecchi, S., Wang, Y., Delgado, J., Casson Moreno, V., Mignot, M., Grénman, H., Murzin, D. Yu., & Leveneur, S. (2021). Bayesian Statistics to Elucidate the Kinetics of γ -Valerolactone from n-Butyl Levulinate Hydrogenation over Ru/C. *Industrial & Engineering Chemistry Research*, 60(31), 11725–11736. <https://doi.org/10.1021/acs.iecr.1c02107>
- Caracotsios, M., & Stewart, W. E. (1985). Sensitivity analysis of initial value problems with mixed odes and algebraic equations. *Computers & Chemical Engineering*, 9(4), 359–365. [https://doi.org/10.1016/0098-1354\(85\)85014-6](https://doi.org/10.1016/0098-1354(85)85014-6)
- Chalid, M., Heeres, H. J., & Broekhuis, A. A. (2012). Green Polymer Precursors from Biomass-Based Levulinic Acid. *Procedia Chemistry*, 4, 260–267. <https://doi.org/10.1016/j.proche.2012.06.036>
- Chauhan, A., Kar, A. K., & Srivastava, R. (2022). Ru-decorated N-doped carbon nanoflakes for selective hydrogenation of levulinic acid to γ -valerolactone and quinoline to tetrahydroquinoline with HCOOH in water. *Applied Catalysis A: General*, 636, 118580. <https://doi.org/10.1016/j.apcata.2022.118580>

- Chen, B., Guo, H., Wan, Z., Xu, X., Zhang, H., Zhao, D., Chen, X., & Zhang, N. (2018). Efficient Catalytic Hydrogenation of Butyl Levulinate to γ -Valerolactone over a Stable and Magnetic CuNiCoB Amorphous Alloy Catalyst. *Energy & Fuels*, 32(4), 5527–5535. <https://doi.org/10.1021/acs.energyfuels.8b00378>
- Chen, W., Yang, Y., Lan, X., Zhang, B., Zhang, X., & Mu, T. (2021). Biomass-derived γ -valerolactone: Efficient dissolution and accelerated alkaline hydrolysis of polyethylene terephthalate. *Green Chemistry*, 23(11), 4065–4073. <https://doi.org/10.1039/D1GC00665G>
- Chia, M., & Dumesic, J. A. (2011). Liquid-phase catalytic transfer hydrogenation and cyclization of levulinic acid and its esters to γ -valerolactone over metal oxide catalysts. *Chemical Communications*, 47(44), 12233–12235. <https://doi.org/10.1039/C1CC14748J>
- Computer-Aided Modeling of Reactive Systems* / Wiley. (n.d.). Wiley.Com. Retrieved October 10, 2022, from <https://www.wiley.com/en-us/Computer+Aided+Modeling+of+Reactive+Systems-p-9780470274958>
- Dakkoune, A., Vernières-Hassimi, L., Leveneur, S., Lefebvre, D., & Estel, L. (2019). Analysis of thermal runaway events in French chemical industry. *Journal of Loss Prevention in the Process Industries*, 62, 103938. <https://doi.org/10.1016/j.jlp.2019.103938>
- Deivayanai, V. C., Yaashikaa, P. R., Senthil Kumar, P., & Rangasamy, G. (2022). A comprehensive review on the biological conversion of lignocellulosic biomass into hydrogen: Pretreatment strategy, technology advances and perspectives. *Bioresource Technology*, 365, 128166. <https://doi.org/10.1016/j.biortech.2022.128166>
- Delgado, J., Vasquez Salcedo, W. N., Bronzetti, G., Casson Moreno, V., Mignot, M., Legros, J., Held, C., Grénman, H., & Leveneur, S. (2022). Kinetic model assessment for the synthesis of γ -valerolactone from n-butyl levulinate and levulinic acid hydrogenation over the synergy effect of dual catalysts Ru/C and Amberlite IR-120. *Chemical Engineering Journal*, 430, 133053. <https://doi.org/10.1016/j.cej.2021.133053>

- Démolis, A., Essayem, N., & Rataboul, F. (2014). Synthesis and Applications of Alkyl Levulinates. *ACS Sustainable Chemistry & Engineering*, 2(6), 1338–1352. <https://doi.org/10.1021/sc500082n>
- Dey, S., & Dhal, G. C. (2020). Applications of Rhodium and Ruthenium Catalysts for CO Oxidation: An Overview. *Polytechnica*, 3(1–2), 26–42. <https://doi.org/10.1007/s41050-020-00023-5>
- Di Menno Di Bucchianico, D., Wang, Y., Buvat, J.-C., Pan, Y., Casson Moreno, V., & Leveneur, S. (2022). Production of levulinic acid and alkyl levulinates: A process insight. *Green Chemistry*, 24(2), 614–646. <https://doi.org/10.1039/D1GC02457D>
- Dutta, S., Yu, I. K. M., Tsang, D. C. W., Ng, Y. H., Ok, Y. S., Sherwood, J., & Clark, J. H. (2019). Green synthesis of gamma-valerolactone (GVL) through hydrogenation of biomass-derived levulinic acid using non-noble metal catalysts: A critical review. *Chemical Engineering Journal*, 372, 992–1006. <https://doi.org/10.1016/j.cej.2019.04.199>
- Falcchi Corrêa, L. F., de Pelegrini Soares, R., & Ceriani, R. (2019). Solubility behavior of γ -valerolactone + n-tetradecane or diesel mixtures at different temperatures. *Fluid Phase Equilibria*, 484, 239–244. <https://doi.org/10.1016/j.fluid.2018.11.012>
- Feng, J., Gu, X., Xue, Y., Han, Y., & Lu, X. (2018). Production of γ -valerolactone from levulinic acid over a Ru/C catalyst using formic acid as the sole hydrogen source. *Science of The Total Environment*, 633, 426–432. <https://doi.org/10.1016/j.scitotenv.2018.03.209>
- Feng, J., Li, M., Zhong, Y., Xu, Y., Meng, X., Zhao, Z., & Feng, C. (2020). Hydrogenation of levulinic acid to γ -valerolactone over Pd@UiO-66-NH₂ with high metal dispersion and excellent reusability. *Microporous and Mesoporous Materials*, 294, 109858. <https://doi.org/10.1016/j.micromeso.2019.109858>
- Fernandes, D. R., Rocha, A. S., Mai, E. F., Mota, C. J. A., & Teixeira da Silva, V. (2012). Levulinic acid esterification with ethanol to ethyl levulinate production over solid acid

- catalysts. *Applied Catalysis A: General*, 425–426, 199–204. <https://doi.org/10.1016/j.apcata.2012.03.020>
- Gawad, E. (2019). URANIUM REMOVAL FROM NITRATE SOLUTION BY CATION EXCHANGE RESIN (AMBERLITE IR 120), ADSORPTION AND KINETIC CHARACTERISTICS. *Nuclear Sciences Scientific Journal*, 8(1), 213–230. <https://doi.org/10.21608/nssj.2019.30142>
- Goddard, J. D., Yamaguchi, Y., & Schaefer, H. F. (1992). The decarboxylation and dehydration reactions of monomeric formic acid. *The Journal of Chemical Physics*, 96(2), 1158–1166. <https://doi.org/10.1063/1.462203>
- Grilc, M., & Likozar, B. (2017). Levulinic acid hydrodeoxygenation, decarboxylation and oligomerization over NiMo/Al₂O₃ catalyst to bio-based value-added chemicals: Modelling of mass transfer, thermodynamics and micro-kinetics. *Chemical Engineering Journal*, 330, 383–397. <https://doi.org/10.1016/j.cej.2017.07.145>
- Havasi, D., Mizsey, P., & Mika, L. T. (2016). Vapor–Liquid Equilibrium Study of the Gamma-Valerolactone–Water Binary System. *Journal of Chemical & Engineering Data*, 61(4), 1502–1508. <https://doi.org/10.1021/acs.jced.5b00849>
- He, N., & Li, Z. H. (2016). Palladium-atom catalyzed formic acid decomposition and the switch of reaction mechanism with temperature. *Physical Chemistry Chemical Physics*, 18(15), 10005–10017. <https://doi.org/10.1039/C6CP00186F>
- Hengst, K., Schubert, M., Carvalho, H. W. P., Lu, C., Kleist, W., & Grunwaldt, J.-D. (2015). Synthesis of γ -valerolactone by hydrogenation of levulinic acid over supported nickel catalysts. *Applied Catalysis A: General*, 502, 18–26. <https://doi.org/10.1016/j.apcata.2015.05.007>
- Herbst, A., & Janiak, C. (2016). Selective glucose conversion to 5-hydroxymethylfurfural (5-HMF) instead of levulinic acid with MIL-101Cr MOF-derivatives. *New Journal of Chemistry*, 40(9), 7958–7967. <https://doi.org/10.1039/C6NJ01399F>

- Horikawa, Y. (2022). Structural diversity of natural cellulose and related applications using delignified wood. *Journal of Wood Science*, 68(1), 54. <https://doi.org/10.1186/s10086-022-02061-2>
- Hsiao, C.-Y., Chiu, H.-Y., Lin, T.-Y., & Lin, K.-Y. A. (2021). A comparative study on microwave-assisted catalytic transfer hydrogenation of levulinic acid to γ -valerolactone using Ru/C, Pt/C, and Pd/C. *Chemical Engineering Communications*, 208(11), 1511–1522. <https://doi.org/10.1080/00986445.2020.1791833>
- Huang, Y.-B., Yang, T., Luo, Y.-J., Liu, A.-F., Zhou, Y.-H., Pan, H., & Wang, F. (2018). Simple and efficient conversion of cellulose to γ -valerolactone through an integrated alcoholysis/transfer hydrogenation system using Ru and aluminium sulfate catalysts. *Catalysis Science & Technology*, 8(23), 6252–6262. <https://doi.org/10.1039/C8CY01971A>
- Inyang, V., Laseinde, O. T., & Kanakana, G. M. (2022). Techniques and applications of lignocellulose biomass sources as transport fuels and other bioproducts. *International Journal of Low-Carbon Technologies*, 17, 900–909. <https://doi.org/10.1093/ijlct/ctac068>
- Isikgor, F. H., & Becer, C. R. (2015). Lignocellulosic biomass: A sustainable platform for the production of bio-based chemicals and polymers. *Polymer Chemistry*, 6(25), 4497–4559. <https://doi.org/10.1039/C5PY00263J>
- Jung, H. M., Choi, J. H., Lee, S. O., Kim, Y. H., Park, J. H., & Park, J. (2002). Facile Synthesis of $(\eta^5\text{-Ph}_4\text{C}_4\text{COH})(\text{CO})_2\text{RuCl}$ and Catalytic Oxidation of Alcohols with Chloroform. *Organometallics*, 21(25), 5674–5677. <https://doi.org/10.1021/om020516m>
- Kamm, B. K. M. (2004). Principles of biorefineries. *Appl Microbiol Biotechnol*, 64, 137–145. <https://doi.org/10.1007/s00253-003-1537-7>
- Kasar, G. B., Medhekar, R. S., Bhosale, P. N., & Rode, C. V. (2019). Kinetics of Hydrogenation of Aqueous Levulinic Acid over Bimetallic Ru–Ni/MMT Catalyst. *Industrial &*

- Engineering Chemistry Research*, 58(43), 19803–19817.
<https://doi.org/10.1021/acs.iecr.9b03748>
- Kerkel, F., Markiewicz, M., Stolte, S., Müller, E., & Kunz, W. (2021). The green platform molecule gamma-valerolactone – ecotoxicity, biodegradability, solvent properties, and potential applications. *Green Chemistry*, 23(8), 2962–2976.
<https://doi.org/10.1039/D0GC04353B>
- Kluson, P., & Cervený, L. (1995). Selective hydrogenation over ruthenium catalysts. *Applied Catalysis A: General*, 128(1), 13–31. [https://doi.org/10.1016/0926-860X\(95\)00046-1](https://doi.org/10.1016/0926-860X(95)00046-1)
- Kopyscinski, J., Choi, J., & Hill, J. M. (2012). Comprehensive kinetic study for pyridine hydrodenitrogenation on (Ni)WP/SiO₂ catalysts. *Applied Catalysis A: General*, 445–446, 50–60. <https://doi.org/10.1016/j.apcata.2012.08.027>
- Kulasinski, K., Keten, S., Churakov, S. V., Derome, D., & Carmeliet, J. (2014). A comparative molecular dynamics study of crystalline, paracrystalline and amorphous states of cellulose. *Cellulose*, 21(3), 1103–1116. <https://doi.org/10.1007/s10570-014-0213-7>
- Kumar, A., Shende, D. Z., & Wasewar, K. L. (2020). Production of levulinic acid: A promising building block material for pharmaceutical and food industry. *Materials Today: Proceedings*, 29, 790–793. <https://doi.org/10.1016/j.matpr.2020.04.749>
- Kumar, R., Kumar, A., & Pal, A. (2022). Overview of hydrogen production from biogas reforming: Technological advancement. *International Journal of Hydrogen Energy*, 47(82), 34831–34855. <https://doi.org/10.1016/j.ijhydene.2022.08.059>
- Kuwahara, Y., Kango, H., & Yamashita, H. (2017). Catalytic Transfer Hydrogenation of Biomass-Derived Levulinic Acid and Its Esters to γ -Valerolactone over Sulfonic Acid-Functionalized UiO-66. *ACS Sustainable Chemistry and Engineering*, 5(1), 1141–1152.
<https://doi.org/10.1021/acssuschemeng.6b02464>
- Levulinic Acid Market Global Industry Growth Forecast to 2030* (No. CM10120; p. 170). (2022). <https://www.psmarketresearch.com/market-analysis/levulinic-acid-market>
- Li, F., France, L. J., Cai, Z., Li, Y., Liu, S., Lou, H., Long, J., & Li, X. (2017). Catalytic transfer hydrogenation of butyl levulinate to γ -valerolactone over zirconium phosphates with

- adjustable Lewis and Brønsted acid sites. *Applied Catalysis B: Environmental*, *214*, 67–77. <https://doi.org/10.1016/j.apcatb.2017.05.013>
- Liguori, F., Moreno-Marrodan, C., & Barbaro, P. (2015). Environmentally friendly synthesis of γ -valerolactone by direct catalytic conversion of renewable sources. *ACS Catalysis*, *5*(3), 1882–1894. <https://doi.org/10.1021/cs501922e>
- Lomate, S., Sultana, A., & Fujitani, T. (2018). Vapor Phase Catalytic Transfer Hydrogenation (CTH) of Levulinic Acid to γ -Valerolactone Over Copper Supported Catalysts Using Formic Acid as Hydrogen Source. *Catalysis Letters*, *148*(1), 348–358. <https://doi.org/10.1007/s10562-017-2241-z>
- Lomba, L., Giner, B., Bandrés, I., Lafuente, C., & Pino, M. R. (2011). Physicochemical properties of green solvents derived from biomass. *Green Chemistry*, *13*(8), 2062. <https://doi.org/10.1039/c0gc00853b>
- Luo, W., Deka, U., Beale, A. M., van Eck, E. R. H., Bruijninx, P. C. A., & Weckhuysen, B. M. (2013). Ruthenium-catalyzed hydrogenation of levulinic acid: Influence of the support and solvent on catalyst selectivity and stability. *Journal of Catalysis*, *301*, 175–186. <https://doi.org/10.1016/j.jcat.2013.02.003>
- Luo, W., Sankar, M., Beale, A. M., He, Q., Kiely, C. J., Bruijninx, P. C. A., & Weckhuysen, B. M. (2015). High performing and stable supported nano-alloys for the catalytic hydrogenation of levulinic acid to γ -valerolactone. *Nature Communications*, *6*(1), 6540. <https://doi.org/10.1038/ncomms7540>
- Mäki-Arvela, P., Hájek, J., Salmi, T., & Murzin, D. Yu. (2005). Chemoselective hydrogenation of carbonyl compounds over heterogeneous catalysts. *Applied Catalysis A: General*, *292*, 1–49. <https://doi.org/10.1016/j.apcata.2005.05.045>
- Mamun, O., Saleheen, M., Bond, J. Q., & Heyden, A. (2017). Importance of Angelica Lactone Formation in the Hydrodeoxygenation of Levulinic Acid to γ -Valerolactone over a Ru(0001) Model Surface. *The Journal of Physical Chemistry C*, *121*(34), 18746–18761. <https://doi.org/10.1021/acs.jpcc.7b06369>

- Matera, S., Schneider, W. F., Heyden, A., & Savara, A. (2019). Progress in Accurate Chemical Kinetic Modeling, Simulations, and Parameter Estimation for Heterogeneous Catalysis. *ACS Catalysis*, 9(8), 6624–6647. <https://doi.org/10.1021/acscatal.9b01234>
- McDonald, M. A., Bromig, L., Grover, M. A., Rousseau, R. W., & Bommarius, A. S. (2018). Kinetic model discrimination of penicillin G acylase thermal deactivation by non-isothermal continuous activity assay. *Chemical Engineering Science*, 187, 79–86. <https://doi.org/10.1016/j.ces.2018.04.046>
- Meinita, M. D. N., Amron, A., Trianto, A., Harwanto, D., Caesarendra, W., Jeong, G.-T., & Choi, J.-S. (2021). Levulinic Acid Production from Macroalgae: Production and Promising Potential in Industry. *Sustainability*, 13(24), 13919. <https://doi.org/10.3390/su132413919>
- Melchiorre, M., Amendola, R., Benessere, V., Cucciolito, M. E., Ruffo, F., & Esposito, R. (2020). Solvent-free transesterification of methyl levulinate and esterification of levulinic acid catalyzed by a homogeneous iron(III) dimer complex. *Molecular Catalysis*, 483, 110777. <https://doi.org/10.1016/j.mcat.2020.110777>
- Mitani, M., Matsumoto, H., Gouda, N., & Koyama, K. (1990). Chemoselective reduction of oxiranes by methylmetals in the presence of a copper(I)-phosphine complex. *Journal of the American Chemical Society*, 112(3), 1286–1287. <https://doi.org/10.1021/ja00159a082>
- Mizugaki, T., Nagatsu, Y., Togo, K., Maeno, Z., Mitsudome, T., Jitsukawa, K., & Kaneda, K. (2015). Selective hydrogenation of levulinic acid to 1,4-pentanediol in water using a hydroxyapatite-supported Pt–Mo bimetallic catalyst. *Green Chemistry*, 17(12), 5136–5139. <https://doi.org/10.1039/C5GC01878A>
- Molleti, J., Tiwari, M. S., & Yadav, G. D. (2018). Novel synthesis of Ru/OMS catalyst by solvent-free method: Selective hydrogenation of levulinic acid to γ -valerolactone in aqueous medium and kinetic modelling. *Chemical Engineering Journal*, 334, 2488–2499. <https://doi.org/10.1016/j.cej.2017.11.125>
- Murzin, D. Y., & Salmi, T. (2005). *Catalytic Kinetics*. Elsevier.

N-Amyl levulinate / *C10H18O3* / *ChemSpider*. (n.d.). Retrieved February 1, 2023, from <http://www.chemspider.com/Chemical-Structure.79805.html>

Nechita, P., Mirela, R., & Ciolacu, F. (2021). Xylan Hemicellulose: A Renewable Material with Potential Properties for Food Packaging Applications. *Sustainability*, *13*(24), 13504. <https://doi.org/10.3390/su132413504>

Niju, S., Swathika, M., & Balajii, M. (2020). Pretreatment of lignocellulosic sugarcane leaves and tops for bioethanol production. In *Lignocellulosic Biomass to Liquid Biofuels* (pp. 301–324). Elsevier. <https://doi.org/10.1016/B978-0-12-815936-1.00010-1>

Nishiyama, Y. (2009). Structure and properties of the cellulose microfibril. *Journal of Wood Science*, *55*(4), 241–249. <https://doi.org/10.1007/s10086-009-1029-1>

Piskun, A. S., Ftouni, J., Tang, Z., Weckhuysen, B. M., Bruijninx, P. C. A., & Heeres, H. J. (2018). Hydrogenation of levulinic acid to γ -valerolactone over anatase-supported Ru catalysts: Effect of catalyst synthesis protocols on activity. *Applied Catalysis A: General*, *549*, 197–206. <https://doi.org/10.1016/j.apcata.2017.09.032>

Piskun, A. S., van de Bovenkamp, H. H., Rasrendra, C. B., Winkelman, J. G. M., & Heeres, H. J. (2016). Kinetic modeling of levulinic acid hydrogenation to γ -valerolactone in water using a carbon supported Ru catalyst. *Applied Catalysis A: General*, *525*, 158–167. <https://doi.org/10.1016/j.apcata.2016.06.033>

Polshettiwar, V., & Varma, R. S. (2009). Revisiting the Meerwein–Ponndorf–Verley reduction: A sustainable protocol for transfer hydrogenation of aldehydes and ketones. *Green Chemistry*, *11*(9), 1313. <https://doi.org/10.1039/b913079a>

PubChem. (n.d.). *Methyl levulinate*. Retrieved January 5, 2023, from <https://pubchem.ncbi.nlm.nih.gov/compound/69354>

PubChem Compound Summary for CID 11579, Levulinic acid. (2022). National Center for Biotechnology Information. <https://pubchem.ncbi.nlm.nih.gov/compound/Levulinic-acid>.

- Putrakumar, B., Nagaraju, N., Kumar, V. P., & Chary, K. V. R. (2015). Hydrogenation of levulinic acid to γ -valerolactone over copper catalysts supported on γ -Al₂O₃. *Catalysis Today*, 250, 209–217. <https://doi.org/10.1016/j.cattod.2014.07.014>
- Qi, L., & Horváth, I. T. (2012). Catalytic Conversion of Fructose to γ -Valerolactone in γ -Valerolactone. *ACS Catalysis*, 2(11), 2247–2249. <https://doi.org/10.1021/cs300428f>
- Rajesh Banu, J., Kavitha, S., Yukesh Kannah, R., Poornima Devi, T., Gunasekaran, M., Kim, S.-H., & Kumar, G. (2019). A review on biopolymer production via lignin valorization. *Bioresource Technology*, 290, 121790. <https://doi.org/10.1016/j.biortech.2019.121790>
- Ramírez, E., Bringué, R., Fité, C., Iborra, M., Tejero, J., & Cunill, F. (2021). Assessment of ion exchange resins as catalysts for the direct transformation of fructose into butyl levulinate. *Applied Catalysis A: General*, 612, 117988. <https://doi.org/10.1016/j.apcata.2021.117988>
- Rasool, M. A., & Vankelecom, I. F. J. (2019). Use of γ -valerolactone and glycerol derivatives as bio-based renewable solvents for membrane preparation. *Green Chemistry*, 21(5), 1054–1064. <https://doi.org/10.1039/C8GC03652G>
- Raud, M., Rooni, V., & Kikas, T. (2016). Explosive decompression pretreatment: Nitrogen vs. Compressed air. *Agronomy Research*, 569–578.
- Registration Dossier—ECHA*. (n.d.). Retrieved January 5, 2023, from <https://echa.europa.eu/registration-dossier/-/registered-dossier/23920/4/7>
- Ruppert, A. M., Jędrzejczyk, M., Sneká-Płatek, O., Keller, N., Dumon, A. S., Michel, C., Sautet, P., & Grams, J. (2016). Ru catalysts for levulinic acid hydrogenation with formic acid as a hydrogen source. *Green Chemistry*, 18(7), 2014–2028. <https://doi.org/10.1039/C5GC02200B>
- Russo, V., Tesser, R., Rossano, C., Cogliano, T., Vitiello, R., Leveneur, S., & Di Serio, M. (2020). Kinetic study of Amberlite IR120 catalyzed acid esterification of levulinic acid with ethanol: From batch to continuous operation. *Chemical Engineering Journal*, 401, 126126. <https://doi.org/10.1016/j.cej.2020.126126>

- Serrano-Ruiz, J. C., Luque, R., & Sepúlveda-Escribano, A. (2011). Transformations of biomass-derived platform molecules: From high added-value chemicals to fuels via aqueous-phase processing. *Chemical Society Reviews*, 40(11), 5266. <https://doi.org/10.1039/c1cs15131b>
- Shen, Q., Zhang, Y., Zhang, Y., Tan, S., & Chen, J. (2019). Transformations of biomass-based levulinate ester into γ -valerolactone and pyrrolidones using carbon nanotubes-grafted N-heterocyclic carbene ruthenium complexes. *Journal of Energy Chemistry*, 39, 29–38. <https://doi.org/10.1016/j.jechem.2019.01.007>
- Shokri, S., Hedjazi, S., Lê, H. Q., Abdulkhani, A., & Sixta, H. (2022). High-purity cellulose production from birch wood by γ -valerolactone/water fractionation and IONCELL-P process. *Carbohydrate Polymers*, 288, 119364. <https://doi.org/10.1016/j.carbpol.2022.119364>
- Siengalewicz, P., Mulzer, J., & Rinner, U. (2014). 6.09 Synthesis of Esters and Lactones. In *Comprehensive Organic Synthesis II* (pp. 355–410). Elsevier. <https://doi.org/10.1016/B978-0-08-097742-3.00612-1>
- Slotboom, Y., Bos, M. J., Pieper, J., Vrieswijk, V., Likozar, B., Kersten, S. R. A., & Brilman, D. W. F. (2020). Critical assessment of steady-state kinetic models for the synthesis of methanol over an industrial Cu/ZnO/Al₂O₃ catalyst. *Chemical Engineering Journal*, 389, 124181. <https://doi.org/10.1016/j.cej.2020.124181>
- Stewart, W. E., & Caracotsios, M. (2008). *Computer-Aided Modeling of Reactive Systems* (1st ed.). Wiley. <https://doi.org/10.1002/9780470282038>
- Stewart, W. E., Caracotsios, M., & Sørensen, J. P. (1992). Parameter estimation from multiresponse data. *AIChE Journal*, 38(5), 641–650. <https://doi.org/10.1002/aic.690380502>
- Stoessel, F. (2008). Fundamentals of Thermal Process Safety. In *Thermal Safety of Chemical Processes* (pp. 31–58). John Wiley & Sons, Ltd. <https://doi.org/10.1002/9783527621606.ch2>

- Sudhakar, M., Kumar, V. V., Naresh, G., Kantam, M. L., Bhargava, S. K., & Venugopal, A. (2016). Vapor phase hydrogenation of aqueous levulinic acid over hydroxyapatite supported metal (M = Pd, Pt, Ru, Cu, Ni) catalysts. *Applied Catalysis B: Environmental*, *180*, 113–120. <https://doi.org/10.1016/j.apcatb.2015.05.050>
- Tabanelli, T., Paone, E., Blair Vásquez, P., Pietropaolo, R., Cavani, F., & Mauriello, F. (2019). Transfer Hydrogenation of Methyl and Ethyl Levulinate Promoted by a ZrO₂ Catalyst: Comparison of Batch vs Continuous Gas-Flow Conditions. *ACS Sustainable Chemistry & Engineering*, *7*(11), 9937–9947. <https://doi.org/10.1021/acssuschemeng.9b00778>
- Tabasso, S., Grillo, G., Carnaroglio, D., Calcio Gaudino, E., & Cravotto, G. (2016). Microwave-Assisted γ -Valerolactone Production for Biomass Lignin Extraction: A Cascade Protocol. *Molecules*, *21*(4), 413. <https://doi.org/10.3390/molecules21040413>
- Tan, J., Cui, J., Deng, T., Cui, X., Ding, G., Zhu, Y., & Li, Y. (2015). Water-Promoted Hydrogenation of Levulinic Acid to γ -Valerolactone on Supported Ruthenium Catalyst. *ChemCatChem*, *7*(3), 508–512. <https://doi.org/10.1002/cctc.201402834>
- Tan, J., Cui, J., Ding, G., Deng, T., Zhu, Y., & Li, Y. (2016). Efficient aqueous hydrogenation of levulinic acid to γ -valerolactone over a highly active and stable ruthenium catalyst. *Catalysis Science & Technology*, *6*(5), 1469–1475. <https://doi.org/10.1039/C5CY01374G>
- Tang, X., Chen, H., Hu, L., Hao, W., Sun, Y., Zeng, X., Lin, L., & Liu, S. (2014). Conversion of biomass to γ -valerolactone by catalytic transfer hydrogenation of ethyl levulinate over metal hydroxides. *Applied Catalysis B: Environmental*, *147*, 827–834. <https://doi.org/10.1016/j.apcatb.2013.10.021>
- Tay, B. Y., Wang, C., Phua, P. H., Stubbs, L. P., & Huynh, H. V. (2016). Selective hydrogenation of levulinic acid to γ -valerolactone using in situ generated ruthenium nanoparticles derived from Ru–NHC complexes. *Dalton Transactions*, *45*(8), 3558–3563. <https://doi.org/10.1039/C5DT03366G>

- Tejero, M. A., Ramírez, E., Fité, C., Tejero, J., & Cunill, F. (2016). Esterification of levulinic acid with butanol over ion exchange resins. *Applied Catalysis A: General*, *517*, 56–66. <https://doi.org/10.1016/j.apcata.2016.02.032>
- Thompson, A., & Wolfrom, M. L. (1957). ESTERS. In *The Carbohydrates* (pp. 138–187). Elsevier. <https://doi.org/10.1016/B978-0-12-395709-2.50007-5>
- Tukacs, J. M., Sylvester, Á., Kmecz, I., Jones, R. V., Óvári, M., & Mika, L. T. (2019). Continuous flow hydrogenation of methyl and ethyl levulinate: An alternative route to γ -valerolactone production. *Royal Society Open Science*, *6*(5), 182233. <https://doi.org/10.1098/rsos.182233>
- Upare, P. P., Lee, J.-M., Hwang, D. W., Halligudi, S. B., Hwang, Y. K., & Chang, J.-S. (2011). Selective hydrogenation of levulinic acid to γ -valerolactone over carbon-supported noble metal catalysts. *Journal of Industrial and Engineering Chemistry*, *17*(2), 287–292. <https://doi.org/10.1016/j.jiec.2011.02.025>
- Vafaezadeh, M., & Fattahi, A. (2015). DFT investigations for “Fischer” esterification mechanism over silica-propyl-SO₃H catalyst: Is the reaction reversible? *Computational and Theoretical Chemistry*, *1071*, 27–32. <https://doi.org/10.1016/j.comptc.2015.07.028>
- Van Boekel, M. a. j. s. (1996). Statistical Aspects of Kinetic Modeling for Food Science Problems. *Journal of Food Science*, *61*(3), 477–486. <https://doi.org/10.1111/j.1365-2621.1996.tb13138.x>
- van Maris, A. J. A., Abbott, D. A., Bellissimi, E., van den Brink, J., Kuyper, M., Luttik, M. A. H., Wisselink, H. W., Scheffers, W. A., van Dijken, J. P., & Pronk, J. T. (2006). Alcoholic fermentation of carbon sources in biomass hydrolysates by *Saccharomyces cerevisiae*: Current status. *Antonie van Leeuwenhoek*, *90*(4), 391–418. <https://doi.org/10.1007/s10482-006-9085-7>
- van Spronsen, J., Cardoso, M. A. T., Witkamp, G.-J., de Jong, W., & Kroon, M. C. (2011). Separation and recovery of the constituents from lignocellulosic biomass by using ionic liquids and acetic acid as co-solvents for mild hydrolysis. *Chemical Engineering and*

Processing: Process Intensification, 50(2), 196–199.
<https://doi.org/10.1016/j.cep.2010.12.010>

- Verma, S., Baig, R. B. N., Nadagouda, M. N., & Varma, R. S. (2016). Sustainable Strategy Utilizing Biomass: Visible-Light-Mediated Synthesis of γ -Valerolactone. *ChemCatChem*, 8(4), 690–693. <https://doi.org/10.1002/cctc.201501352>
- Vishtal, A., & Kraslawski, A. (n.d.). *CHALLENGES IN INDUSTRIAL APPLICATIONS OF TECHNICAL LIGNINS*. 22.
- Wang, A., Lu, Y., Yi, Z., Ejaz, A., Hu, K., Zhang, L., & Yan, K. (2018). Selective Production of γ -Valerolactone and Valeric Acid in One-Pot Bifunctional Metal Catalysts. *ChemistrySelect*, 3(4), 1097–1101. <https://doi.org/10.1002/slct.201702899>
- Wang, Y., Cipolletta, M., Vernières-Hassimi, L., Casson-Moreno, V., & Leveneur, S. (2019). Application of the concept of Linear Free Energy Relationships to the hydrogenation of levulinic acid and its corresponding esters. *Chemical Engineering Journal*, 374, 822–831. <https://doi.org/10.1016/j.cej.2019.05.218>
- Wang, Y., Plazl, I., Vernières-Hassimi, L., & Leveneur, S. (2020). From calorimetry to thermal risk assessment: γ -Valerolactone production from the hydrogenation of alkyl levulinates. *Process Safety and Environmental Protection*, 144, 32–41. <https://doi.org/10.1016/j.psep.2020.07.017>
- Wang, Y., Vernières-Hassimi, L., Casson-Moreno, V., Hébert, J.-P., & Leveneur, S. (2018). Thermal Risk Assessment of Levulinic Acid Hydrogenation to γ -Valerolactone. *Organic Process Research & Development*, 22(9), 1092–1100. <https://doi.org/10.1021/acs.oprd.8b00122>
- Werpy, T., & Petersen, G. (2004). *Top Value Added Chemicals from Biomass: Volume I -- Results of Screening for Potential Candidates from Sugars and Synthesis Gas* (DOE/GO-102004-1992, 15008859; p. DOE/GO-102004-1992, 15008859). <https://doi.org/10.2172/15008859>
- Wong, C. Y. Y., Choi, A. W.-T., Lui, M. Y., Fridrich, B., Horváth, A. K., Mika, L. T., & Horváth, I. T. (2017). Stability of gamma-valerolactone under neutral, acidic, and basic

- conditions. *Structural Chemistry*, 28(2), 423–429. <https://doi.org/10.1007/s11224-016-0887-6>
- Xiao, C., Goh, T.-W., Qi, Z., Goes, S., Brashler, K., Perez, C., & Huang, W. (2016). Conversion of Levulinic Acid to γ -Valerolactone over Few-Layer Graphene-Supported Ruthenium Catalysts. *ACS Catalysis*, 6(2), 593–599. <https://doi.org/10.1021/acscatal.5b02673>
- Xu, R., Liu, K., Du, H., Liu, H., Cao, X., Zhao, X., Qu, G., Li, X., Li, B., & Si, C. (2020). Falling Leaves Return to Their Roots: A Review on the Preparation of γ -Valerolactone from Lignocellulose and Its Application in the Conversion of Lignocellulose. *ChemSusChem*, 13(24), 6461–6476. <https://doi.org/10.1002/cssc.202002008>
- Xu, S., Chansai, S., Xu, S., Stere, C. E., Jiao, Y., Yang, S., Hardacre, C., & Fan, X. (2020). CO Poisoning of Ru Catalysts in CO₂ Hydrogenation under Thermal and Plasma Conditions: A Combined Kinetic and Diffuse Reflectance Infrared Fourier Transform Spectroscopy–Mass Spectrometry Study. *ACS Catalysis*, 10(21), 12828–12840. <https://doi.org/10.1021/acscatal.0c03620>
- Xue, Z., Zhao, X., Sun, R., & Mu, T. (2016). Biomass-Derived γ -Valerolactone-Based Solvent Systems for Highly Efficient Dissolution of Various Lignins: Dissolution Behavior and Mechanism Study. *ACS Sustainable Chemistry & Engineering*, 4(7), 3864–3870. <https://doi.org/10.1021/acssuschemeng.6b00639>
- Yamada, T., Yamaguchi, M., Kubo, S., & Hishikawa, Y. (2015). Direct Production of Alkyl Levulinates from Cellulosic Biomass by a Single-Step Acidic Solvolysis System at Ambient Atmospheric Pressure. *BioResources*, 10(3), 4961–4969. <https://doi.org/10.15376/biores.10.3.4961-4969>
- Yan, K., Lafleur, T., Jarvis, C., & Wu, G. (2014). Clean and selective production of γ -valerolactone from biomass-derived levulinic acid catalyzed by recyclable Pd nanoparticle catalyst. *Journal of Cleaner Production*, 72, 230–232. <https://doi.org/10.1016/j.jclepro.2014.02.056>
- Yan, K., Lafleur, T., Wu, G., Liao, J., Ceng, C., & Xie, X. (2013). Highly selective production of value-added γ -valerolactone from biomass-derived levulinic acid using the robust Pd

- nanoparticles. *Applied Catalysis A: General*, 468, 52–58. <https://doi.org/10.1016/j.apcata.2013.08.037>
- Yan, K., Yang, Y., Chai, J., & Lu, Y. (2015). Catalytic reactions of gamma-valerolactone: A platform to fuels and value-added chemicals. *Applied Catalysis B: Environmental*, 179, 292–304. <https://doi.org/10.1016/j.apcatb.2015.04.030>
- Yan, Z. P., Lin, L., & Liu, S. (2009). Synthesis of γ -valerolactone by hydrogenation of biomass-derived Levulinic acid over Ru/C catalyst. *Energy and Fuels*, 23(8), 3853–3858. <https://doi.org/10.1021/ef900259h>
- Yang, C.-G., Reich, N. W., Shi, Z., & He, C. (2005). Intramolecular Additions of Alcohols and Carboxylic Acids to Inert Olefins Catalyzed by Silver(I) Triflate. *Organic Letters*, 7(21), 4553–4556. <https://doi.org/10.1021/ol051065f>
- Yang, Y., Gao, G., Zhang, X., & Li, F. (2014). Facile fabrication of composition-tuned Ru-Ni bimetallics in ordered mesoporous carbon for levulinic acid hydrogenation. *ACS Catalysis*, 4(5), 1419–1425. <https://doi.org/10.1021/cs401030u>
- Yousuf, A., Pirozzi, D., & Sannino, F. (2020). Fundamentals of lignocellulosic biomass. In *Lignocellulosic Biomass to Liquid Biofuels* (pp. 1–15). Elsevier. <https://doi.org/10.1016/B978-0-12-815936-1.00001-0>
- Zhang, L., Fu, L., Wang, H., & Yang, B. (2017). Discovery of Cellulose Surface Layer Conformation by Nonlinear Vibrational Spectroscopy. *Scientific Reports*, 7(1), 44319. <https://doi.org/10.1038/srep44319>
- Zhong, H., Li, Q., Liu, J., Yao, G., Wang, J., Zeng, X., Huo, Z., & Jin, F. (2017). New Method for Highly Efficient Conversion of Biomass-Derived Levulinic Acid to γ -Valerolactone in Water without Precious Metal Catalysts. *ACS Sustainable Chemistry & Engineering*, 5(8), 6517–6523. <https://doi.org/10.1021/acssuschemeng.7b00623>
- Zhou, Y., Woo, L. K., & Angelici, R. J. (2007). Solid acid catalysis of tandem isomerization-lactonization of olefinic acids. *Applied Catalysis A: General*, 333(2), 238–244. <https://doi.org/10.1016/j.apcata.2007.09.013>

Zhu, S., Xue, Y., Guo, J., Cen, Y., Wang, J., & Fan, W. (2016). Integrated Conversion of Hemicellulose and Furfural into γ -Valerolactone over Au/ZrO₂ Catalyst Combined with ZSM-5. *ACS Catalysis*, 6(3), 2035–2042. <https://doi.org/10.1021/acscatal.5b02882>

Annexes

List of figures

Figure 1-1 - The main components and structure of lignocellulose. “Gl” represents glucuronic acid, and “Fer” represents esterification with ferulic acid. Reproduced from (Isikgor & Becer, 2015) with permission from the Royal Society of Chemistry.....	19
Figure 1-2 - Lignocellulosic Feedstock Biorefinery (LCF-Biorefinery, Phase III) Reproduced with permission from Springer Nature. Licence 5519390807757 (Kamm, 2004).....	21
Figure 1-3 – Molecular structure of The Top Sugar-derived Building Blocks. Based on (Bozell & Petersen, 2010; Werpy & Petersen, 2004)	22
Figure 1-4 - Reaction scheme for 5-HMF production from glucose. Taken from (Herbst & Janiak, 2016) with an CCCN 3.0 licence	23
Figure 1-5 - Chemical structure of levulinic acid	23
Figure 1-6 - Synthesis of alkyl levulinates from various biomass reactants. Reprinted with permission from (Démolis et al., 2014),. Copyright 2014, American Chemical society.	25
Figure 1-7 - Transesterification of methyl levulinate (a) and esterification of levulinic acid (b) (ML: methyl levulinate, LAE: levulinic acid ester) Reprinted from(Melchiorre et al., 2020) with permission of Elsevier 5519410053276.....	25
Figure 1-8 – n-alkyl levulinates up to 5 chain carbon substituents.....	26
Figure 1-9 - Structure of γ -valerolactone	28
Figure 1-10 – Lignocellulosic biomass-derived products obtained using GVL as solvent. Reproduced from (Alonso et al., 2013)nwith permission from the Royal Society of Chemistry	30
Figure 1-11 - Ring opening of GVL as a new versatile route to produce polymer precursors. Reproduced from (Isikgor & Becer, 2015) with permission from the Royal Society of Chemistry.	31

Figure 1-12 – Representation of the leading products obtained from GVL. Synthesized from (Alonso et al., 2013; Chalid et al., 2012; Isikgor & Becer, 2015).....	31
Figure 1-13 - Emitted smoke concentration at full load as a function of engine speed. (Bereczky et al., 2014) Public licence CCCN 4.0	32
Figure 1-14 - Fractionation of lignocellulosic biomass and reaction pathways to produce GVL from hemicellulose and cellulose. Reproduced from (Alonso et al., 2013) with permission from the Royal Society of Chemistry	33
Figure 1-15 - Intramolecular Hydroalkoxylation of olefins. Reprinted with permission from (C.-G. Yang et al., 2005). Copyright 2005, American Chemical Society.....	33
Figure 1-16 – Reaction of epoxide with (MeLi)CuBr(PBu ₃) complex. Adapted with permission from (Mitani et al., 1990), Copyright 1990, American Chemical Society.....	33
Figure 1-17 - Reaction scheme: Reaction pathway of hydrogenation of LA to GVL Reprinted from (Putrakumar et al., 2015) with permission from Elsevier.	34
Figure 1-18 - Catalytic transfer hydrogenation of levulinic acid (1, R1 = H) and its esters (1, R1 = C _x H _{2x+1}) to γ -valerolactone (5) using a secondary alcohol as the hydrogen donor (2, R2 = C _y H _{2x+1}). Used with permission of Royal Society of Chemistry, from (Chia & Dumesic, 2011), permission conveyed through Copyright Clearance Center, Inc.	35
Figure 1-19 – γ -valerolactone production from levulinic acid with formic acid as a hydrogen source. Used with permission of Royal Society of Chemistry from (Ruppert et al., 2016); permission conveyed through Copyright Clearance Center, Inc.....	36
Figure 1-20 - Decomposition reactions for formic acid. Reproduced from (Goddard et al., 1992), with the permission of AIP Publishing.	36
Figure 1-21 – Graphic representation of deactivation of rhodium and ruthenium catalysts by contacting with poisoning compounds. Reproduced from (Dey & Dhal, 2020) with permission from Springer	37
Figure 1-22 - Production of GVL by hydrogenation of alkyl levulinates and levulinic acid with molecular hydrogen.....	37

Figure 1-23 - Classic mechanism for acid-catalyzed Fisher esterification. Reprinted from (Vafaezadeh & Fattahi, 2015) with permission of Elsevier.	38
Figure 1-24 - Levulinic acid keto and enol forms. Representation made from (Bruice, 2010)	39
Figure 2-1 – Scheme of the experimental setup for kinetic experiments by autoclave. (Capecci, Wang, Delgado, et al., 2021).....	46
<i>Figure 2-2 - Mettler Toledo RC1 Mx calorimeter. Picture of reactor (left) and schema of heating mechanism (right) from Mettler Toledo.</i>	<i>47</i>
Figure 2-3 - Tian Calvet C80 micro-calorimeter. Picture (left) and schema for cells (right) ..	48
Figure 2-4 - Hastelloy reversal mixing cells in C80 microcalorimeter.....	48
Figure 2-5 - Batch reactor used for transesterification reactions.	49
Figure 2-6 - IKA RV 10 digital rotavapor.....	49
Figure 2-7 - GC FID used for experiments.	50
Figure 2-8 – Chromatogram on GC-FID with methanol as solvent. From left to right: methanol, ethanol, n-propanol, n-butanol, n-pentanol, γ -valerolactone, and alkyl levulinates (methyl, ethyl, n-propyl and n-butyl levulinate) studied.	51
Figure 2-9 - Micrometrics 3 Flex used (left) and VacPrep 061 sample degasser system (right)	52
Figure 2-10 – Adsorption and Desorption isotherms (up) and DFT Pore size distribution (down) for Ru/C catalyst.....	53
Figure 2-11 - Reaction scheme of Hydrogenation of alkyl levulinates into GVL	54
Figure 3-1 - Temperature effect on BL(A) and BHP (B) conversion at 20 bars. Experiments 2, 5, and 6.	59
Figure 3-2 - The effect of temperature and total pressure on the vapor–liquid equilibria for a binary system hydrogen–levulinic acid; equilibrium mole fraction of H ₂ in the liquid phase. Used with permission of Elsevier Science & Technology Journals, from (Grilc & Likozar, 2017) permission conveyed through Copyright Clearance Center, Inc	60

Production of γ -valerolactone, a green platform molecule

Figure 3-3 - Hydrostatic pressure effect in BL (A) and BHP (B) at 100°C with a Ru catalyst loading of 0.5g. Experiments 7, 9, and 10.....	61
Figure 3-4 - Catalyst loading effect on BL (1) and BHP (B) at 150°C and 20 bars. Experiments 3 and 5.	62
Figure 3-5 – Schema for hydrogenation step adsorption models based on Langmuir Hinshelwood non-competitive mechanism with (1) and without (2) dissociation of hydrogen; competitive with (3) and without (4) dissociation of hydrogen and (5) Eley-Rideal mechanisms.(Sites for adsorption: * and ^)	63
Figure 3-6 - Parity Plots for Model 4	72
Figure 3-7 - Parity plots for Model 2	73
Figure 3-8 - Parity plots for Model 8.	75
Figure 3-9 - Fit of Model 8 (Non-competitive Langmuir-Hinshelwood with no dissociation of Hydrogen) to the experimental data.	76
Figure 4-1 - Reaction scheme for butyl levulinate production from fructose alcoholysis (Ramírez et al., 2021; Démolis et al., 2014; Di Menno Di Bucchianico et al., 2022)	79
Figure 4-2 - Effect of Temperature: Comparison between exp 3&4. Hydrogenation and Cyclization reaction steps. (P:20bar, 0.5g Ru/C, 0g Amberlite).....	82
Figure 4-3 - Effect of pressure: Comparison between exp 3&5. Hydrogenation and Cyclization reaction steps.(0.5g Ru/C, 0g Amberlite).....	83
Figure 4-4 - Effect of Ru/C loadings: Comparison between exp 7&8. Hydrogenation and Cyclization reaction steps. (T: 403.15K, P: 20 bar, 0g Amberlite).....	84
Figure 4-5 - Effect of Amberlite IR120 concentration on the kinetics: Comparison between exp 9&10. Hydrogenation and Cyclization reaction steps.(T: 403.15K, P:20 bar, 0.5g Ru/C).....	85
Figure 4-6 - Effect of LA concentration: Comparison between exp 3&6. Hydrogenation and Cyclization reaction steps. (T:403.15K, P:20 Bar, 0.5g Ru/C, 0g, Amberlite).....	86
Figure 4-7 - Parity plots for the NCLH1.2 model	99

Figure 4-8 - Fit of Model NCLH1.2 to the experimental concentrations with prediction intervals.	101
Figure 4-9 - Parity plots for concentrations with the NCHL2.2 modeling results.	107
Figure 4-10 - Fit of Model NCLH2.2 with prediction intervals to the experimental concentrations.....	107
Figure 4-11 - Coefficient of determinations for training, test, and all for the different models.	112
Figure 5-1 - Procedure to estimate hydrogenation and cyclization enthalpies for alkyl levulinates and levulinic acid.	116
Figure 5-2 – Experimental procedure in RC1 experiments.....	118
<i>Figure 5-3 – Transesterification of methyl levulinate (ML) into propyl levulinate (n-PrL)..</i>	119
Figure 5-4 - Amberlite IR120 H form, normal picture of catalyst (left) and SEM image at 500 μ m (right, with permission from (Gawad, 2019))	120
Figure 5-5 - Heat-flow rate normalized by the initial intermediate concentration for the cyclization of MHP, BHP and EHP and with 0.01 mol/L of H ₂ SO ₄ in GVL solvent at 60°C versus time.....	122
Figure 5-6 - Evolution of heat-flow rate for BL hydrogenation at 130°C, 35 bars of hydrogen and with an initial BL concentration of 2.03 mol/L in GVL solvent.	124
Figure 5-7 - Heat-flow rate evolution for the hydrogenation of BL in GVL solvent at different temperatures.	125
Figure 5-8. BL concentration effect on heat-flow rate at isothermal and isobaric conditions: at 130°C and hydrogen pressure of 35 bars.....	126
Figure 5-9. Solvent effect on the heat-flow rate of BL hydrogenation at isothermal and isobaric conditions: 100 °C and 35 bar of hydrogen.....	128
Figure 5-10. Effect of substituent on the normalized heat-flow rate of hydrogenation at 130°C and 35 bars of hydrogen for substrates in GVL.	130

Figure 5-11. Effect of substituent on the normalized heat-flow rate of hydrogenation at 130°C and 35 bars of hydrogen for pure substrates. 131

List of Tables

Table 1-1 - The top sugar-derived building blocks (Bozell & Petersen, 2010; Werpy & Petersen, 2004).....	22
Table 1-2 – Physical properties of levulinic acid (PubChem Compound Summary for CID 11579, Levulinic Acid, 2022)	24
Table 1-3 - Physical properties of alkyl levulinates studied (N-Amyl Levulinate C ₁₀ H ₁₈ O ₃ ChemSpider, n.d.; PubChem, n.d.; Registration Dossier - ECHA, n.d.).....	26
Table 1-4 - Physical properties of γ -valerolactone (Alonso et al., 2013; Havasi et al., 2016; Kerkel et al., 2021).....	28
Table 1-5 - Preparation of GVL catalyzed by noble metal catalysts. Used with permission of WILEY - VCH VERLAG GMBH & CO. KGAA, from (R. Xu et al., 2020) permission conveyed through Copyright Clearance Center, Inc.	40
Table 2-1 - Materials bought for analysis and experiments.	45
Table 2-2 - Surface area and pore size volume values of Ru/C catalyst.....	52
Table 3-1 - Experimental matrix for kinetic experiments	57
Table 3-2 - Rate expressions for the hydrogenation step of the reaction system.	64
Table 3-3 - Tested models for the hydrogenation of BL to GVL.....	67
Table 3-4 - Modeling results from Bayesian statistics	71
Table 3-5 - Estimated values at Tref (403.15K) and statistical data for Model 4.....	71
Table 3-6 - Normalized parameter covariance matrix for Model 4	72
Table 3-7 - Estimated values at Tref 403.15K and statistical data for Model 2.....	73
Table 3-8 - Normalized parameter covariance matrix for Model 2	74

Table 3-9 - Estimated values at $T_{ref}=403.15K$ and statistical data for Model 8	74
Table 3-10 - Normalized parameter covariance matrix for Model 8	75
Table 4-1 - Experimental matrix	80
Table 4-2 - Rate expressions for hydrogenation steps	91
Table 4-3 - Regression parameters for each model	96
Table 4-4 - Estimated Values at $T_{ref} = 392.72 K$ and statistical Data for NCLH1.2	98
Table 4-5 - Normalized parameter covariance matrix for Model NCLH1.2.....	100
Table 4-6 - Estimated Values at $T_{ref} = 392.72 K$ and Statistical Data for NCLH2.2	104
Table 4-7 - Normalized parameter covariance matrix for Model NCLH2.2.....	105
Table 4-8 - Distribution of the 14 experiments in the seven folds	110
Table 4-9 - Different sets for regression and validation.....	111
Table 4-10 - $CV_{(K)}$ and standard deviation for each model	111
Table 5-1. Operating conditions and experimental results for the cyclization experiments in C80 calorimeter in isothermal conditions.	121
Table 5-2. GC and RC1 results for experiments in isothermal conditions at different temperatures for the hydrogenation of BL in GVL solvent at 35 bars of hydrogen.	125
Table 5-3. GC and RC1 results for experiments in isothermal conditions at different initial BL concentrations for the hydrogenation of BL in GVL solvent at 35 bars of hydrogen.....	126
Table 5-4. GC and RC1 results for experiments in isothermal and isobaric conditions for the hydrogenation of BL in GVL solvent and in butanol solvent at $100^{\circ}C$ and 35 bar of hydrogen.	127
Table 5-5. GC and RC1 results for experiments in isothermal conditions for the hydrogenation of substrates at $130^{\circ}C$ and 35 bar of hydrogen.	129
Table 5-6. GC and RC1 results for experiments in isothermal conditions for the hydrogenation of EL-BL mixture in GVL solvent at $130^{\circ}C$ and 35 bar of hydrogen.	132

Table 5-7 - Operating conditions for the cyclization experiment in C80 in isothermal conditions at 60 °C and 0.01 mol/L of H_2SO_4 in GVL solvent.....	133
Table 5-8 - GC and RC1 results for experiments at isothermal conditions for the hydrogenation of substrates at 130°C, 35 bar of hydrogen, reaction mass of 550 g and 6.3 g of Ru/C	133
Table 5-9 - Operating conditions for the cyclization experiment in C80 in isothermal conditions at 60 °C and 10 mol/m ³ of H_2SO_4 in GVL solvent.	134
Table 5-10 - GC and RC1 results for experiments at isothermal conditions for the hydrogenation of substrates at 130°C, 35 bar of hydrogen, reaction mass of 0.550 kg and 0.0063 kg of Ru/C (containing 50 wt% of water).....	134
Table 5-11 - Mean values for hydrogenation reaction enthalpies for LA and AL between 100 and 130 °C at 35 bar of Hydrogen.....	135
Table 5-12 - Mean values for cyclization reaction enthalpies for AL at 60°C	135